Modelling and Experimental Investigation of Nonlinear Properties of YBa$_2$Cu$_3$O$_7$ and NdBa$_2$Cu$_3$O$_7$ Superconducting Films and Resonators for Applications in Microwave Circuits

A thesis presented in partial fulfilment of the requirements for the degree of

Doctor of Philosophy

in

Electrical Engineering

at

James Cook University, Townsville, Australia

Dmytro Ledenyov

2018

ABSTRACT

Nonlinear effects arising in High Temperature Superconductors (HTS) under elevated electromagnetic signal power levels can significantly limit HTS superior microwave characteristics. Understanding the extent of those limitations and possibly predicting them by modelling microwave properties of high temperature superconductors can yield a substantial advantage at early stages of microwave device design and manufacturing. Therefore, one of the main objectives of this thesis is **to *investigate if it is feasible to expand modelling of microwave properties of superconductors including nonlinear effects in more details.*** In addition, an experimental investigation was conducted in this thesis focusing on the question *if there is any HTS material that exhibits smaller nonlinear effects than found in the widely utilised* $YBa_2Cu_3O_7$ *(YBCO) superconductor*.

A novel approach towards the development of an advanced lumped element model of HTS materials that can accurately represent nonlinear effects in a microwave resonator is presented in this thesis. The theoretical model engineered by the author, more comprehensively represents superconducting phenomena than the standard two-fluid model. Simulation results demonstrated close correspondence with the measured characteristics of HTS films under test. The developed model could be suitable for advanced CAD tools applicable for design of HTS electronic circuits, that need to take into account the complex nature of nonlinear effects.

In reference to the experimental investigation, microwave properties of $YBa_2Cu_3O_7$ thin films and improved $NdBa_2Cu_3O_7$ (NdBCO) **thin films** on MgO substrates were examined by the author. In addition, a comprehensive microwave investigation of YBCO and NdBCO **microstrip resonators** manufactured at Tsinghua University (China) utilising thin films, manufactured in the same laboratory (Ceraco) using the same thermal co-evaporation technique, was also conducted. The measurements for the thin films and resonators were performed at frequencies of 25GHz and 2.1GHz respectively, as a function of temperature and varying RF input power (from -5dBm to +30dBm). A thorough analysis

of the onset of nonlinear effects in YBCO and NdBCO thin films and resonators is presented and comparatively discussed. The performed investigations show that NdBCO thin films and NdBCO resonators demonstrated higher values of the onset of nonlinearities than YBCO thin films and YBCO resonators. Smaller nonlinear effects observed in NdBCO films and NdBCO microstrip resonators could give them an advantage over YBCO films and resonators for applications in microwave circuits.

ACKNOWLEDGEMENTS

I would like to begin by offering my sincerest thanks to my supervisor, Prof. Janina Mazierska, who presented me with an opportunity to undertake my PhD in Australia and supported me in obtaining both the International Postgraduate Research Scholarship at the James Cook University and a prestigious Graduate Fellowship award from IEEE Microwave Theory and Technique Society (MTT-S), USA. Her research expertise, guidance and support have been invaluable for the past years.

I would also like to extend my gratitude to Prof. Bin Wei of Tsinghua University, China for his valuable input and contribution. My thanks also go to Dr. Kenneth Leong and Prof. Mohan Jacob for their relevant inputs and discussions.

I would also like to thank you all staff at the Electrical and Engineering Department at James Cook University for the opportunity to work with such an experienced team of academics, engineers and technicians.

Finally, I would like to pass my warm thanks to all my family and friends for making everything that I have undertaken possible.

CONTENTS

FIGURES

LIST OF PUBLICATIONS

[1] J. Mazierska, K. Leong, D. Ledenyov, A. Rains, N. Zuchowski, J. Krupka, "Microwave Measurements of Surface Resistance and Complex Conductivity of NdBaCuO Films", *Advances in Science and Technology*, vol. 95, pp. 162-168, 2014.

[2] J. Mazierska, D. Ledenyov, M. Jacob, J. Krupka, "Precise Microwave Characterization of *MgO* Substrates for *HTS* Circuits with Superconducting Post Dielectric Resonator", *Superconductor Science and Technology,* vol. 18, pp. 18–23, 2005.

[3] J. Mazierska, J. Krupka, M. Jacob, D. Ledenyov, "Complex Permittivity Measurements at Variable Temperatures of Low Loss Dielectric Substrates Employing Split Post and Single Post Dielectric Resonators", *Proceedings of IEEE MTT-S International Microwave Symposium,* Fort Worth, Texas, USA, vol. **3**, pp. 1825 – 1828, 2004.

[4] D. Ledenyov, J. Mazierska, G. Allen, M. Jacob, "Lumped Element Modelling of Nonlinear Properties of High Temperature Superconductors in a Dielectric Resonator", *Proceedings of the XV International Microwaves, Radar and Wireless Communications Conference MIKON 2004,* Warsaw, Poland, vol. 3, pp. 824-827, 2004.

[5] D. Ledenyov, J. Mazierska, G. Allen, M. Jacob, "Simulations of Nonlinear Properties of *HTS* Materials in a Dielectric Resonator Using Lumped Element Models", *Proceedings of International Superconductive Electronics Conference ISEC 2003,* Sydney, Australia, 2003.

[6] M. Jacob, J. Mazierska, K. Leong, D. Ledenyov, J. Krupka, "Surface Resistance Measurements of *HTS* Thin Films using SRLAO Dielectric Resonator", *IEEE Transactions on Applied Superconductivity,* vol. 13, no. 2, pp. 2909-2912, 2003.

[7] M. Jacob, J. Mazierska, D. Ledenyov, J. Krupka, "Microwave Characterisation of CaF_2 at Cryogenic Temperatures Using Dielectric Resonator Technique", *Journal of*

European Ceramic Society, Elsevier, The Netherlands, vol. 23, no. 14, pp. 2617-2622, 2003.

[8] K. Leong, J. Mazierska, M. Jacob, D. Ledenyov, "Comparing Unloaded Q-factor of a High-Q Dielectric Resonator Measured Using the Transmission Mode and Reflection Mode Methods Involving S-Parameter Circle Fitting", *Proceedings IEEE MTT-S International Symposium*, Seattle, Washington, USA, vol. 3, pp. 1665–1668, 2002.

[9] J. Mazierska, M. Jacob, K. Leong, D. Ledenyov, J. Krupka, "Microwave Characterisation of *HTS* Thin Films using *SrLaAlO₄* and Sapphire Dielectric Resonators", *Proceedings 7th Symposium on High Temperature Superconductors in High Frequency Fields,* Cape Cod, MA, USA, 2002.

CHAPTER 1

Introduction

A number of electronic devices and systems being used around the world continues to increase at an astounding rate. Our society and lifestyles are quickly forced to evolve into a globally networked economy, a development that is being shaped by the convergence of electronic systems, computing power, advanced materials and communication technologies. Such rapid developments coupled with limited available technological resources have created needs for both improving the system performance and developing materials with enhanced microwave properties to better address the technological demands of the current generation. High Temperature Superconductor (HTS) compounds provide prospects for such improvements and developments to be achieved.

A very brief history of superconductivity, HTS and their applications follows, to establish a foundation for the objectives of this thesis.

The phenomenon of superconductivity was first unexpectedly discovered by Onnes in 1911 [1] in mercury at the temperature below 4.19K, while conducting investigation on resistance of platinum, gold and mercury at very low temperatures. For this ground-breaking discovery Onnes was awarded the Nobel Prize only two years later, in 1913.

Superconductivity is characterised by two key fundamental attributes, that differentiate it from normal conductivity, such as the suddenly vanishing electrical resistance that becomes zero at Direct Current (DC) below the critical temperature (T_C), and the perfect diamagnetism - spontaneous exclusion of external magnetic fields, first detected in 1933 and known as the 'Meissner effect' [2]. These unique

characteristics of superconducting state occur in the phase region below certain critical values of external magnetic field (H_C), current density (J_C), and frequency (f_C).

The discovery of superconductivity was one of the fundamental scientific achievements of the 20th century, opening the way to exciting new applications in electronics and beyond. In 1913, superconductivity was found in *lead* below 7K, and later in *niobium nitride* below 16K. During seventy-five years after the discovery of superconductivity, a significant number (more than 5000) of compounds, elements and alloys were discovered to be superconducting. The maximum critical temperature achieved was 23K in Nb_3Ge [3]. Such low temperatures were achievable only with expensive liquid helium.

While discovered in 1911, the effective understanding of the superconducting phenomenon occurred only in 1957 [4], when a Bardeen-Cooper-Schrieffer (BCS) theory explaining the superconducting current as a superfluid of Cooper pairs was proposed, the concept that received the Nobel Prize in Physics in 1972. Due to the severe cryogenic requirements at that time, only a few very specialised applications of superconductors were developed, such as microwave mixers and detectors for highly challenging radio astronomy applications; and superconducting magnets for high-energy physics and magnetic resonance imaging (MRI) applications.

Enthusiasm for research and applications of superconductivity was renewed in 1986 with the surprising discovery of High Temperature superconductivity in copper oxides (cuprates) [5], which are poor conductors. La_2BaCuO_4 (LBCO) exhibited the critical temperature of 30K, and this discovery received the Nobel Prize one year later, in 1987. The same year, a new superconducting cuprate was developed, $YBa_2Cu_3O_7$ (YBCO) [6], that exhibited superconductivity at temperatures up to 92K, a material widely used now mostly in a thin film form.

For High Temperature Superconductors (HTS) with T_C above 77K, liquid nitrogen could be used for cooling, significantly decreasing the costs. Hence, since the discovery of High Temperature Superconductors, substantial efforts have been

made towards the development of superconductive applications. These include such areas as *Information and Electronics* with custom microwave systems, superconducting transistors, satellite technology and mobile communication developments [7, 8]; *Defence* with advanced radars and deep space detection [9]; *Medical Care* with MRI and SQUID for living body measurements [9]; *Environment and Energy* with applications in power generators, current limiters, superconducting magnetic energy storage and large magnet for nuclear fusion furnace [9]; *Transportation* with magnetically levitated transportation [9]. The most recent development, of the 17-Qubit superconducting computer chip, by Intel in the late 2017 [10] presents an important step towards the realisation of quantum computing. In this dissertation, a focus is on the Information and Electronics area of the applications, specifically on microwave superconducting devices.

A wide range of HTS circuits operating at microwave frequencies have been developed and built, such as filters, mixers, delay lines and antennas. Superconducting materials are appealing for implementation in passive microwave circuits for a number of reasons. First, it is their surface resistance (R_S), very low in comparison to the best conventional materials [11]. For example, the $YBa_2Cu_3O_7$ superconductor, used in microwave applications, exhibits the surface resistance at 1GHz of nearly $1x10^{-6}\Omega$ versus copper of approximately $3x10^{-3}\Omega$ under equivalent conditions [11]. Second, it is their high critical current density (J_C) in high quality superconducting films. These performances enable microwave HTS filters to possess exceptional characteristics, such as very low insertion losses, extremely high out-of-band rejections, very narrow bandwidth, very steep skirt slopes, and compact resonant structures with extremely high quality factors [12]. Taking advantage of the low-loss properties of superconductors, the fabrication of microwave circuits in a more compact geometry than their normal-metal counterparts is feasible.

However, despite the superior characteristics of HTS superconductors at low power levels, an increase of the losses at elevated microwave powers, referred to as the nonlinear phenomenon, degrade the performance of high-power HTS microwave devices. The nonlinearity appears in the form of a dependence of the surface

impedance (Z_S) of superconductors on the input RF power level, which was also observed in low T_C superconductors [13, 14]. Nonlinear effects in HTS thin films have been observed and analysed by several researchers [15-24] and found that they might be caused by one or more of the following phenomena: thermal effects, weak links, non-homogeneities, non-equilibrium excitation, unconventional pairing and others. Each of the above phenomena occurs under certain conditions and can be described by either linear, quadratic and exponential dependence on the RF magnetic field.

Simple modelling of the superconducting phenomenon is usually done using a lumped element equivalent circuit based on the two fluid model [25], consisting of a resistor representing the current flow of normal electrons and an inductor representing superconducting Cooper pairs. While this model (in the basic form or in its modifications [26-27]) represents the basic phenomena of superconductivity very well despite its simplicity, it does not accurately characterise the nonlinear effects. More precise modelling of the nonlinear behaviour of HTS materials could allow for more accurate simulation of HTS based circuits and hence better design of HTS filters.

Thus, the first aim of this dissertation was *to develop an advanced lumped element model of microwave properties of superconducting materials including nonlinear effects for the purpose of application of the model to analysis of performance of HTS circuits*.

The second goal of this thesis was *to investigate if there is any other HTS material that exhibits smaller nonlinear effects than found in the widely used YBCO superconductor that could be used in microwave superconducting circuits.*

The commercial microwave implementation of High Temperature Superconducting thin films demands double-sided homogeneous films on large areas with low surface resistance. Since the discovery of HTS materials, the $YBa_2Cu_3O_7$ compound has been unquestionably the most widely researched of the rare-earth copper oxide materials, leading to its dominance in the market of microwave

applications. This was due to commercial availability of high quality YBCO films. However, development of HTS films with better power handling capabilities than those observed in YBCO films would be highly beneficial for microwave devices.

The bulk $NdBa_2Cu_3O_7$ (NdBCO) cuprate, first developed in 1987 [28], exhibited a higher critical temperature (~94K) than YBCO [29, 30], and a higher critical current density (J_C) [31-33]. The surface resistance (R_S) of NdBCO films on MgO substrate was reported as low as $230\mu\Omega$ at 10GHz and 77K [30], lower than of YBCO films (typically $300-400\mu\Omega$ at 10GHz and 77K [31]). Hence, the NdBCO thin films could be good candidates for applications for microwave circuits. However, nonlinear properties of NdBCO cuprates have never been examined in the past, to the author's knowledge.

Therefore, in this dissertation, single sided NdBCO thin films were selected to be investigated to establish if they exhibited smaller nonlinear effects than the YBCO thin films. Microwave investigation was based on measurements of the quality factor Q_0 (and subsequent calculation of the surface resistance) as a function of temperature and microwave input power. To achieve high accuracy of microwave measurements of HTS films the Hakki-Coleman dielectric resonator [34] was utilised, and the Transmission Mode Quality Factor (TMQF) technique used for data processing [35].

In order to perform a proper assessment of microwave properties of NdBCO films and to enable the adequate comparison, the YBCO films deposited with the same thermal co-evaporation technique in the same laboratory were also investigated. Additionally, YBCO and NdBCO microstrip resonators were designed and manufactured (in cooperation with Prof. Bin Wei of Tsinghua University, China) in order to enable a comparison of nonlinear effects not only in superconducting thin films, but also in microwave devices. The resonators were designed for frequency of 2.1GHz and manufactured using double sided films. Having superconducting films and devices analysed independently could provide additional verification of the results.

The structure of the thesis is as described below:

Chapter 2 is divided into two subchapters to cover the topics of superconducting materials and their microwave properties in a more comprehensive way. Chapter 2.1 concentrates on an introduction to superconductivity and its applications. Special emphasis was made on the overview of theories of the superconducting phenomenon with physics and material properties of superconductors discussed. Also, main applications of HTS materials from communication devices to medicine have been outlined. Chapter 2.2 analyses microwave properties of superconducting materials including the surface resistance and nonlinear effects. A literature review of experimental results related to nonlinear properties of the surface resistance R_S in the form of the dependences on both the external DC and RF magnetic fields is presented. Possible sources of nonlinearity considering extrinsic and intrinsic approaches are discussed. Also, included in this chapter is a review of microwave measurement techniques used by laboratories around the world.

In Chapter 3, the literature review of lumped element modelling of microwave properties of superconductors and superconducting resonators has been presented. An analytical review investigating equivalent circuits proposed by various authors to represent superconducting resonators has been shown and examined by the author of this dissertation.

The development of an advanced lumped element model to simulate nonlinear microwave characteristics of superconducting materials, conducted by the author of this thesis, is described in Chapter 4. Three lumped element models of the resonator incorporating superconductors have been proposed and analysed by the author. Also, to investigate nonlinear effects, three mathematical dependences of superconducting model elements on RF magnetic field (linear, quadratic, and exponential) have been

applied. Power responses of the developed models have been simulated using the algorithm developed in Matlab software [36].

Chapter 5 shows experimental investigation of microwave properties of $YBa_2Cu_3O_7$ and $NdBa_2Cu_3O_7$ thin films and microstrip resonators. The measurement system for the microwave characterisation of HTS thin films is presented together with the results of the microwave characterisation and discussions. The thin films and microstrip resonators have been investigated as a function of temperature and microwave input power. The onset of nonlinear effects in the YBCO and NdBCO films and resonators has been defined and analysed using the two segment linear approximation technique.

The summary of results and conclusions to the thesis are presented in Chapter 6.

REFERENCES

[1]   K. Onnes, *Leiden Comm.*, 120b, 122b, 124c, 1911.

[2]   W. Meissner and R. Ochenfeld, *Naturwissenschaften*, v. 21, p. 787, 1933.

[3]   M. Nisenoff, "Microwave superconductivity Part: History, properties and early applications", *IEEE MTT-S International Microwave Symposium Digest*, 2011.

[4]   J. Bardeen, et.al., "Theory of Superconductivity", *Phys. Rev.,* v. 108, p. 1175, 1957.

[5]   J. Bednorz K. Muller, "Possible high T_c superconductivity in the Ba-La-Cu-O system" *Z. Phys.*, B64, p. 189, 1986.

[6]   K. Wu et al., "Superconductivity at 93K in a new mixed phase Y-Ba-Cu-O compound system at ambient pressure", *Phys. Rev. Let.*, vol. 58., p. 908, 1987.

[7]   H. Piel et.al., "High temperature superconductors in high frequency fields – fundamentals and applications", *Advances in Superconductivity IV*, pp. 925–930, 1992.

[8]   Li Chunguang et al., "Topical Review: Progress on applications of high temperature superconducting microwave filters", *Supercond. Sci. Technol.*, v. 30, 073001, pp.1-14, 2017.

[9]   Sumitomo Electric Industries, www.global-sei.com (accessed: October, 2017)

[10]   Intel, www.newsroom.intel.com, (accessed: October, 2017)

[11]   H. Piel and G. Muller, "The microwave surface impedance of high-T_C superconductors", IEEE Trans. on Magnetics, vol. 27, no. 2, pp. 854-862, 1991.

[12]   J. Mazierska and M. Jacob, "High-temperature superconducting planar filters for wireless communication", Chapter 6 in "Novel technologies for microwave and millimeter - wave applications" edited by J.-F. Kiang, *Springer Science*, pp. 123-151, 2004.

[13]   R. Parmenter, "Nonlinear electrodynamics of superconductors with a very small coherence distance", *RCA Rev.* 23, pp. 323, 1962.

[14] P. Nozieres, W. Viven, "The motion of flux in type II superconductors", Phil. Mag.: J. Theor. Experim. and Appl. Phys., v. 8, pp. 667-688, 1966.

[15] J. Halbritter, RF residual losses, surface impedance, and granularity in superconducting cuprates, *Appl. Phys.*, v. 68, p. 6315, 1990.

[16] D. Oates, et al., "Measurements and Modeling of Linear and Nonlinear Effects in Striplines", *Journal of Superconductivity,* vol. 5, no. 4, pp. 361-369, 1992.

[17] P. Nguyen et al., "Nonlinear Surface Impedance for $YBa_2Cu_3O_{7-x}$ Thin Films: Measurements and Coupled-Grain Model", *Phys. Re. B.,* v. 48, p. 6400, 1993.

[18] D. Oates, et al., "Nonlinear Surface Impedance of YBCO Thin Films: Measurements, Modeling, and Effects in Devices", *Journal of Superconductivity,* vol. 8, no. 6, pp. 725-733, 1995.

[19] S. Sridhar, Nonlinear microwave impedance of superconductors and ac response of the critical state, *Appl. Phys. Lett.,* vol. **65,** no. 8, pp. 1054-1056, 1994.

[20] A. Andreone, et al., "Nonlinear Microwave Properties of Nb_3Sn sputtered superconducting films", *Journal of Applied Physics,* vol. 82, no. 4, pp 1736-1742, 1997.

[21] J. Wosik et al., Thermally induced nonlinearities in the surface impedance of superconducting YBCO thin films, *IEEE Trans. Appl. Supercond.*, v. 7, p. 1470, 1997.

[22] A. Velichko, et al., "Non-linear Microwave Properties of High-Tc Thin Films – Topical Review", *Supercon. Sci. Technol.*, vol. 18, R24-R49, 2005.

[23] J. Booth, et al., "Measurement of the microwave nonlinear response of combined ferroelectric-superconductor transmission lines", *IEEE Trans. Appl. Superc.*, vol. 9, 3, pp. 940-943, 2009.

[24] N. Enaki and S. Colun, "Nonlinear effects in the theory of superconductivity", *J. Phys.: Conf. Ser. 338*, 2012.

[25] C. Gorter and H. Casimir, "On superconductivity I", *Physica 1*, no. 4, pp. 306-320, 1934.

[26] M. Lancaster, "Fundamental Consideration of Superconductors at Microwave Frequencies", Microwave Superconductivity edited by H. Weinstock and M.

Nisenoff, *NATO Science Series E: Applied Science, Kluwer Academic Press,* v. 375, pp. 1-20, 2001.

[27] D. Oates, "Microwave measurements of fundamental properties of superconductors", *Chapter 8 in "100 Yeas of Superconductivity", edited by H. Rogalla and P. Kes*, 2011.

[28] S. Takekawa et al., *Jpn. J. Appl. Phys*, v. 26, no.12, L2076, 1987.

[29] C. Cantoni et al., "Structural and Transport Properties of Epitaxial NdBCO Thin Films on Single Crystal and Ni Metal Substrates", *Physica C*, v. 324, p. 177, 1999.

[30] R. Semerad, et al., "RE-123 thin films for microwave applications", *Physica C*, 378-381, pp.1414-1418, 2002.

[31] B. Utz et al., "Deposition of YBCO and NBCO films on areas of 9 inches in diameter", *IEEE Trans. Appl. Supercond.*, v. 7, no. 2, pp. 1272-1277, 1997.

[32] Z. Mori et al., "In-situ annealing effect of sputter-deposited NdBCO thin films", *Thin Solid Films*, v. 354, pp. 195-200, 1999.

[33] C. Cantoni et al., "Structural and Transport Properties of Epitaxial NdBCO Thin Films on Single Crystal and Ni Metal Substrates", *Physica C*, v. 324, p. 177, 1999.

[34] J. Mazierska, "Dielectric Resonators as a Possible Standard for Characterisation of High Temperature Superconducting Films for Microwave Applications", *Journal of Superconductivity,* vol. 10**,** 2, p. 73, 1997.

[35] K. Leong and J. Mazierska, "Accurate measurements of surface resistance of HTS films using a novel transmission mode Q-factor technique", *J. Supercond.*, v. 14, pp. 93-103, 2001.

[36] Matlab software, www.mathworks.com.

CHAPTER 2.1

Superconductivity and applications of superconducting materials

The aim of this chapter is to make an introduction to the phenomenon of superconductivity and its applications. The basic concepts of microscopic electromagnetic theories, developed over the past century towards better understanding of superconductivity, are presented here. It should be mentioned that this chapter is intended to serve as an introductory background for the coming chapters and does in no way describe all aspects of superconductivity.

2.1.1 Superconductivity

The discovery of superconductivity, revealed in 1911 by H. K. Onnes [1] at the Leiden University in the Netherlands, was one of the biggest physics breakthroughs of the past century. Later in 1913, Onnes was awarded a Nobel Prize in physics for his ground-breaking investigations in the area of superconductivity. As was known for a long time, the electrical resistance of metals would decrease continuously once they are cooled down below room temperatures. Nevertheless, the resistance limiting values at the temperatures reduced towards the absolute zero were not identified at that time. Onnes, during his successful investigations in liquefying helium (see Fig. 2.1-1 for the equipment setup), was able to achieve temperatures as low as 1K. Later, he observed that instead of a smooth decrease, as for other metals, the resistance of mercury decreases sharply to zero at about 4K. Onnes recognised that below 4K mercury reached a new state where electrical properties of the material differed from anything accepted before. This new state was characterised as the *superconducting state*. The threshold temperature below which a material starts to

display superconducting properties, in other words losses resistance, has been referred to as the *critical temperature* (T_C).
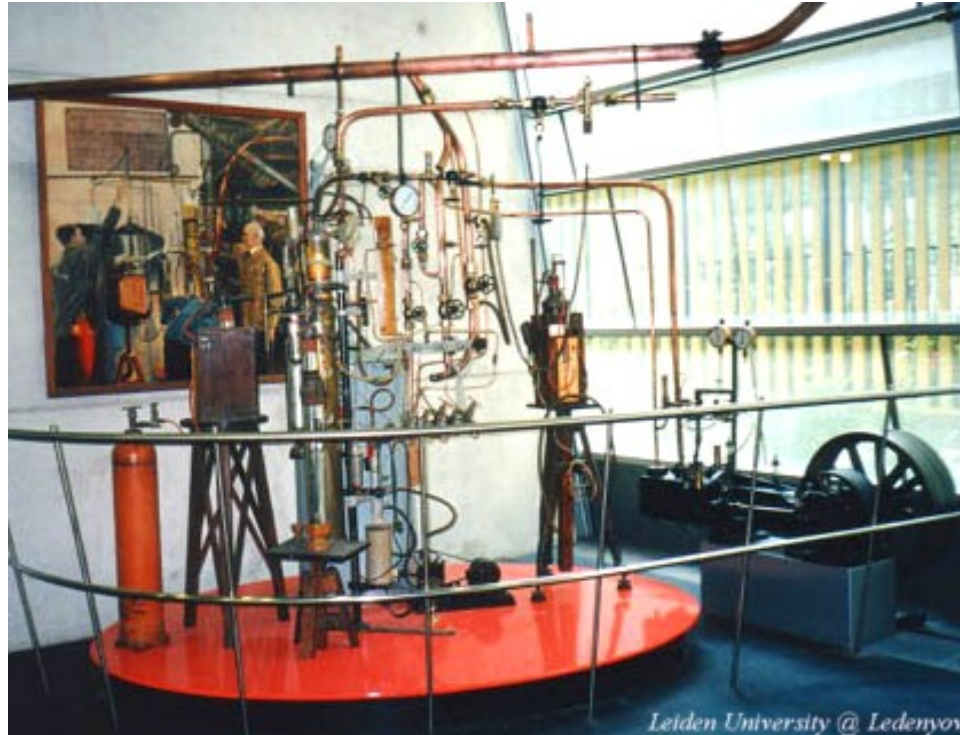
Fig. 2.1-1 Experimental equipment used by K. Onnes to discover the superconductivity phenomenon at Leiden University in 1911. (Photo *taken by the author of this thesis at Leiden University*)

Over the years, different superconducting materials have been discovered with various critical temperatures as shown in Fig. 2.1-2. Before 1986, there was a number of metallic elements and alloys exhibiting superconducting properties below 30K, with the element tungsten having the lowest critical temperature of 0.016K, and the inter-metallic compound Nb_3Ge showing the highest T_C of 23K at that time. The main challenge was to achieve the highest critical temperature possible, as the higher the T_C, the easier and cheaper the manufacturing and operation of cryogenic systems required for cooling of the superconducting materials. The breakthrough came in 1986 when Bednorz and Mueller [2], researchers at the IBM Research Laboratory in Switzerland, discovered a new class of materials – complex layered copper oxide compounds. The critical temperature of $La_{2-x}Ba_xCuO_4$ compound was 30K, that was

almost 10 degrees higher than the maximum T_C of metallic superconductors known previously. This significant increase in critical temperature prompted widespread research that quickly led to materials that are superconducting at temperatures of 90K and higher, such as $YBa_2Cu_3O_7$ (YBCO) compound with T_C of 93K discovered in 1987. These oxide materials were referred to as **High Temperature Superconductors** (HTS). The highest critical temperature T_C detected at ambient pressure for a material formed stoichiometrically (by formula) stands at 138K for the thallium doped mercuric cuprate $(Hg_{0.8}Tl_{0.2})Ba_2Ca_2Cu_3O_{8.33}$ [3]. Therefore, two classification classes of superconducting materials exist, Low Temperature Superconductors (LTS) and HTS. Also, it has to be mentioned, that the two classes of materials have different underlying mechanism responsible for the superconductivity phenomenon.
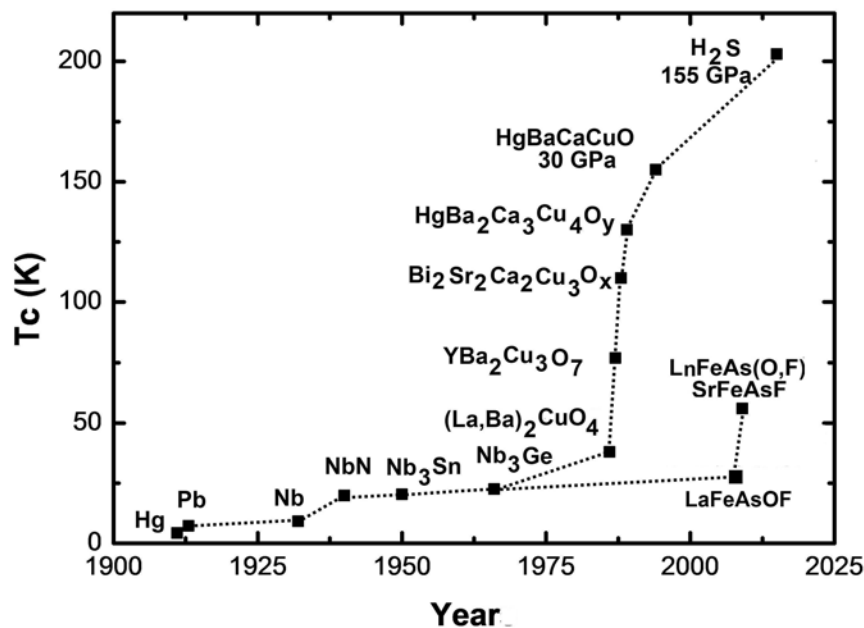
Fig. 2.1-2 Chronological progress of the critical temperature of superconductors.

Conventional low temperature superconductivity have been discovered to occur in organic and non-organic materials, while high temperature superconductors are mostly cuprates (copper oxide compounds). In 2006, the superconductivity was discovered in an iron-based compound LaFePO at 4K [4]. The iron-based superconductors were investigated further in 2008, when analogous material

$LaFeAsO_{1-x}F_x$ was found with T_C of 26K [5], and reaching 43K under pressure [6]. Subsequently, other families of the iron-based superconductors emerged with T_C up to 56K for LnFeAs(O,F) and SrFeAsF compounds [7, 8]. The Fe formed superconductors currently possess the second highest critical temperature, behind the cuprates.

Examples of high temperature superconducting coper oxide compounds are:

- $YBa_2Cu_3O_7$ (often called 'YBCO') with $T_C = 93K$;
- $NdBa_2Cu_3O_7$ (NdBCO) with $T_C = 98K$;
- $Bi_2(Sr_2Ca)Cu_2O_8$ (often called 'BSCCO') with $T_C = 110K$;
- $Tl_2Ba_2Ca_2Cu_3O_{10}$ (often called 'TBCCO') with the highest $T_C = 125K$;
- $HgBa_2Ca_2Cu_3O_8$ with the highest $T_C = 135K$;

The high temperature superconducting ceramics have a layered crystal structure consisting of CuO_2 planes with either oxygen or rare earth layers in between as shown for the $YBa_2Cu_3O_7$ compound in Fig. 2.1-3 [9].
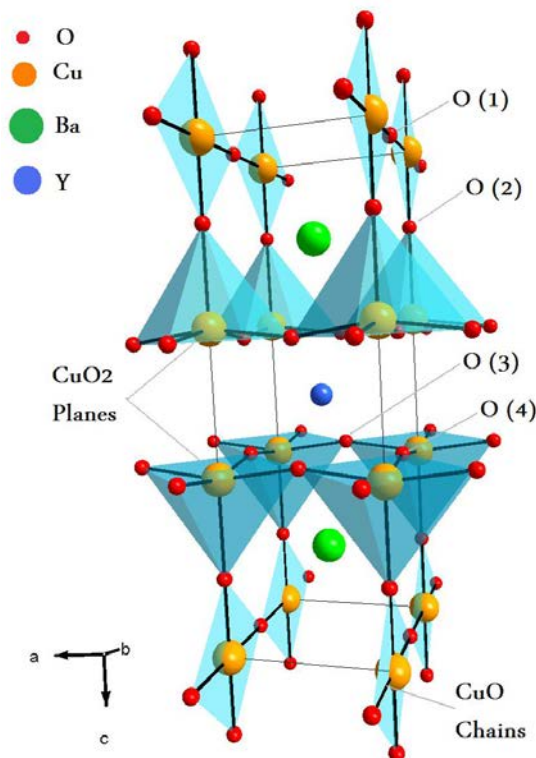
Fig. 2.1-3 YBCO crystal structure (after [9]).

It needs to be stated that the NdBCO superconductor has the same crystal structure as the YBCO compound [10]. The electrical conductivity and superconductivity are associated with the copper oxide planes, whereas the other layers stabilise the structure chemically. The more layers of CuO_2 planes (up to 3 or 4 maximum), the higher T_C.

2.1.2 Fundamental properties of High-T_C Superconductors

Superconductors possess two fundamental phenomena related to their physical properties, such as the vanishing resistance phenomenon and diamagnetic behaviour. The important concepts of critical parameters of superconductors that need to be satisfied to enable the superconductivity phenomena are discussed in this section. A principle behind the classification of superconductors known as *Type-I* and *Type-II* is also featured.

2.1.2.1   Disappearing resistance

As well known, the electrical resistivity of all metals and alloys declines once they are cooled down [11]. The nature of this effect is described at a microscopic level, the current in a conductor is carried by electrons, while the perfect periodicity of a crystal lattice is affected by impurities and thermal vibrations of the microscopic structure, thus introducing resistance to the current flow. Although achieving zero resistance is hypothetically possible with a "perfect" metallic specimen at 0K, it cannot be considered as the phenomenon of superconductivity. No metal sample can be perfectly pure and it always contains some impurities. In this context, the nature of superconductivity is very remarkable, as when superconductors are cooled down their electrical resistance decreases initially in the usual way. However, on reaching a

certain critical temperature the electrical resistance suddenly drops to zero as illustrated in Fig. 2.1-4 [12].

The fact that a superconductor has no resistance means that there is no voltage decline in the material when the current passes through it, and no power is produced. The phenomenon of "zero" resistance exists only for a DC and not for an AC current.
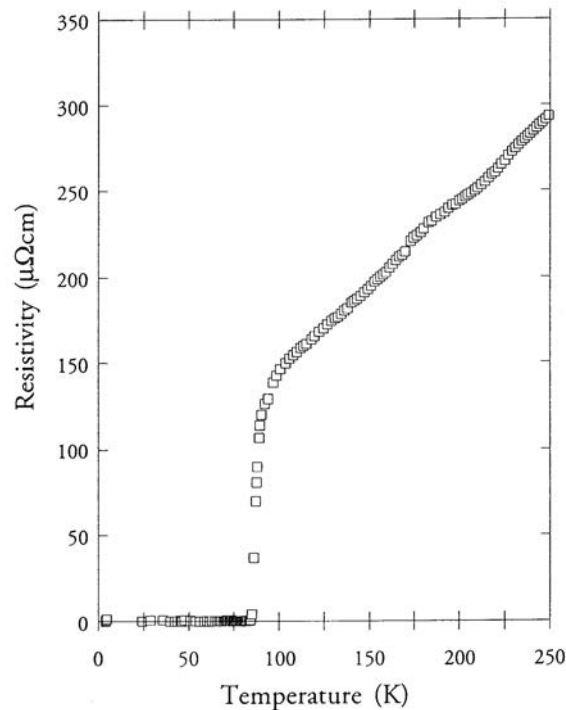
Fig. 2.1-4 Temperature dependence of DC resistivity in an YBCO superconductor (after [12]).

The AC resistance of a superconductor is not zero when the field is applied, however its value is still much lower than observed in the best conventional conductors at microwave frequencies. The phenomenon behind the AC resistivity can be easily explained by the so-called 'two fluid model' [13], considered in more details later in this chapter.

2.1.2.2   Diamagnetic behaviour - Meissner effect

As mentioned in the previous subchapter, superconducting materials do not act as perfect conductors. The resistance is zero in a perfect conductor, meaning that current within a perfect conductor flows without losing energy to resistance. Therefore, the amount of magnetic flux within the perfect conductor will not change and it will be constant with time (dB/dt=0). Thus, when a perfect conductor is cooled to a very low temperature and the magnetic field is applied after the cooling process, the field will not enter the sample due to *screening currents* induced to keep the magnetic field unchanged. However, when the magnetic field is applied to a perfect conductor before the cooling process, the magnetic flux density inside the material will be identical to the external field. The flux distribution would remain unaffected when the sample is cooled down to low temperatures in this scenario. Now, if the applied magnetic field is removed, currents will be generated within the perfect conductor in order to maintain the flux inside unchanged, Fig. 2.1-5 (a). The magnetic induction B can be described as (2.1), where μ is the permeability (for a superconductor: μ equals zero), and H is the magnetic field.

$$B = \mu H \tag{2.1}$$

In the contrary, superconductors behave in a different way when the magnetic field is applied before the cooling process ($T > T_C$). A phenomenon, called the *Meissner effect*, was discovered by Meissner and Ochsenfeld in 1933 [14], when the flux distribution of metallic superconductors was measured when cooled down to their critical temperatures with applied magnetic field. Unexpectedly, it was observed that the magnetic flux density was not allowed to exist within a superconductor, thus exhibiting *perfect diamagnetism*, Fig. 2.1-5 (b).
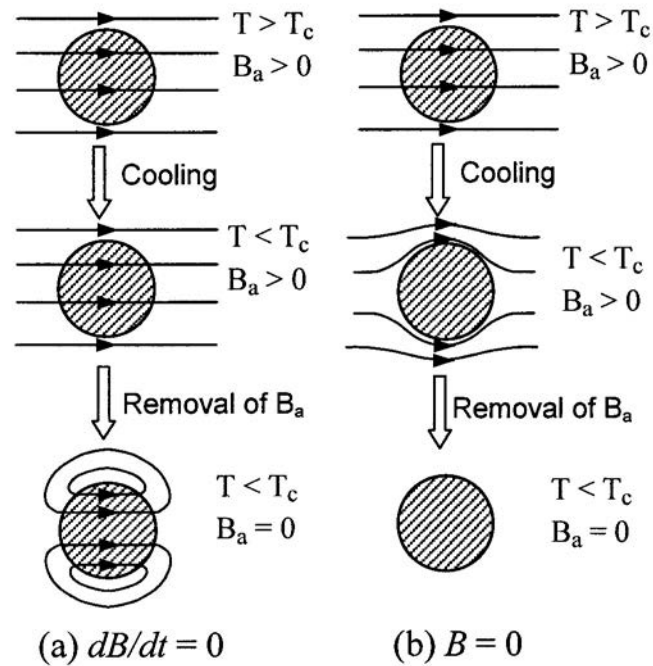
Fig. 2.1-5 Magnetic behaviour of: (a) "perfect" conductor,
and (b) superconductor. B_a – *applied* magnetic induction. (after [14])

On the other hand, it should be mentioned that currents, which circulate to cancel the applied magnetic flux inside a superconducting sample, are not restricted entirely to the surface. Therefore, the applied magnetic field is not completely screened out from the superconductor. In fact, the field penetrates a small distance into the material (around 10^{-5}cm [13]), and transport currents flow within this very thin surface layer. The magnetic flux density decays exponentially as it penetrates into the metal. The depth where the field drops exponentially of the field at the surface is defined as the *penetration depth (λ)* [13, 15], described in more details later in this chapter.

2.1.2.3   Critical parameters of superconductors

Superconducting materials are characterised by certain critical parameters, such as: *critical temperature* T_C (introduced earlier in this chapter), *critical magnetic field* H_C, and *critical current density* J_C. The material loses its superconducting properties when any of the above critical parameter values are exceeded. The critical parameters are interconnected between each other as illustrated in Fig 2.1-6, where the transition boundary between the superconducting and normal states is shown.
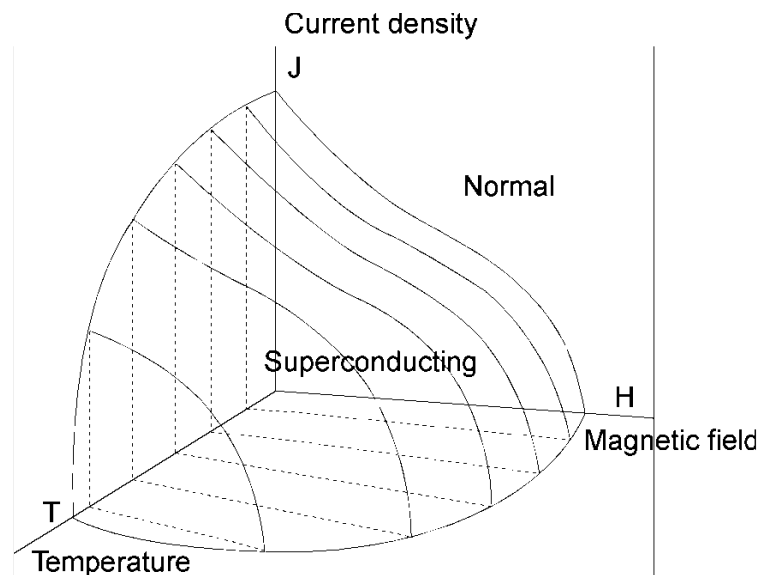
Fig. 2.1-6 Interdependence of critical parameters of a superconductor (after [16]).

The critical field above which the superconducting state disappears is dependent on the temperature, as shown in (2.2). Typically, the critical magnetic field shows a zero value at the critical temperature, reaching its maximum at the absolute zero temperature [16].

$$H_C(T) = H_C(0)(1 - (^T/_{T_C})^2) \tag{2.2}$$

When the value of the applied magnetic field is increased, the screening currents must also increase, and when the critical current density is reached by the screening currents

the material loses its superconductivity. This destruction of superconductivity by a sufficiently strong magnetic field is one of the most important properties of a superconductor.

In addition to T_C and H_C, the third important parameter, as mentioned above, is the maximum *current density* J_C, that a superconducting material can uphold without resistance. The current density is temperature dependent, as expressed in eq. (2.3) [17], it increases as the temperature is decreased below the critical temperature [17].

$$J_C(T) = J_C(0)(T_C - T)/T_C \qquad (2.3)$$

The correlation between the *critical current* I_C and the critical magnetic field H_C was formulated by Silsbee, where he postulates that "The threshold value of the current is that at which the magnetic field due to the current itself is equal to the critical magnetic field" [18].

$$I_C = 2\pi a H_C \qquad (2.4)$$

where *a* is the radius of the conductor.

It needs to be mentioned that the *critical current* I_C depends on the size of the conductor, thus not forming an intrinsic property of the material. I_C gets bigger as the diameter of the superconductor is increased, while the *critical current density* J_C behaves differently, declining as the diameter is increased.

$$J_C = 2H_C/a \qquad (2.5)$$

This phenomenology characterises the so-called *Type-I* superconductors. This class of materials has a single critical field H_C, ranging from 10^{-2} to 10^{-1} Tesla at temperature of 0K [19]. The Type-I superconductor loses its zero resistance, when, at any point on its surface, the magnitude of strength of total magnetic field $H = H_I + H_e$, which is generated by the transport current and by the external magnetic field, reaches the critical field strength H_C. All superconducting metals, excluding Niobium (Nb), are characterised as *Type-I* superconductors.

Another class of superconductors is the *Type-II*, where additional phenomena are observed. Apart from the normal and superconducting states associated with *Type-I* materials, the *Type II* superconductors can be in a *mixed state*, where the magnetic flux partially enters the superconductor and the Meissner effect does no longer exist. They are also unique in possessing two critical magnetic fields, a lower field H_{C1} (2.6) and an upper field H_{C2} (2.7) [20].

$$H_{C1} \approx (H_C \cdot \ln k)/k \cdot \sqrt{2} \tag{2.6}$$

$$H_{C2} = H_C \cdot k \sqrt{2} \tag{2.7}$$

Below the lower critical field H_{C1} the superconductor is in a diamagnetic state with a very small concentration of normal electrons, however when the external magnetic field surpasses the threshold value of H_{C1}, the superconductor transforms into a mixed phase. This phase holds a large number of quantum magnetic vortices, where each vortex has the normal metal core with radius around the size of the *coherence length* ξ (defined below) and trapped *magnetic flux quantum* $\phi_0 = 2,0679 \times 10^{-15}$ Wb [21]. A unique condition occurs in the mixed state, where substantial parts of the superconductor are in the normal state, however superconducting currents can still flow via the material [15]. When the external magnetic field exceeds the higher critical field H_{C2}, the superconducting effect entirely vanishes. It needs to be mentioned, that this manuscript deals nearly completely with *Type-II* superconductors, and *Type-I* superconductors are included here for comprehensiveness only.

Before further considerations, certain important parameters need to be briefly defined here, with their more detailed examination followed in this or later chapters. These parameters are:

- *Penetration depth*, λ. This characteristic length is a measure of the depth of flux penetration into a superconductor. The currents which prevent flux penetration into the interior of the material flow in a layer of this thickness λ.

- *Coherence length, ξ.* This length describes the dimensional correlation of superconducting electrons. It can also be characterised as the minimum thickness of the surface between normal and superconducting regions [14]. In impure materials, ξ value is also influenced by the electron mean free path. Typical values are around 5nm for Type-II superconductors and significantly bigger for *Type-I* (Al ~ 1600nm, Pb ~ 83nm).

- *Ginzburg-Landau parameter*, k. This is the dimensionless ratio of the two parameters introduced above: $k = \lambda/\xi$. This parameter is used to distinguish between *Type-I* and *Type-II* superconductors; those with a value $< 1/\sqrt{2}$ are *Type-I*.

The penetration depth λ is smaller for the *Type-I* superconductor than the coherence length ξ, while for the *Type-II* materials the penetration depth has bigger values than the coherence length ($\xi < \lambda$).

The mentioned earlier two critical fields in the *Type-II* superconductors have distinct temperature dependences as shown in Fig. 2.1-7. The upper critical field H_{C2} are usually much higher than the critical field H_C of the *Type-I* superconductors. The *Type-II* material can have the H_{C1} values above 10 Tesla while the *Type-I* H_C is below 0.2 Tesla. Therefore, the *Type-II* superconductors have found applications requiring strong magnets such as in particle accelerators for creation of very strong magnetic fields.
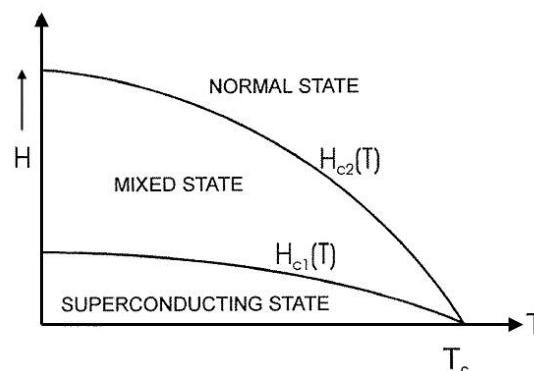
Fig. 2.1-7 Critical magnetic fields of *Type-II* superconductors (after [19]).

The *Type-II* superconductors are very sensitive to impurities in terms of their current carrying capabilities. As known, point-like impurities can be the reason for *Type-II* materials having small critical current values [14], meaning that the superconductivity phenomena may be present in such materials, but the ability to conduct the superconducting current is suppressed. However, on the other hand, big critical currents can be observed in the materials with large inhomogeneities with effective dimension of d≥ξ [21], where d is a diameter of a superconductor.

To make this review complete another critical parameter needs to be defined. A frequency at which the photons of electromagnetic waves energise superconducting electrons to force them to the normal state is defined as a *critical frequency, f_C*. The values of the frequency forcing a material to lose its superconducting properties lie within the range of 100GHz [19]. On the other hand, superconducting electronic applications are generally concentrated well below 100GHz, meaning that the critical frequency parameter would not be important for practical applications of superconductors.

In the following sections the main theories of the superconductivity at zero magnetic field and in the mixed state are briefly described.

2.1.3 Theories toward understanding of superconductivity

The discovery of the Meissner effect, described earlier in this chapter, was fundamental for the development of phenomenological theories of superconductivity. Two of such theories were developed right after the discovery of the Meissner effect, they were the 'Two-fluid' model theory of the Gorter and Casimir [22] in 1934 and the London theory proposed in 1935 [23]. Other important theoretical work, developed later, is also presented in the following sections.

2.1.3.1   Two-fluid model

Gorter and Kasimir in their theory [22] postulate the existence of two currents in superconductors: a normal current with a carrier density n_n, and a superconducting current with a carrier density n_S, yielding a total carrier density $n = n_n + n_S$. The normal electrons experience resistance due to interactions with the crystal lattice or the collisions with other electrons, just like the conduction electrons in a normal metal. However, the superconducting electrons pass through the superconductor without any resistance. It should be noted, that in a special case of the direct current (DC), all current in a superconductor is carried entirely by the superconducting electrons (superelectrons).

Densities of the normal and superconducting electrons in a superconductor are temperature dependant. At zero temperature, all electrons act as superconducting electrons, however, when the temperature is increased, some electrons transform to normal electron behaviour. Additionally, the percentage of the normal electrons increases when the temperature is raised further. As a result, when the critical temperature of the material is reached, all the electrons turn to normal and superconducting properties disappear. At temperatures below T_C, the equilibrium portions of normal and superconducting electrons n_n/n and n_s/n, change with absolute temperature T, as [20]

$$\frac{n_n}{n} = \left(\frac{T}{T_C}\right)^4 \; , \; \frac{n_S}{n} = 1 - \left(\frac{T}{T_C}\right)^4 \tag{2.8}$$

Certain material properties of superconductors such as the current density and the conductivity can be determined using the Two-Fluid model due to its simplicity in terms of the practical understanding. The total current density J in a superconductor based on the Two-Fluid approximation is given as the sum of the superconducting and normal currents [15], resulting in a complex conductivity.

$$\vec{J} = \vec{J_n} + \vec{J_s} = (\sigma_1 - i\sigma_2)\vec{E} \tag{2.9}$$

where σ_1 and σ_2 are the real and imaginary parts of the complex conductivity respectively, given by:

$$\sigma_1 = \frac{n_n e^2 \tau}{m(1+\omega^2\tau^2)} \quad \text{and} \quad \sigma_2 = \frac{n_S e^2}{m\omega} + \frac{n_n e^2 (\omega\tau)^2}{m\omega(1+\omega^2\tau^2)} \quad (2.10)$$

where e is a fundamental unit of charge; n_n and n_s are the densities of normal and superconducting electrons respectively; m is the mass of an electron; ω is the radian frequency; and τ is the momentum relaxation time.

The real part σ_1 of the complex conductivity in (2.10) describes only the normal state, while the imaginary part σ_2 includes contributions from both normal and superconducting states.

The Two-Fluid model can be represented by an equivalent circuit model consisting of two elements connected in parallel: a normal conductor with fixed inductance and resistance, and a perfect conductor with zero resistance that is represented only by an inductance [24] as discussed in more details in chapter 3. The Two-Fluid model is a standard working approximation for understanding electrical losses in superconductors, so that dissipation can be anticipated and minimised for various types of applications. It also needs to be mentioned that the Two-Fluid model approximation has been used by the author of this thesis for the development of the lumped element modelling of microwave properties of superconductors, described in details in chapter 4.

2.1.3.2   London theory of electrodynamics

The phenomenological theory created by brothers H. and F. London characterises the dimensional distribution of currents and fields within a superconductor [23], focusing on the influence of magnetic fields on the material properties. The Londons postulated that the magnetic flux was not completely expelled from a superconductor, but it penetrated the surface of the material on the

penetration depth λ, declining exponentially. The electrodynamics of conventional superconductors in weak fields can be formulated by the renowned London equations [19]:

$$\frac{\partial}{\partial t}\vec{J_S} = \frac{\vec{E}}{\mu_0\lambda_L^2}$$

$$\mathrm{curl}\,\vec{J_S} = -\frac{1}{\mu_0\lambda_L^2}\vec{B}$$

(2.11)

where B and E are the magnetic field density and electric field intensity respectively inside the material, J_S is the superconducting current density, and λ_L is the London penetration depth, defined as:

$$\lambda_L = \sqrt{\frac{m_S}{\mu_0 n_S e^2}}$$

(2.12)

where m_S is the mass of superconducting charge carrier.

The first London equation (2.11 - top formula) describes the no-resistance property of a superconductor showing a change in the superconducting current produced by the applied electric field, or that there is no electric field in the metal unless the current is changing. The second London equation (2.11 – bottom formula) shows the relation between the magnetic field and the superconducting current. It determines how the magnetic field penetrates in the superconductor in the Meissner state. The magnetic flux density B can be obtained as a function of distance x inside the superconductor, eqn. (2.13), when the magnetic field is applied parallel to the surface, eqn. (2.13), illustrating that the flux density B decays exponentially inside a superconductor as depicted in Fig. 2.1-8.

$$B(x) = B_a exp\left(\frac{-x}{\sqrt{\alpha}}\right)$$

(2.13)

where B_a is the magnetic flux density at the surface of the superconductor, and the constant $\alpha=\lambda_L{}^2=m/\mu_0 n_s e^2$.
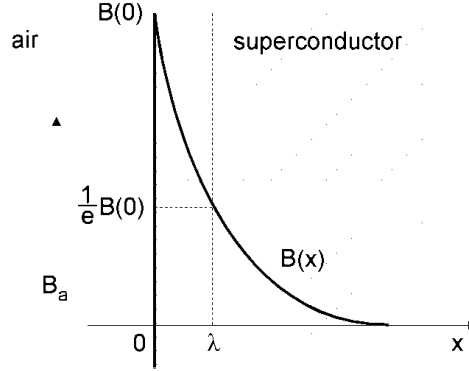
Fig. 2.1-8 Penetration of the magnetic field into a superconductor (after [19]).

2.1.3.3   Ginsburg-Landau (GL) theory

Ginsburg and Landau, in 1950 in Moscow, announced their remarkable phenomenological theory [26] that integrated the electrodynamics, quantum mechanical and thermodynamic properties of superconductors. They attributed an order parameter Ψ to the superconductor, with certain qualities of a quantum-mechanical wave function. The density of superconducting electrons n_S equals $|\Psi|^2$. The wave function Ψ is defined as zero for a normal metal region and characterises the density of superconducting electrons at various points in a superconductor. As mentioned, it has a quantum mechanical nature but no classical analogue.

The two prominent equations developed from the GL theory are given as [14]:

$$\left\{ \frac{1}{4m}[\nabla - 2ie\mathbf{A}]^2 - \beta^{-1}\left[\frac{T_c - T}{T_c} - \frac{1}{n}|\psi|^2 \right] \right\}\psi = 0 \tag{2.14}$$

$$\mathbf{J} = \frac{-ie}{2m}[\psi^*\nabla\psi - \psi\nabla\psi^*] - \frac{2e}{m}\mathbf{A}|\psi|^2 \tag{2.15}$$

where $\mathbf{A}$ is the magnetic vector potential, $\mathbf{J}$ is the superconducting current density; m and e are the mass and charge of a superconducting electron; $\beta=[7\zeta(3)/6(\pi T_c)^2]E_F$, where E_F is the Fermi energy. The first Ginsburg-Landau (GL) equation, (2.14), establishes interrelation of the kinetic energy of the superconducting electrons with the energy of their condensation in a superconducting state. The second equation, (2.15), describes

quantum interrelation of the superconducting current with a gradient of the wave function $\nabla\Psi$ and the vector-potential **A**. The result of the theory is a generalisation of the London theory for situations in which the superconducting electron volume density n_S varies in space. It also deals with nonlinear responses to the fields and currents strong enough to change n_S.

Ginsburg and Landau introduced the parameter κ, mentioned earlier in this Chapter. Their results indicated that, if κ has a value bigger than $1/\sqrt{2}$, then superconductivity can be sustained up to fields of $H=(\kappa/\sqrt{2})H_C$.

Also, at the beginning of 1950s, Pipard, at Cambridge, was investigating microwave surface resistance in superconductors and metals. He observed that in impure metals the electron properties were not influenced by the electric and magnetic fields, but by the electron mean free path l. An electron passing from a normal to a superconducting region cannot suddenly modify its wave function Ψ – the transformation should occur over certain set distance. This distance, as stated before in this Chapter, is referred to as *coherence length* ξ_0 [26]. Pipard predicted that for pure metals, $\xi_0 \approx 1\mu$m. The Pipard theory presented variations to the penetration depth. For a pure superconductor, where $l >> \xi_0$, the penetration depth is specified as:

$$\lambda_\infty = [\left(\frac{\sqrt{3}}{2\pi}\right)\xi_0\lambda_L^2]^{1/3} \tag{2.16}$$

where λ_L is the penetration depth, eqn. (2.12).
For alloys, where $l << \xi_0$, the theory gives a novel (bigger) value, for the penetration depth:

$$\lambda = \lambda_L(\frac{\xi_0}{l})^{1/2} \tag{2.17}$$

and also, much smaller value for coherence length,

$$\xi_{alloy} = (\xi_0 l)^{1/2} \tag{2.18}$$

The GL theory also introduced a characteristic temperature dependent length, usually called the (GL) *coherence length* ξ_{GL} [19]:

$$\xi_{GL}(T) = \frac{\hbar}{|2m^*\alpha(T)|^{1/2}}$$ (2.19)

where, m^* is the mass of superconducting electrons and $\hbar$ is the reduced Plank's constant.

In a pure superconductor for temperatures much below T_C, $\xi_{GL}(T) \approx \xi_0$. Near T_C, however, the GL coherence length follows the following rule: $\xi_{GL}(T) \propto (T_C - T)^{-1/2}$. Therefore, these two coherence lengths ξ_{GL} and ξ_0 are related, but have distinct quantities.

The Ginsburg-Landau κ can be approximately defined as:

$$\kappa = \frac{\lambda(T)}{\xi_{GL}(T)}$$ (2.20)

Near T_C, λ and ξ behave as $\sim (T_C - T)^{-1/2}$, and κ is approximately independent of temperature. For alloy superconductors with l very small, k can be quite large, around 25 for niobium based alloys, and larger 100 for oxide HTS.

The GL theory have an advantage over the London theory that it can be implemented to research the performance of superconductors at high magnetic fields and at temperatures near the critical temperature, where the London theory is not applicable. The GL theory can also be practical for estimating values of critical fields in very thick or very thin films.

The Bardeen-Cooper-Schrieffer (BCS) microscopic theory of superconductivity was formulated next, introduced in detail in the following section.

2.1.3.4   BCS theory of superconductivity

In 1957, J. Bardeen, L. Cooper and J. Schrieffer published the microscopic theory of superconductivity, known as the BCS theory [27]. This awarded theory, recognised with the Nobel Prize in Physics in 1972, is widely accepted to describe conventional (low temperature) superconductors. It viewed superconductivity as a microscopic quantum mechanical effect, proposing that two electrons with opposite momentums $\mathbf{p_1} = - \mathbf{p_2}$ and opposite spins $s_1(\uparrow) = - s_2(\downarrow)$ can become paired forming the so-called *Cooper pairs,* charge carriers in superconductors that carry current without resistance. Cooper in 1956 presented the basic idea that even a weak attraction can force pairs of electrons into a formed state [28].

In many superconductors, the interaction between the electrons and the phonons (crystal lattice) indirectly form attractive connections between electrons, required to create Cooper pairs. When an electron travels in a conductor, a minor surge of positive charge densities is generated in the lattice around it. This increase in densities can attract another electron, and grip two together with some binding energy. All Cooper pairs behave as a cluster with a single momentum and the coherent wave function in the area near the Fermi surface with the thickness $\delta\mathbf{p} \sim 2\Delta \cdot p_F/\varepsilon_F$.

Due to the electrical resistance originating from the carrier scattering effect, the single momentum shared by all carriers in the superconducting state explains the zero-resistance property. The bound energy of a Cooper pair is called the *energy gap* $\Delta(T)$, which is a function of temperature [29]. At T=0K energy gap has the maximum value:

$$\Delta(0) = 2\hbar\omega_D \cdot \exp[-1/N(0)V] \qquad (2.21)$$

where ω_D is the high limiting frequency of crystal lattice oscillations, $N(0)$ is the density of the electrons states on Fermi surface, V is potential of the electron-phonon interaction.

It needs to be mentioned that these presented hypothesises such us energy gaps, phonons and electron pairs had been proposed before in superconductivity, however Bardeen, Cooper, and Schrieffer combined them all together for the first time, creating a unified theoretical framework. The energy gap has the critical temperature dependence as shown in eq. (2.22):

$$2\Delta \approx 3.5 k_B T_C \tag{2.22}$$

At the critical temperature T_C, the energy gap disappears causing the Cooper pair to break. This explains the transition from the superconducting state to the normal state at T_C. The BCS theory explains the low T_C metal and alloy superconductor behaviour very well and has been verified by many experiments [30].

The surface resistance of superconductors in BCS theory can be expressed as [31]:

$$R_S \approx (\Delta(T)/k_B T) \, \omega^{3/2} \exp(-\Delta(T)/k_B T) \tag{2.23}$$

This expression is important for the current manuscript, and it will be examined in more details in the following Chapters.

In 1957, Abrikosov developed the theory of magnetic properties of *Type-II* superconductors [32], on the basis of GL theory, mentioned earlier in this Chapter, for the case when $\kappa > 1/\sqrt{2}$. Abrikosov's mathematical solution presented that above the critical magnetic field H_{C1}, flux vortices are formed each having a normal core with a radius ξ, and superconducting currents circulating over a radius λ. With the increase of the applied magnetic field, a number of vortices grow until the normal cores overlap at the upper critical field $H_{C2} = \sqrt{2}\kappa H_{C0} = \Phi_0/2\pi\mu_0\xi^2$.

Later in 1959, Gor'kov showed [33] that the GL theory is a direct consequence of the microscopic BCS theory, deriving coefficients in the GL theory from the BCS. This trilogy of theoretical work by Russian scientists is known as GLAG (Ginsburg-Landau-Abrikosov-Gorkov) theory. For any superconductor, when the normal state

mean free path of the electrons l is decreased, ξ increases, λ becomes bigger, and κ rises. When alloys are added, when l is reduced, κ grows.

In summary, the mathematically-complex microscopic BCS theory explained superconductivity on the basis of electron-phonon interactions. However, for High Temperature Superconductors (HTS), the BCS theory became inadequate to comprehensively explain mechanisms behind superconductivity. Even now, three decades since the discovery of HTS, no agreed theory exists to explain high temperature superconductivity. However, it needs to be stated that the above listed theories provide valuable concepts of superconducting current existence, and understanding of the main properties of superconductors.

2.1.4   Applications of superconductors

The discovery of superconductivity more than a century ago looked very promising in terms of practical applications in several areas. However, the further understanding of material properties of superconductors brought a realisation that their critical parameters in forms of temperature, current, and magnetic field were one of the main obstacles towards the application progress. Also, refrigeration systems posed a substantial cost-effective obstacle for commercial applications of superconductors due to the need for costly liquid helium (4.2K) for the refrigeration purposes. As a consequence, everyday applications of superconductivity were limited and mostly confined to specialised laboratory devices.

It has to be mentioned that the first actual applications of superconductors were developed in the 1960's, such as extremely sensitive magnetometers, RF cavities with high quality factors, and electromagnets designed for high-field operations. The main role in the development also played the fact of discoveries of both NbTi, making superconducting wire feasible, and the Josephson junctions, applicable in the SQUID

devices. Electromagnets for MRI systems are possibly the biggest use of superconductivity up to date.

The discovery of High Temperature Superconductors (HTS) in 1986 with critical temperatures above 90K sparked excitement around the world and restored enthusiasm towards various superconductor applications. The temperature of 90K can be achieved with liquid nitrogen at a fraction of the costs than the functional temperatures of conventional superconducting materials. Also, the important factor is that modern cryogenic refrigerators can deliver refrigeration to HTS materials on an uninterrupted basis with high reliability, making HTS technology applicable for use in RF applications.

Since the discovery of High Temperature Superconductors, certain progress have been achieved on many technological frontiers, enabling successful commercial applications of superconductors. In the following sections, various applications of superconducting materials are summarised with a special attention to those directly related to the scope of this thesis, i.e. wireless communication technologies [34, 35].

2.1.4.1   Review of applications of HTS materials

High-temperature superconductors can be manufactured in various forms such as wires, tapes, ribbons, and films. Superconducting wires are generally used in low-power magnets, antennas, power transmission lines, medium torque motors, and compact electrical generators. Superconducting tapes are most useful where large lengths of material are required and must meet strict weight and size requirements. Ribbons are most suitable for space-borne and airborne superconducting devices, where implementation of monolithic microwave integrated circuit (MMIC) technology is highly desirable. Thin films are most suitable for passive RF and microwave devices, optical detectors, and microelectronic circuits, due to their low loss properties and desirable size reductions. Superconducting thick films are widely

used in high-power microwave cavities, high-power lifting magnets, and propulsion systems. Some general applications of High-T$_C$ superconductors are summarised in Fig. 2.1-9 [36].

Superconducting films can be used in manufacturing advanced HTS filters for wireless communications exhibiting superior features than conventional filters. As this topic is in particular interest to this thesis, it is discussed in more details in the following sub-chapter.
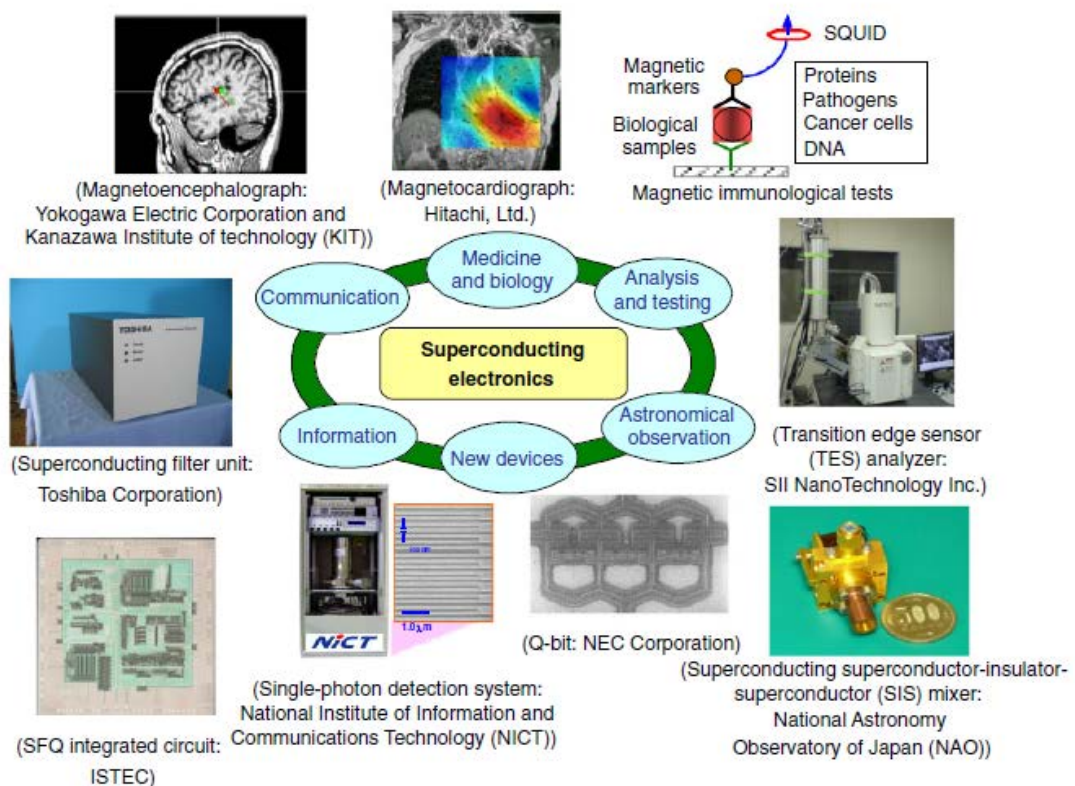
Fig. 2.1-9 Possible applications of high temperature superconductors (after [36]).

2.1.4.2   HTS filters for wireless communications

Practical   realisation   of   microwave   components   using   High-T$_C$ superconductors has mostly focused on the use of microstrip designs implementing thin film technology [37]. Advanced microwave properties of superconductors, such

as low losses of HTS films deliver outstanding RF performance, also considerably reducing size of microwave components. Microwave superconducting resonators with very high quality factors enable filters with small insertion losses, even in the case when bandwidth is extraordinary narrow. When these superconducting filters are integrated into mobile networks, they continuously deliver supreme frequency selectivity and extreme sensitivity of the receiver, unlike conventional filters. A comparison between a superconducting and a conventional cellular base station filters based on field data of Conductus [38] is given in Fig. 2.1-10.
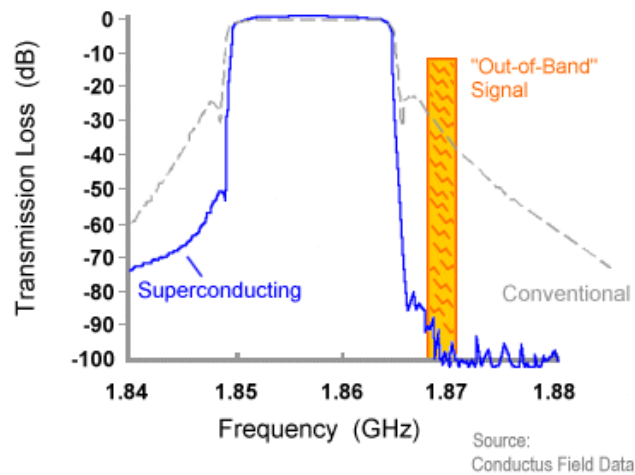
Fig. 2.1-10 Measured characteristics of a conventional and HTS cellular filters [38].

As can be observed, HTS filters are very affective at eliminating out-of-band signals, especially the ones adjacent to the wanted frequency band. The unique properties of superconducting filters enable the production of devices with either extraordinary steep skirts, or exceptionally narrow bandwidth. In either case, very low insertion losses are still reachable for such filters. The importance of manufacturing extremely sharp skirted filters is emphasised in their ability to keep reasonably wideband range, significant for commercial wireless bands. On the other hand, the capability of producing very narrowband filters is crucial for receiving weak signals in crowded RF environment.

HTS filters have certain technical advantages that result in reduced band interference, improved spectrum utilisation, and better coverage. These advantages are [35, 39, 40]:

- Lower insertion loss;
- Smaller out-of-band interference;
- Lower noise;
- Sharper skirt;

Therefore, practical benefits of using HTS technology in wireless communication can lead to increased data traffic, better coverage with fewer cells, improved audio quality, and smaller number of dropout calls. The current mobile environment along with emerging wireless applications set rigorous requirements on the overall technical network performance. Therefore, HTS high-performance components may be necessary for some systems in order to achieve the full band utilisation, high quality of service, and high data rate transmission over the network.

However, microwave properties of superconducting materials, especially at elevated power levels, can set certain limitations to superior microwave characteristics of superconductors. In the next chapter, the microwave properties of superconductors are investigated and discussed.

REFERENCES

[1]. K. Onnes, *Leiden Comm.*, 120b, 122b, 124c, 1911.

[2]. J. Bednorz K. Muller, "Possible high T_c superconductivity in the Ba-La-Cu-O system" *Z. Phys.*, B64, p. 189, 1986.

[3]. Website reference: www.superconductors.org, 2017.

[4]. Y. Kamihara, et al., "Iron-Based Layered Superconductor: LaOFeP", *Journal of the American Chemical Society*, vol. 128 (31), pp. 10012–10013, 2006.

[5]. Y. Kamihara, et al., "Iron-Based Layered Superconductor La[$O_{1-x}F_x$]FeAs (x=0.05–0.12) with T_c =26 K", *Journal of the American Chemical Society,* vol. 130 (11), pp. 3296–3297, 2008.

[6]. H. Takahashi, et al., "Superconductivity at 43 K in an iron-based layered compound LaO1-$_x$F$_x$FeAs", *Nature,* vol. 453 (7193), pp. 376–378, 2008.

[7]. R. Zhi-An, et al., "Superconductivity and phase diagram in iron-based arsenic-oxides ReFeAsO1−δ (Re=rare-earth metal) without fluorine doping", *EPL,* vol. 83, 17002, 2008.

[8]. G. Wu, et al., "Superconductivity at 56 K in Samarium-doped SrFeAsF", *Journal of Physics: Condensed Matter*, vol. 21 (3), 142203, 2009.

[9]. Z. Xiong and Y. Zhu, "Microstructures and structural defects in high-temperature superconductors", *World Scientific*, 1998.

[10]. G. Dhanaraj, et al., "Handbook of Crystal Growth", *Springler*, 2010.

[11]. R. Serway and J. Jewett, "Principles of Physics", *2nd ed. Saunders College Pub*,1997.

[12]. M. Wu, et al., "Superconductivity at 93K in a new mixed-phase Y-Ba-Cu-O compound system at ambient pressure", *Phys Rev Lett.,* vol. 58, p. 908, 1987.

[13]. A. Rose-Innes and E. Rhoderick, "Introduction to Superconductivity", 2nd Edition, *Pergamon Press,* 1994.

[14]. W. Meissner and R. Ochenfeld, *Naturwissenschaften*, v. 21, p. 787, 1933.

[15]. M. Tinkham, "Introduction to Superconductivity" 2nd Edition*, McGraw-Hill*, 1996.

[16]. I. Firth, "Superconductivity", *Mills & Boon Ltd*, 1972.

[17]. K. Onnes, ibid. 133b, 29, 1913.

[18]. F. Silsbee*, Journal of the Washington Academy of Sciences*, vol. 6, 79, 1916.

[19]. A. Rose-Innes and E. Rhoderick, "Introduction to Superconductivity, 2nd Edition, *Pergamon Press*, 1994.

[20]. C. Kittel, "Introduction to Solid State Physics", *Wiley*, revised edition, 2004.

[21]. T. Van Duzer and C. Turner, "Principles of Superconductive Devices and Circuits", 2nd Edition, *Prentice Hall,* 1999.

[22]. C. Gorter and H. Casimir, "On superconductivity I", *Physica 1*, no. 4, pp. 306-320, 1934.

[23]. F. London and H. London, "The electromagnetic equations of the superconductor", *Proc Roy Soc A*, vol. 149, no. 866, pp. 71-88, 1935.

[24]. W. Lyons and R. Withers, "Passive microwave device applications of high T_c superconducting thin films", *Microwave Journal*, Nov, 1990.

[25]. V. Ginzburg and L. Landau, "To the theory of superconductivity", *Zh. Eksperim. I Teor. Fiz.*, vol. 20, p. 1064, 1950.

[26]. A. Pippard, "The coherence concept in superconductivity", *Physica*, vol. 19, no. 9, pp. 765-774, 1953; "An experimental and theoretical study of the relation between magnetic field and current in a superconductor", *Proc Roy Soc A*, vol. 216, no. 1126, pp. 547-568, 1953.

[27]. J. Bardeen, et.al., "Theory of Superconductivity", *Phys. Rev.,* vol. 108, p. 1175, 1957.

[28]. L. Cooper, "Bound electron pairs in a degenerate Fermi gas", *Phys. Rev.*, vol. 104, pp. 1189-1190, 1956.

[29]. G. Rickayzen, "Theory of Superconductivity" *New York: Willey*, 1965.

[30]. E. Lynton, "Superconductivity" *Mathuen and Co. Ltd*, 1969.

[31]. J. Halbritter, "On the surface resistance of superconductors", Z Physik, vol. 226, pp. 209-217, 1974.

[32]. A. Abrikosov, *J. Experim. Theoret. Phys.*, vol. 32, p. 1442, 1957 (translation: Soviet Phys. – JETP 5, p. 1174, 1957)

[33]. L. Gor'kov, *Zh. Eksperim. I Teor. Fiz.*, vol. 36, 1959. (Sov. Phys. –JEPT, vol. 9, p. 1364, 1959)

[34]. A. Velichko, et al., "Non-linear Microwave Properties of High-Tc Thin Films - TOPICAL REVIEW", *Supercon Sci Technol,* vol. 18, R24-R49, 2005.

[35]. J. Mazierska and M. Jacob, "High Temperature Superconducting Filters for Wireless Communication", Novel Technologies for Microwave and Millimeter-wave Applications, edited by Jean-Fu Kiang, *Kluwer Academic/Plenum Publishers,* pp. 123-152, 2003.

[36]. K. Kitazawa, "Superconductivity: 100th Anniversary of Its Discovery and Its Future", *Japanese Journal of Applied Physics*, vol. 51, pp. 1-14, 2012.

[37]. T. Dahm and D. Scalapino, "Theory of intermodulation in a superconducting microstrip resonator", *J Appl Phys,* vol. 81**,** pp. 2002-2009, 1997.

[38]. www.conductus.com, (accessed Nov 2017).

[39]. A. Knack, "Thesis: Design and Implementation of HTS Technology for Cellular Base Stations: An Investigation into Improving Cellular Communication", *JCU Townsville*, 2006.

[40]. A. Saito A, et al., "Resonator Structures and Power-Handling Capability for Superconducting Transmit Band-Pass Filters", *HF-P08 International Superconductive Electronics Conference,* 2009.

CHAPTER 2.2

Microwave properties of superconducting materials

As mentioned earlier in Chapter 1, investigating microwave properties of superconductors is important in terms of applied superconductivity, development of advanced applications of superconducting materials, as well development of scientific concepts and theories associated with high temperature superconductivity. Limited power handling capabilities of high temperature superconductors (HTS) have narrowed the number of applications of HTS microwave devices. For microwave HTS filter applications, it is necessary for the HTS filter to be able to operate with relatively high levels of microwave power propagating through it. However, it is known that undesirable behaviour can occur at elevated power levels. HTS filter performance can be significantly degraded when internal microwave power reaches certain high levels. Other HTS microwave devices can also exhibit significant degradation in performance when operating at desired power levels. While the negative impact of high microwave power on HTS devices is well documented, there is still no physical theory that explains the link between microwave properties and the onset of performance degradation for a given microwave power level.

2.2.1 Theoretical background

To characterise the electromagnetic properties of either a superconductor or a normal conductor the surface impedance (Z_S) is used. Z_S describes the behaviour of microwave electromagnetic waves at the surface of conducting materials. The surface impedance is a complex quantity that can be defined as [1]:

$$Z_S = \left(\frac{E_x}{H_y}\right)_{surf} = R_S + jX_S \tag{2.2.1}$$

where E_x and H_y are the tangential electrical and magnetic field components of the electromagnetic wave on the surface of a sample, R_S is the surface resistance, X_S is the surface reactance.

The surface resistance can be determined experimentally. In the linear regime, the surface impedance is independent from the amplitude of the electromagnetic field and includes only contributions from the sample properties.

In *a normal conductor*, the electromagnetic wave decays exponentially on the characteristic penetration depth δ, called the skin depth, which has a frequency dependence f [2, 3] as shown in eqn. (2.2.2):

$$\delta = \sqrt{\frac{1}{\pi f \sigma \mu}} \tag{2.2.2}$$

where μ and σ are the magnetic permeability and the conductivity of the material respectively. The skin depth declines with frequency, leading to increased resistance to current flow at high frequencies.

For a normal conductor the imaginary part of the complex conductivity can be neglected. In that case the conductivity becomes real and equal to, as [4]:

$$Z_S = \sqrt{\frac{\omega \mu_0}{2\sigma}}\,(1 + j) \tag{2.2.3}$$

This relation is valid for the normal skin effect in conductors, where the penetration depth is larger than the normal carriers mean free path and where the sample thickness is much greater than the penetration depth of the electromagnetic field. Also, the real and imaginary parts of the surface impedance are equal for the normal conductor.

For a brief historical overview of microwave conductors and superconductors, it needs to be mentioned that an important breakthrough of the microwave studies happened in 1940 when H. London was investigating tin (Sn) samples [5]. London described experiments of the surface resistance (R_S) of tin at 3.8K at the normal (non-superconducting) condition, just above T_C. The obtained R_S was approximately three times larger than typically calculated. London explained this big value of R_S by the influence of increased l (electron mean free path) at low temperatures compared to δ_{eff} (effective penetration depth) of the fields. This occurrence, where l is bigger than δ_{eff}, is referred to as the anomalous skin effect.

Later, Pippard [6] conducted comprehensive surface resistance measurements on a range of metals at normal state. At low temperatures those measurements showed that the surface resistance became independent of the penetration depth and therefore the electron mean free path. To explain this behaviour where $l>>\delta_{eff}$, Pippard created a basic model [7], suggesting that electrons almost parallel to the surface are substantially more effective as screening currents than those at bigger angles. This rational formed an assumption that the surface impedance is proportional to $\omega^{2/3}(l/\sigma)^{1/3}$.

A more comprehensive Z_S theory of an isotropic normal conductor was proposed by Reuter and Sondheimer [8]. Their calculations assumed an electron model where the mean free path l and the effective mass m, and electron scattering effects are taken into account.

In a superconductor, the surface impedance can be rewritten as a function of the complex conductivity σ_S [9]:

$$Z_S = R_S + jX_S = \sqrt{\frac{j\omega\mu_0}{\sigma_S}} \tag{2.2.4}$$

The real part of the surface impedance (R_S) is connected to microwave power loss in the superconductor and the imaginary part (X_s) describes the stored magnetic energy [10, 11]. R_S, X_S and the complex conductivity can be expressed as [12, 13]:

$$R_S = \frac{\sigma_1}{2\sigma_2}\left(\frac{\omega\mu}{\sigma_2}\right)^{1/2}$$
(2.2.5)

$$X_S = \left(\frac{\omega\mu}{\sigma_2}\right)^{1/2}$$
(2.2.6)

$$\sigma_S = \sigma_1 - j\sigma_2 = \frac{2\omega\mu_0 R_S X_S}{\left(R_S^2 + X_S^2\right)^2} - j\frac{\omega\mu_0\left(X_S^2 - R_S^2\right)}{\left(R_S^2 + X_S^2\right)^2}$$
(2.2.6a)

or sometimes, depending on the convention used, as [14]:

$$\sigma_S = \sigma_1 + j\sigma_2$$
(2.2.6b)

where σ_1 and σ_2 are conductivities related to the normal current (in regards to the two-fluid model) and the superconducting current respectively. In this thesis the equation (2.2.6a) is implemented.

The real and imaginary parts of the conductivity can also be written as [1]:

$$\sigma_1(T) = \frac{\sigma_n(T)}{1+\left(\omega\tau(T)\right)^2} \quad ; \quad \sigma_2(T) = \frac{1}{\mu_0\omega\lambda^2(T)}$$
(2.2.7)

where $\sigma_n = n_n e^2\tau/m$, n_n is the normal electrons density, n_s - the superconducting electrons density, where $n_n(T)+n_s(T)=1$.

The real part σ_1 is connected to the δ (skin depth) of the superconductor, and the imaginary part σ_2 is linked to the λ (penetration depth), as can be seen in (2.2.7) [13, 14]:

$$\delta = \sqrt{\frac{2}{\omega\mu\sigma_1}} \tag{2.2.8}$$

$$\lambda = \sqrt{\frac{1}{\omega\mu\sigma_2}} \tag{2.2.9}$$

The surface resistance and reactance are dependent on the RF magnetic field H_{rf} or current density J_{rf}. This is also referred to as power dependence, as it contributes to variations in feedback characteristics of the device as the power varies past it. Based on the two-fluid model, equations for R_S and X_S can be rewritten as [15]:

$$R_S(H_{rf}) = \frac{\mu_0\omega^2\lambda^3(H_{rf})\sigma_n(H_{rf})}{2} \tag{2.2.10}$$

$$X_S(H_{rf}) = \omega L_S(H_{rf}) = \omega\mu_0\lambda(H_{rf}) \tag{2.2.11}$$

where σ_n is the conductivity of normal electrons in a superconductor and $L_S = \mu_0\lambda$ is the surface inductance.

The relationship of the surface impedance in the time-frequency domain was investigated in [16], where a rigorous approach based on the time-domain nonlinear London equations and the two-fluid model was implemented.

The relationship between R_S and X_S for various materials is illustrated in Fig. 2.2-1 [15].
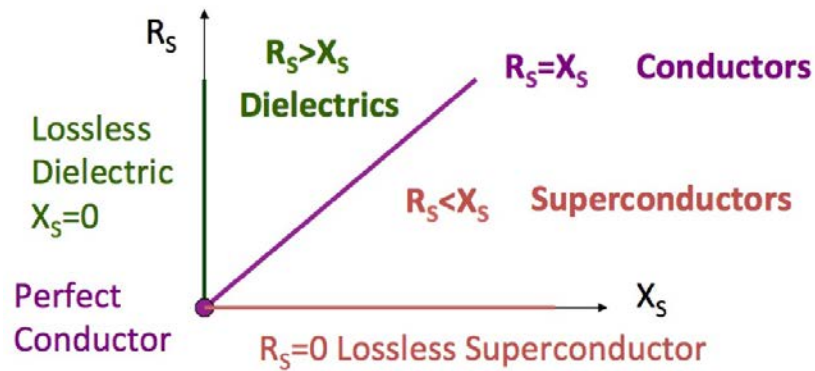
Fig. 2.2-1 Relationship between the surface resistance R_S and the surface reactance X_S for different materials (after [15]).

The investigation of the surface impedance of superconducting materials is often conducted with the use of thin films, which can be represented as a multilayered structure: superconducting thin film – dielectric substrate - metal plate. They can also include a very thin buffer layer(s) between the film and the substrate which will be neglected in the next description.

When the thickness of the superconducting thin film is $t_S \leq min\ (\lambda,\ \delta)$, the relation for Z_S becomes more complex. This is due to the penetration of the electromagnetic field through the thin film sample and interaction with the substrate and any supporting layers.

For the general case of the multilayered structure mentioned above, the surface impedance is given by the effective quantity $Z_{S,eff}$ based on the impedance transformation [17]:

$$Z_{S,eff} = Z_{S,\omega} \frac{Z_{d,eff} + iZ_{S,\omega}\tan\ (k_{S,\omega}t_S)}{Z_{S,\omega} + iZ_{S,eff}\tan\ (k_{S,\omega}t_S)} \tag{2.2.12}$$

where $Z_{d,eff}$ is the effective surface impedance of the substrate, $Z_{S,\omega}$ and $k_{S,\omega}$ are the wave impedance and the wave propagation constant in the superconducting thin film. The latter two parameters coincide exactly with the plane wave Z_S and $k_S = \mu_0\omega/Z_S$ for

Transverse Electromagnetic (TEM) wave propagation and most of the time for Transverse Electric (TE) operated resonators [17]. Thus, the 'ω' superscript will be omitted from now on.

The effective surface impedance of the substrate can be represented similar to the film, taking into account the bulk impedance of the underlying metallic plate (Z_m) [18]:

$$Z_{S,eff} = Z_d \frac{Z_m + iZ_d\tan(k_d t_d)}{Z_d + iZ_m\tan(k_d t_d)} \tag{2.2.13}$$

where Z_d is the characteristic impedance of substrate, which is a material dependent parameter; k_d and t_d are the propagation constant and the thickness of the substrate respectively.

In the case of $|Z_{d,eff}| \gg |Z_S|$, the substrate contribution can be neglected and the equation (2.2.12) reduces to the intrinsic surface impedance of the film:

$$Z_{S,eff} \cong Z_{s,i} = -iZ_S\cot(k_S t_S) \tag{2.2.14}$$

which, if $t_S \ll min(\lambda, \delta)$, gives the so-called thin-film approximation (Z_f):

$$Z_{S,eff} \cong Z_f = \frac{1}{\sigma_S t_S} \tag{2.2.15}$$

The value of the surface impedance defines the quality of superconducting thin films for microwave applications. Measurement techniques used for RF characterisation of the films are presented in the following subchapter.

2.2.2 Measurement techniques

The system for microwave characterisation of HTS, and development of techniques to extract the necessary system parameters have to be undertaken with a great care to satisfy a number of criteria. This is due to the fact that a measurement technique used for accurate microwave characterisation of superconductors need to ensure low uncertainty, high accuracy, and high reproducibility. A measurement set up should not modify the physical properties of the superconductor under test, and all the effects introduced by the measurement system needed to be accounted for.

There are various methods for the measurement of Z_S at microwave frequencies. The available methods include both resonant techniques (involving resonators such as cavity resonators, dielectric resonators (DR), microstrip resonators etc.) and non-resonant reflection or transmission methods. The non-resonant methods are not widely used due to the low sensitivity and the necessity for the complex analytical modelling, therefore they will be introduced first and only briefly in this subchapter.

The transmission type measurements are built around the detection of the power transmitted through the sample. Using this method, the complex conductivity σ of a superconducting film can be identified. The measurement cell consists of a rectangular waveguide with the emphasis on the TE_{01} mode. The superconducting film sample on the dielectric substrate is placed perpendicular to the waveguide axis. To extract the complex conductivity – reflection from the boundaries of the sample needs to be taken into account. The method was presented by Glover and Tinkham in 1957 [19] to investigate the frequency dependence of the complex conductivity for quasi-optical frequencies and implemented later for HTS films [20-22]. In the HTS case, the complex conductivity can be determined from the transmission coefficient S_{21} using the following relation [21]:

$$S_{21} = \frac{2}{\left(\dfrac{Z_g}{Z_{bi}}\right) + 1 + \sigma d Z_g}$$

(2.2.16)

where Z_{bi} is the reflective impedance of the dielectric layers at the interface with the superconducting film, and Z_g is the wave impedance of the waveguide.

Measurements of the reflected power are based on conditions where the superconducting sample short circuits the waveguide or coaxial cable. The reflected power gives the surface resistance of the sample. With the reflection measurements, the uncertainty in R_S is much larger than in the transmission method.

All resonant techniques related for the surface impedance investigations can be separated into planar resonator and bulk resonator techniques. Fig 2.2-2 illustrates various types of microwave resonators used for the thin film characterisation.
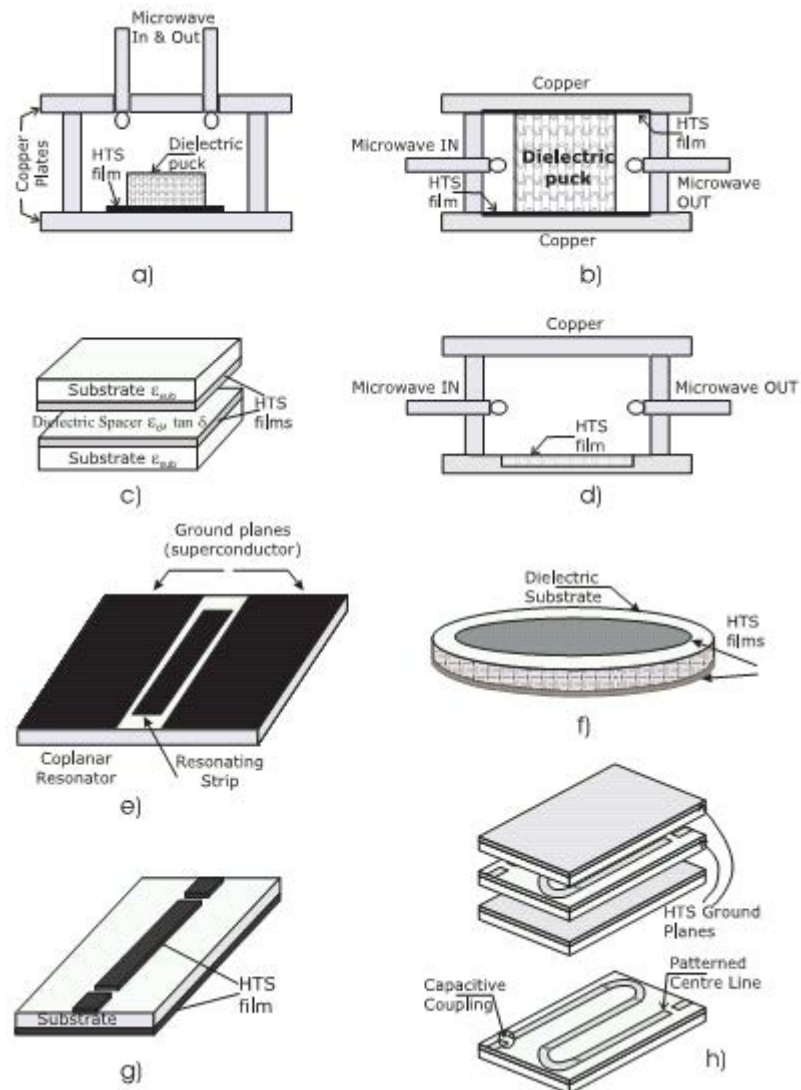
Fig. 2.2-2 Main types of microwave resonators used for thin film characterisation: (a) open-ended dielectric resonator; (b) Hakki–Coleman dielectric resonator; (c) parallel plate resonator; (d) cavity resonator; (e) coplanar resonator; (f) disc resonator; (g) microstrip resonator; (h) stripline resonator (after [23]).

All resonant techniques for measuring superconducting Z_S are based on a resonator, with HTS films forming an integral part of the resonant structure. The quality factor of the structure is measured and the surface resistance of the film is identified from the loss equation [24]:

$$\frac{1}{Q_0} = \frac{1}{Q_S} + \frac{1}{Q_c} + \frac{1}{Q_d} + \frac{1}{Q_{rad}}$$ (2.2.17)

where Q_0 is the unloaded quality factor and Q_S, Q_c, Q_d, and Q_{rad} are the quality factors related to superconductor, metal, dielectric, and radiation losses respectively. Superconductor and metal losses are formulated by the respective surface resistances (R_S, R_{met}), and dielectric losses by the loss tangent [24], as shown in (2.2.17a). The radiation losses are assumed to be negligible.

$$\frac{1}{Q_S} = \frac{R_S}{A_S}; \frac{1}{Q_c} = \frac{R_{met}}{A_{met}}; \frac{1}{Q_d} = p_d \, tan\delta; \qquad (2.2.17a)$$

$$\frac{1}{Q_0} = \frac{R_S}{A_S} + \frac{R_{met}}{A_{met}} + \frac{tan\delta}{A_{diel}} \qquad (2.2.18)$$

where A_S, A_{met} are geometrical factors of the superconducting and metal parts respectively, and p_d is the electric energy filling factor. The HTS films thickness needs to be bigger (at least three times) than the penetration depth, in order to limit the influence of the substrate and the backing plate of the resonator on the Q_0 factor and thus R_S.

The following types of the *bulk resonators* are normally used for microwave measurements on unpatterned films: cavity resonators [25], dielectric resonators [26, 27], parallel plate resonators [28]. In general, differences between each resonator type result in different sensitivity, accuracy, and simplicity of measurements. The bulk resonator techniques possibly provide the most accurate information on the film properties as they are least affected by extensive film handling and patterning. It needs to be mentioned, that the copper cavity resonant technique was the first method successfully used for surface resistance measurements of High Temperature Superconductors [29, 30].

The bulk cavity resonators have been used in the past for investigations of the superconducting R_S at frequencies above 30GHz. However, for lower frequencies of 1GHz or even 10GHz (suitable for applications of HTS films), the size of the empty cavities is too big to fit standard HTS films with areas such as 1cm^2 and 2.5cm^2. It also

needs to be stated that producing large area HTS thin films with uniform properties is fairly difficult and costly.

Cavity resonators are normally excited on the lowest order TE or TM modes. In the rectangular and cylindrical cavities (widely used), corresponding unidirectional and cylindrical currents are induced on the flat surfaces. Electromagnetic fields in the cavity resonators are well described in the literate due to the simplicity of geometry, that in turn simplifies its design and operation. Other advantages of the cavity resonators include: large Q-factor at low temperature (up to 10^5); geometric factor can be calculated analytically; easy sample mounting; measurements are generally reproducible. Regarding disadvantages associated with cavity resonators, their sensitivity to the film quality is not at the level required for accurate assessment of highest quality HTS films. Experimentally, the resistance of the sample under test can be extracted on the basis of a single measurement, where the resistance of the sample is unknown, while the resistance of the other conducting surface is precisely known in advance [31].

Bob Taber [32] in 1989 proposed the parallel plate resonator for accurate measurements of the surface resistance and penetration depth at frequencies of 10GHz. This technique was considered as a standard for precise microwave characterisation of HTS. The parallel plate resonator consists of two superconducting films set in a parallel arrangement where the superconducting sides of the HTS thin films face each other. In this configuration, the two superconducting films have a very thin layer of a dielectric material in between them. For practical measurement requirements, the plates of the resonator need to be parallel to achieve reliable results. Also, the difficulty of detecting the correct mode of resonant frequency is present due to the proximity of different modes. The advantages of the parallel plate resonator include its low geometrical factor and therefore high sensitivity enabling accurate measurements. The average surface resistance R_S of the two HTS films under test is calculated from the loss equation as [32]:

$$Q_0^{-1} = tan\delta + \alpha s + \frac{\beta R_S}{s} \approx \frac{R_S}{\pi\mu_0 f s} \qquad (2.2.19)$$

where s is the separation between the HTS plates (thickness of the dielectric) and α and β are geometrical factors.

Dielectric resonators containing a low loss dielectric piece, placed centrally within the cavity, have been prevalent for investigations of the surface resistance R_S of High Temperature Superconductors. It needs to be mentioned, that dielectric resonators had been implemented for research on the R_S of metals and losses of dielectric materials in the past [33 - 34], before their application for measurements of HTS materials. In 1989, Fiedziuszko [35] proposed the use of dielectric resonators for microwave characterisation of superconductors. Due to the number of advantages such as high accuracy and measurement sensitivity, simple procedure for the resonant frequency mode identification, and extensive range of measured resistances, the dielectric resonator technique is currently one of the most accepted measurement method for microwave investigation of HTS films.

Dielectric resonators implemented for characterisation of HTS are founded on two classical designs: a typical shielded configuration proposed by Hakki-Coleman [36] where two superconducting materials with comparable characteristics are studied; and the one-plate (open-ended) dielectric resonator [37]. The common methodology behind the measurements implies that a substantial portion of the total microwave losses appears in the HTS samples enabling very sensitive measurements of R_S. This is due to the fact that the dielectric permittivity is generally much bigger than the permittivity of free space, thus detaining most of the microwave energy within the dialectic. Outside the dielectric, an almost exponential decay of the electromagnetic field takes place. Therefore, the effect of the base edges and the outer wall contribution on the resulting Q-factor is minimal. Another advantage of the dielectric resonators versus empty cavity resonators lies in the much smaller size of the dielectric resonator at the same working frequency, allowing it to fit standard small size samples (1cm or inch square/round). The Hakki-Coleman dielectric resonator is characterised by high Q factor in the order of 10^6 at low temperatures.

There are few commercially available dielectrics with high permittivity ε_r and low loss: sapphire $\varepsilon_r = 9.8$, rutile $\varepsilon_r = 100$, lanthanum aluminate with $\varepsilon_r = 25$ and various types of ceramics. Sapphire is widely used not only because it is characterised by high ε_r, but also due to its extremely low dielectric losses at microwave frequencies.

The surface resistance of superconductors is obtained from the dielectric resonator loss equation, as [24]:

$$R_S = A_S \left(\frac{1}{Q_0} - \frac{R_{met}}{A_{met}} - \frac{1}{Q_d} \right)$$

(2.2.20)

where $1/Q_d = p_d \tan\delta$ and defines losses occurring in a dielectric. The geometrical factors A_S and A_{met} represent the design and dimensions of the resonator. The constant p_d for dielectric resonators equals around unity and only slightly depends on the size of the resonator.

In general, the quality factor of a resonator can be identified from the reflection coefficient S_{11} or from the transmission coefficient S_{21}. Measurements of S_{21} are more suited for weakly coupled resonators due to the difficulty of measuring S_{11} accurately for those conditions. The loaded quality factor (Q_L) can be obtained easily using the 3dB method (based on three values of S_{21} measured data). More accurate Q_L values can be determined by implementing the multi-frequency measurements [37, 38] and data fitting procedures [39, 40] of the S_{21} coefficient around the resonant frequency. For very small or equal coupling coefficients ($\beta_1 = \beta_2$) the unloaded Q_0 can be calculated from measured Q_L and S_{21} as [24]:

$$Q_0 = \frac{Q_L}{1 - |S_{21}|}$$

(2.2.21)

More accurate calculations can be performed applying the full equation for the unloaded Q_0-factor [24]:

$$Q_0 = Q_L(1 + \beta_1 + \beta_2) \tag{2.2.22}$$

where the coupling coefficients β_1 and β_2 can be found from measurements of S_{11} and S_{22}. This approach is suitable only for intermediate or high coupling. It also needs to be mentioned that for very low coupling coefficients, it can be assumed that the unloaded Q_0-factor approximately equals the loaded Q_L-factor. Therefore, precise investigations of Q_0-factors of dielectric resonators can be achieved for broad range of coupling coefficients.

Another category of resonators employed for the surface impedance measurements are the *planar transmission line resonators,* that are implemented for patterned film microwave characterisations. The most regularly used types, implemented since the 1980s to research thin films of superconductors, include stripline [41-45], microstrip [46-50] and coplanar resonators [51-53]. These resonators can be easily integrated with standard electronic devices incorporated in the microwave circuits. Microwave current in the planar resonators is concentrated in the region of the central conductor of the patterned sample, so that the effect of the sample boundary plays a role. Constant sample thickness is also required, therefore precise manufacturing of the samples is needed to minimise errors in Z_S due to geometrical uncertainties. The geometric factors for planar resonators are very low [54], that enables exceptional sensitivity of the surface impedance. The major disadvantage of planar resonator methods lies in the edge of the patterned HTS resonating lines that can be rough due to the practical limitations of the patterning process. The roughness of the edges may influence the quality of the sample. In addition, planar structures are difficult to analyse due to very non uniform current distribution requiring sophisticated numerical modelling.

Considering each of the above-mentioned planar resonator types separately, it needs to be indicated that the sensitivity of R_S measurements of *microstrip resonators*, shown in Fig. 2.2-2 (g), is affected by the radiation loss that forms a substantial part of the total energy loss, including patterning and current crowding losses. *Stripline*

resonators, illustrated in Fig 2.2-2 (g), are similar to microstrip resonators, apart from having two groundplanes instead of one. The two groundplanes reduce the radiation losses and effectively increase the sensitivity of measurements. All conductors are located on a single plane in *Coplanar resonators* [55], depicted in Fig. 2.2.-2 (e), where a superconducting ribbon positioned in between two normal conducting ground planes. While the coplanar resonators have been popular for measurements of the surface resistance and the penetration depth of HTS films [51-53], they also became very common in the 2000s for photon studies as microwave detectors [56, 57], and as foundational elements for circuit quantum electrodynamics architecture [58, 59]. Coplanar resonators hold certain benefits over stripline and microstrip resonators such as reachable values of quality factors, and simplicity of fabrication. However, they are highly sensitive to grounding and finite edge roughness.

In terms of the nonlinear behaviour (considered in details in the next subchapter 2.2.3), planar resonators have a certain advantage compared to the bulk systems, namely their extreme current crowding at the boundaries of the resonant band. This property makes them convenient for study of nonlinear behaviour at reasonably small microwave powers. On the other hand, planar resonators clearly need patterning, therefore the achieved results only partly denote properties of the HTS films. In this research project two types of resonators have been used extensively, the Hakki-Coleman type and the microstrip resonators. This enabled a comprehensive investigation of nonlinear effects of HTS thin films and their detailed comparative analysis that is presented in the following chapters.

2.2.3 Nonlinear microwave properties of superconductors

The dependence of the surface impedance Z_S on RF magnetic field (Hr_{rf}) or RF current (I_{rf}) defines the nonlinear surface impedance $Z_S(H_{rf}, I_{rf})$. Both elements of the complex surface impedance, the surface resistance R_S and surface reactance X_S, are dependent on H_{rf} and implementing the two-fluid model they can be expressed as equations (2.2.10) and (2.2.11), given earlier in this chapter. While the surface

resistance at low power levels does not necessarily affect microwave performance of very low loss microwave devices, the nonlinear surface impedance still pose severe limitations to many applications where high power handling capability or very linear operations are required. It needs to be mentioned, that nonlinearities normally occur as deviations in the Z_S, however they can also appear in forms of intermodulation distortion and harmonic generation. Although, these types of nonlinear effects evidently have comparable origins, the main focus in this thesis will be on the measurements of $Z_S(H_{rf})$.

It is important to note that nonlinear effects can appear under various circumstances when certain RF power levels are applied. One or more of the following phenomena can contribute to the nonlinearities: thermal effects, weak links, non-homogeneities, non-equilibrium excitation, unconventional pairing and others [60-68], each of which may occur under certain conditions. The usual dependence of the surface resistance R_S of superconducting thin films on the microwave field can be identified by four modes, such as the linear one that occurs at small field, weakly nonlinear dependence, highly nonlinear state, as well as breakdown mode occurring at peak field levels.

It is believed that surface resistance of HTS films in the linear mode is extrinsic in nature and defined by the crystal defects such as weak links at grain boundaries. The coupled-grain model [69] describes the linear state comprehensively. The surface resistance increases gradually with microwave field strength in weakly nonlinear regime, and this behaviour has usually quadratic dependence as a function of power. The weakly nonlinear mode is also believed to originate from the presence of deformations such as weak links at grain boundaries. This mode can be defined by the expanded coupled-grain model, which includes nonlinear inductance of the weak links [70]. The third regime expresses strongly nonlinear behaviour, where the surface resistance increases more rapidly with the microwave power. This region is usually connected with the vortex generation phenomena under a strong microwave magnetic field. The fourth regime can occur at very high microwave power levels, the so-called breakdown region, where the surface resistance increases very sharply. The

breakdown regime is believed to be caused by a heating effect and formation of normal-state domains.

In relation to the nonlinear measurements of Z_S for *unpatterned* films there are two important considerations to notice. The first, high power amplifiers are normally required to obtain adequate power to generate sufficient H_{rf} in the dielectric resonator. This is due to the large volume of the dielectric resonator with reasonably uniform current distribution. In order to maximise the circulating power, it is necessary to have the adjustable input coupling, enabling the maintenance of critical coupling at all power levels and temperatures. While, the output coupling is normally required to be at a weak level for keeping the circulating power at maximum.

The heating effects of the films occurring as a result of the power dissipation form the second consideration in relation to the nonlinear measurements. As dielectric resonators are designed to be controlled by losses in the films, most of the input power is dissipated in the film itself. This means that proper measures need to be taken to manage the heating effects appearing within the vacuum space of the cryocooler. In the measurement setup, the resonator is thermally connected on the one side to the cold finger of the cryocooler, while additional arrangements need to be taken to cool the other side [71].

As far as the nonlinear measurements of Z_S for *patterned* films are concerned, it needs to be mentioned that the large number of measurements of the surface impedance have been conducted implementing patterned superconductors. Those measurements used some of the typical transmission line setups such as stripline, coplanar or microstrip, introduced before in this chapter. The H_{rf} is larger in the patterned geometries than in the dielectric resonators as the distribution of currents is structurally nonuniform with strong peaks occurring at the edges [72] within a reasonably small area. Therefore, reaching high enough RF field levels to produce nonlinear behaviour is relatively easy. As many practical devices are manufactured using patterned films the microwave characterisation and practical investigation of nonlinear effects are important for their applications.

As was stated before, for the comprehensive investigation of nonlinear effects of HTS films in this thesis, two types of resonators have been implemented - the Hakki-Coleman type dielectric resonator and the stripline resonator.

2.2.4 Review of microwave measurement results of HTS with nonlinear properties

Since the discovery of HTS in 1986 numerous research papers on nonlinear properties of HTS superconductors have been published [60, 72-74]. Some results related to the scope of this thesis are presented below.

The same resonators are normally used for the most measurements of $Z_S(H_{rf})$ and characterisation of the linear Z_S. In the microwave experiments the resonant frequency f_0 and the quality factor Q are usually measured in order to determine the physically meaningful quantities such as R_S. Such measurements are completed in the time or frequency domains [75].

The consequence of the nonlinear effects in a resonator is presented in Fig. 2.2-3, where undesirable distortion of the resonant curve is clearly visible at elevated power [76]. It shows the results of measurements of transmitted power versus frequency with a YBCO stripline resonator for a sequence of increasing power levels, indicating the change from linear to highly nonlinear regions as a function of input power.
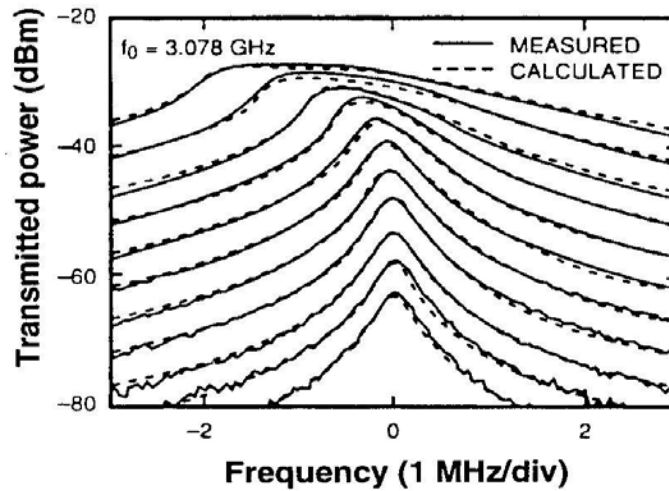
Fig. 2.2-3 Transmitted power vs frequency for a YBCO stripline resonator as a function of input power (after [76]).

The maximum power for Fig. 2.2-3 results is +30dBm with the minimum of -20dBm. The experiment was carried out where input power was set to -20dBm, and the frequency was then swept to provide a power curve of transmitted power versus frequency. The input power was then increased by 5dBm (to give -15dBm of input power), and the frequency sweep was repeated to provide a second power curve. Other power curves were obtained in similar fashion with input power increasing in steps of 5dBm for each run. The result is a family of power curves shown in Fig 2.2-3. The frequency is 3GHz with the temperature at 77K. Solid lines show measured data and dashed lines are calculated [76].

To investigate nonlinear effects in ceramics, a niobium quarter-wave cavity resonator at 821MHz was fabricated by Delayen et al. [77] for the investigation of HTS in RF fields up to 300Oe. Results for broad range of superconductors are presented in Fig. 2.2-4.
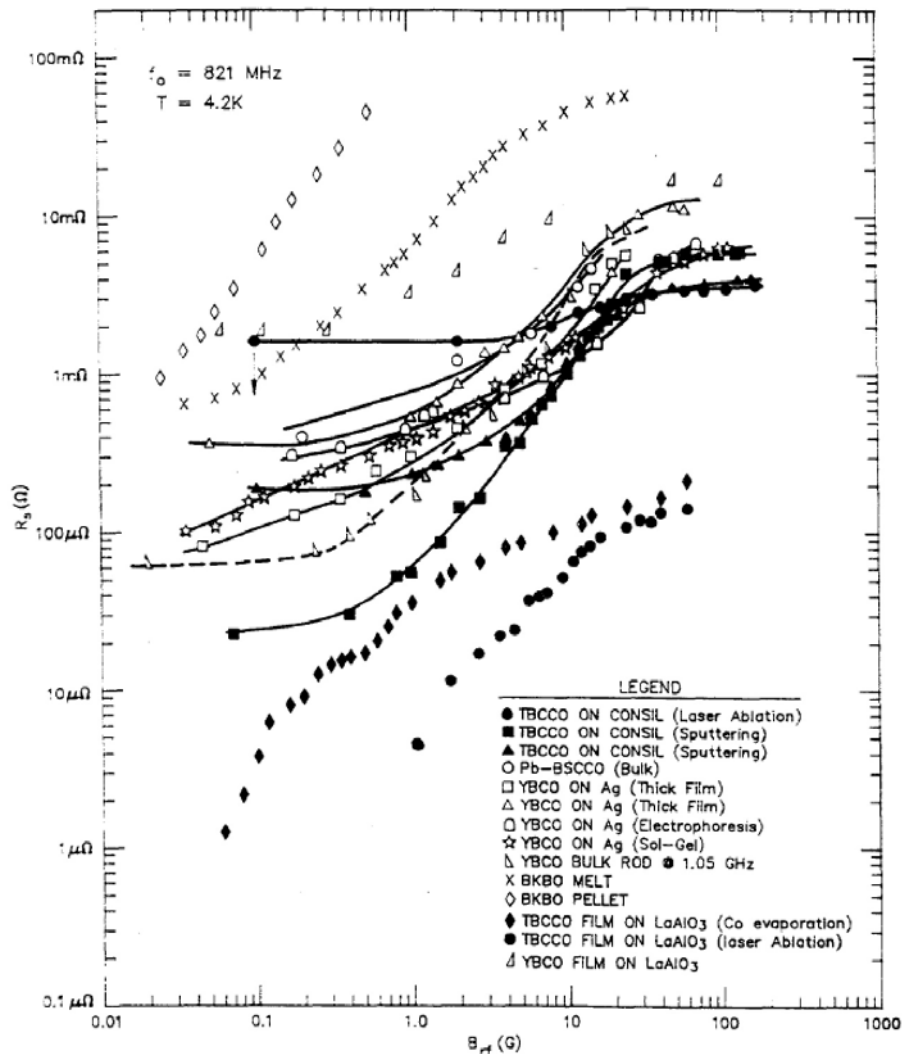
Fig. 2.2-4 Surface resistance vs RF magnetic field at 821MHz and 4.2K for a variety of samples. The behaviour of a ceramic rod is shown for comparison. The high apparent surface resistance of laser-ablated TBCCO on Consil is probably from the edges, which were not coated (after [77]).

As can be seen from the Fig. 2.2-4, all superconductors behave in a similar fashion. At the lower magnetic field range of 0.1-1Oe, the surface resistance increases at a declining rate saturating finally in fields of 10-100Oe. It needs to be mentioned that the surface resistance values at saturation is 10 to 100 times bigger than R_S at the low power values, however they are still only a few percent of the normal state surface resistance.

Kobayashi et al. [78] implemented a dielectric rod resonator for measurements of the R_S power dependence of YBCO ceramics. The surface field H_S up to 10^4A/m (126Oe) was achieved with a four-fold surge in the surface resistance at temperature of 11K.

As far as granular films are concerned, 100μm thick TBCCO films have been investigated in [79] as a function of RF power at 18GHz and showed an increase of R_S at 4K. The results showed that the unoriented film surface resistance saturated at values of 100mΩ in RF magnetic fields of approximately 15Oe. The R_S of the better oriented films grew more gradually without reaching the saturation point, as illustrated in Fig 2.2-5.
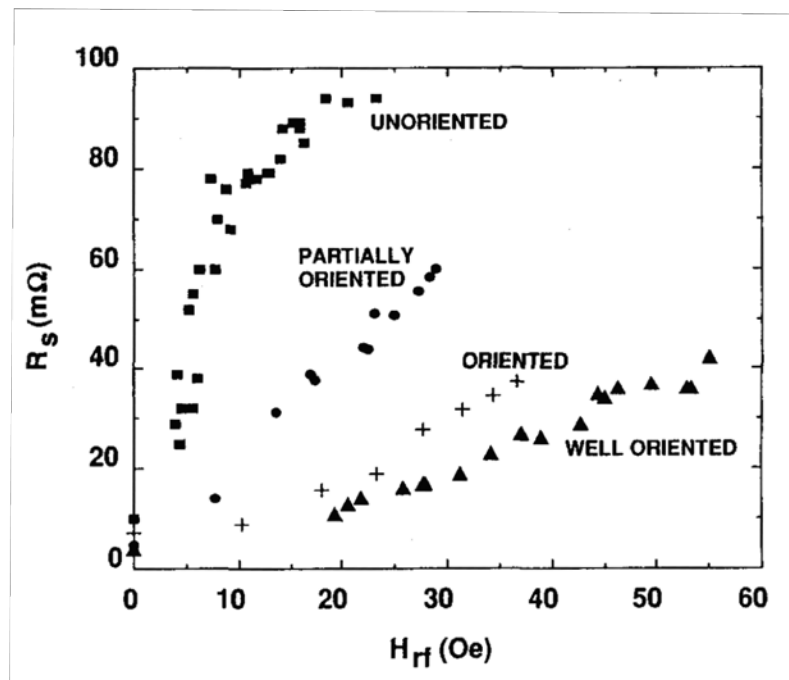
Fig. 2.2-5 Field dependence of R_S of TBCCO thick films for varying degrees of c-axis texturing measured at 18GHz and 4K (after [79]).

The surface resistance at the lowest levels of H_{rf} was below 10mΩ. The R_S was observed to increase with higher H_S, with saturation in the un-oriented film.

Thick films manufactured with electrophoretic deposition technique were developed in [80] for the implementation in resonators at high power levels. The

deposition method involves the 8T magnetic field, positioning the particles in such a way that results in better grain growth and texturing. The results obtained for two thick films (textured and un-textured) measured in a niobium cavity resonator at 21.5GHz and up to 1000A/m (12.6Oe) [81] are presented in Fig. 2.2-6.
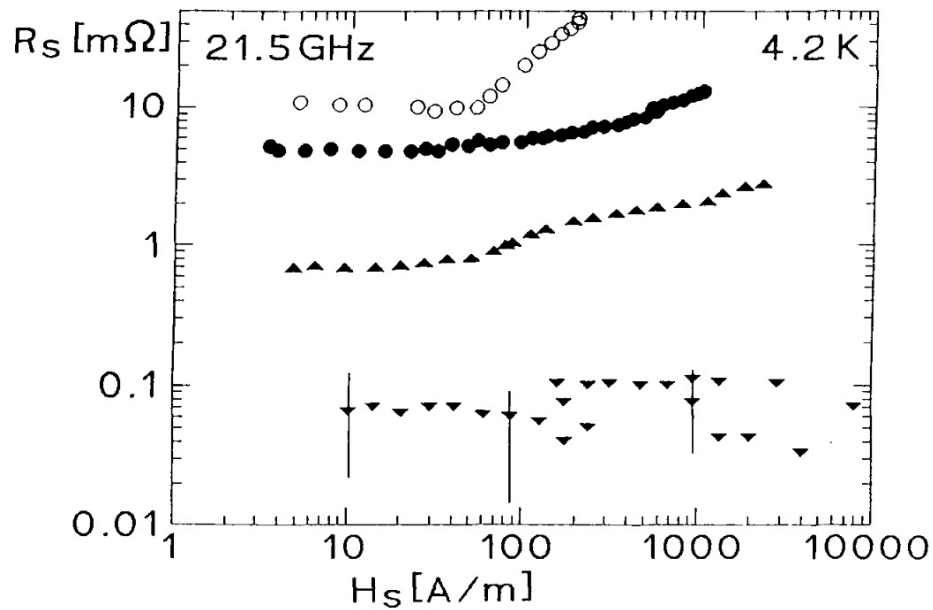
Fig. 2.2-6 Dependence of RF field of the surface resistance of electrophoretically deposited YBCO thick films at 4.2K and 21.5GHz. A highly textured thick film is shown with filled circles and an untextured film is illustrated with open circles. For comparison – two thin films are shown: an electron coevaporated film (inverted triangles) and a CVD film (upright triangles) (after [81]).

Fig 2.2-6 also shows two thin films for comparison: a CVD film (upright triangles) and an electron coevaporated film (inverted triangles). The R_S of the textured film (filled circles) growths as a square root of the microwave field, while the R_S of the untextured film (open circles) is not affected by the field up to approximately 50A/m (0.6Oe) after rising linearly with the field.

It is known, based on various literature publications, that HTS thin films display a wide range of RF microwave field or power dependences of the surface resistance and reactance. There have been various mathematical dependencies

proposed to describe the magnetic field dependence in terms of linear [64, 82], quadratic [64, 82] and exponential representations [83, 84]. Normally, quality films show comparable H^2_{rf} dependence of both the surface resistance and the surface reactance at small fields, which gets steeper than H^2_{rf} with escalating microwave power. Oates and co-authors [44, 54] identified three ranges (stated below) in the surface RF field, while investigating the properties of YBCO thin film on $LaAlO_3$ substrate stripline resonator in high RF field (up to 300Oe) for frequencies of 1.5-20GHz and temperatures of 4-90K:

i.   In the low field region ($H_{rf}<10$Oe) R_S raises very slightly;

ii.   In the intermediate field region ($10<H_{rf}<50$Oe at 77K) the surface resistance increases quadratically with RF field H_{rf} and frequency f as $R_S(H_{rf})=a(f,T)+b(f,T)H^2_{rf}$;

iii.   At elevated magnetic fields $H_{rf}>50\text{-}300$ Oe, with the dependence on temperature and frequency, R_S rises quicker than the earlier quadratic growth. In this field region, R_S surges in a linear way with frequency, demonstrating hysteretic progression [44, 54].

The increase in R_S with elevated RF field at temperature of 67.3K and a frequency range of 1.5-7.5GHz is illustrated in Fig. 2.2-7.
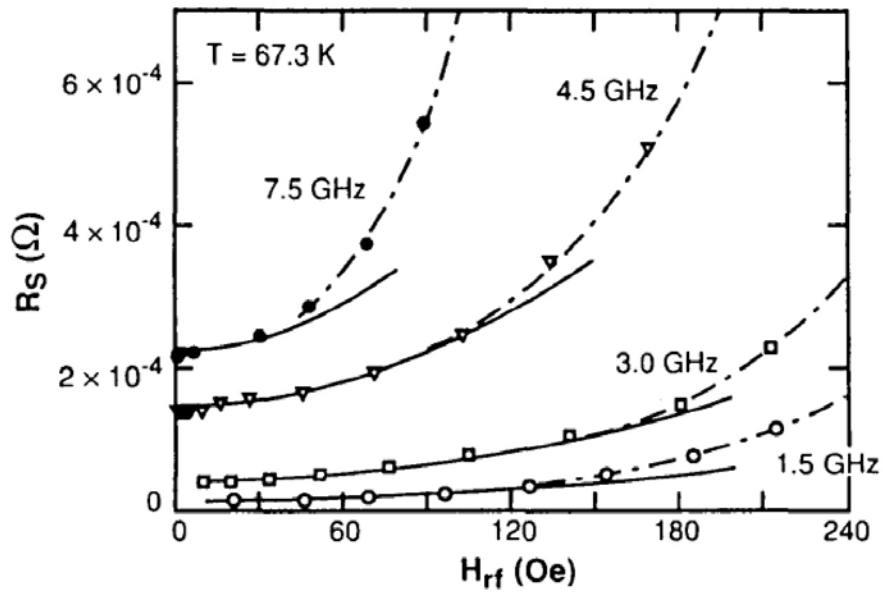
Fig. 2.2-7 Surface resistance vs RF magnetic field at various frequencies. The solid
lines fit the initial parabolic increase. At higher fields R_S increases more rapidly than
the extrapolated quadratic increase (after [54]).

A detailed set of the surface resistance dependence on the RF magnetic field data at
different temperatures for the frequency of 1.5GHz is presented in Fig. 2.2-8.
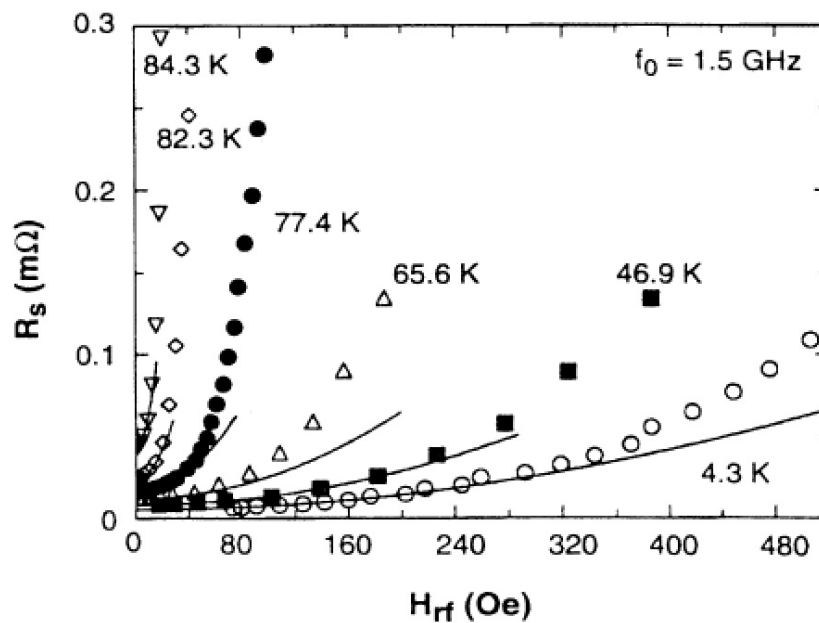
Fig. 2.2-8 R_S vs H_{rf} at 1.5 GHz for the YBCO on LaAlO$_3$ substrate stripline
resonator at different frequencies. The solid lines are quadratic fits (after [44]).

A quadratic fit to the equation $R_S=R_S(0)[1+b_RH^2_{RF}]$ (where b_R is a fitting constant) is shown at various temperatures for different RF field values. As can be seen, all curves illustrate similar behaviour, where at elevated RF magnetic fields the growth in R_S is quicker than H^2_{RF}.

Fig. 2.2-9 shows $\Delta\lambda/\lambda(0)$ versus H_{rf} dependence for the same temperatures as presented in Fig. 2.2-8 apart from the curve at 4.2K.
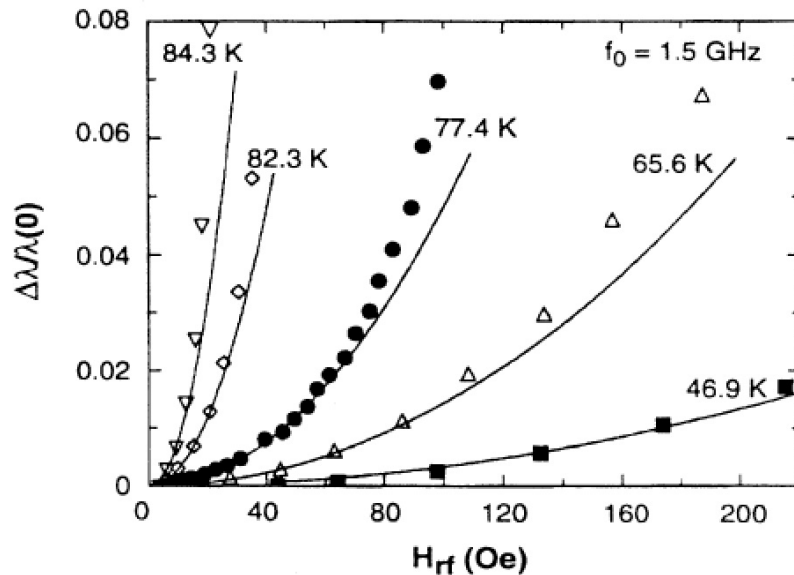
Fig. 2.2-9 The fractional change in the penetration depth λ versus the RF magnetic field H_{rf} at 1.5GHz the YBCO on $LaAlO_3$ stripline resonator at different temperatures. The solid lines are quadratic fits to the data (after [44]).

As can be observed from the Fig. 2.2-9, the functional behaviour of $\lambda(H_{rf})$ is comparable to $R_S(H_{rf})$. However, the fractional variation in λ is minor compared with that of R_S.

Fig. 2.2-10 shows plots of the resonant frequencies of f_0 as functions of RF field for the same set of temperatures as in Fig. 2.2-8 and 2.2-9. These resonant

frequencies were used for the corresponding effective λ in Fig. 2.2-9. The solid curves are quadratic fits.
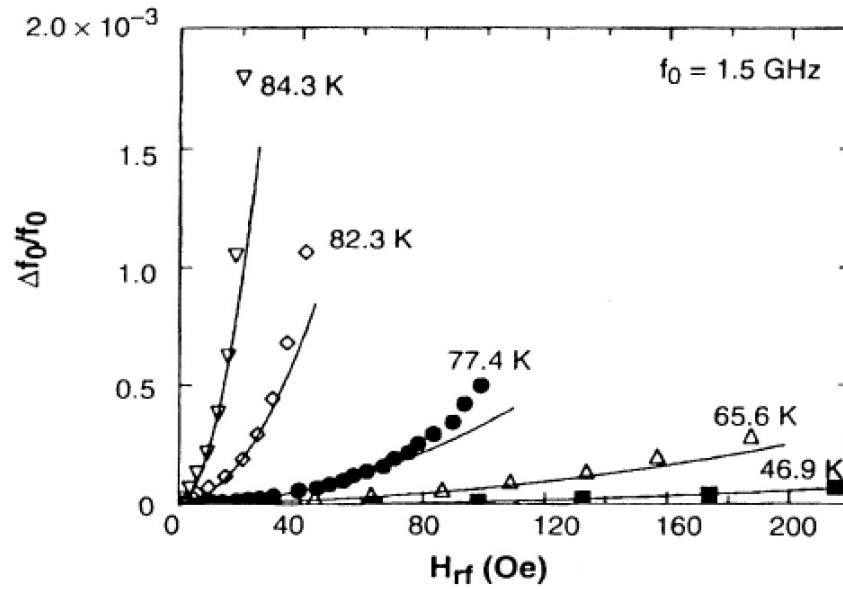
Fig. 2.2-10 $\Delta f_0/f_0$ vs H_{rf} at 1.5GHz for the YBCO on LaAlO$_3$ stripline resonator at the same temperatures as Fig. 2.2-9. The solid lines are quadratic fits to the data. (after [44]).

Fig 2.2-11 shows a typical set of values of both R_S and X_S with increased microwave power for an epitaxial YBCO film measured with the stripline resonator at 1.5GHz and 77.4K [85].
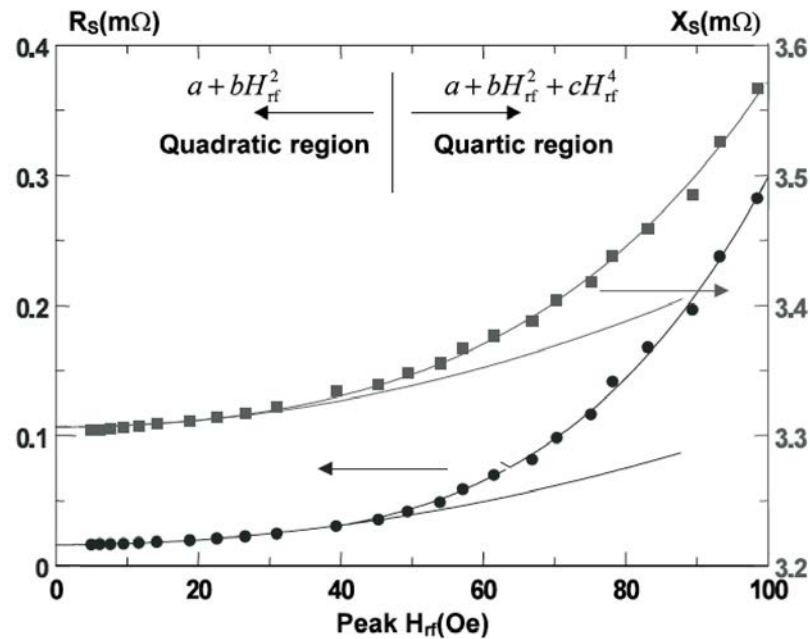
Fig. 2.2-11 Typical power dependence of an epitaxial YBCO film measured with the
stripline resonator at 1.5GHz and 77.4K. (after [85])

The quadratic behaviour at low fields is normally credited to the Ginzburg-Landau
departing mechanism, when the Cooper pairs are destroyed under influence of the
microwave electric field. Subsequently steeper increase (around H^4_{RF} or steeper) in
$Z_S(H_{RF})$ is usually dominated by the vortex penetration into the superconducting
grains [85].

The surface resistance power dependence for various YBCO thin films
deposited on different substrates by various techniques was reported in [86] with the
results shown in Fig. 2.2-12.
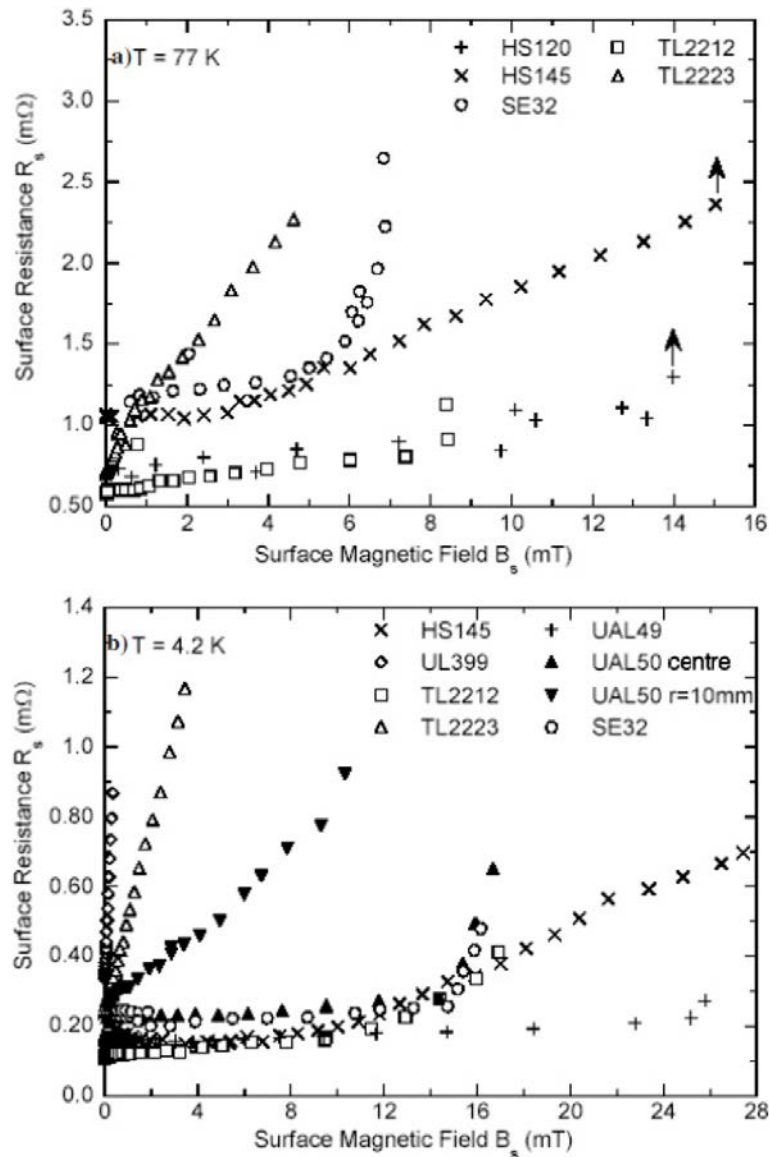
Fig. 2.2-12 A variety of different power dependences for different films on various substrates measured by using the dielectric at 19GHz and (a) 77K and (b) 4.2K. HS—YBCO sputtered on $LaAlO_3$; UAL—YBCO laser deposited on $LaAlO_3$; SE— e-beam co-evaporated on MgO; Tl-2223—$Tl_2Ba_2Ca_2Cu_3O_8$ two-step process on $LaAlO_3$; Tl-2212—$Tl_2Ba_2Ca_1Cu_2O_8$ two-step process on MgO; UL—YBCO laser deposited on CeO_2/Al_2O_3 (after [86]).

Fig. 2.2-12 shows a great variety in responses of $R_S(H_{RF})$ that can be sublinear, linear, quadratic or more rapidly increasing functions of H_{RF} ($\sim H^4_{RF}$). There are also films where the surface resistance is almost unchanged up to relatively high fields of approximately 15mT then starting to increase sharply in a stepwise way.

As far as patterning effects are concerned, the discussion of their influence on microwave properties of HTS films has been ongoing. In order to examine this question, microwave properties of a superconducting sample are studied first in the unpatterned form and after in the patterned state, with further comparison of the obtained results. Extensive measurements of microwave properties of various YBCO films on $LaAO_3$ substrates in both the dielectric and stripline resonators were conducted by Xin et al. in [71]. Various regions of the HTS film, as a result of the difference in field distribution, have been tested for two resonators with the goal to identify the effect of patterning on the nonlinear microwave properties of the HTS films. Fig. 2.2-13 shows microwave current distribution for the two resonators used in [71].
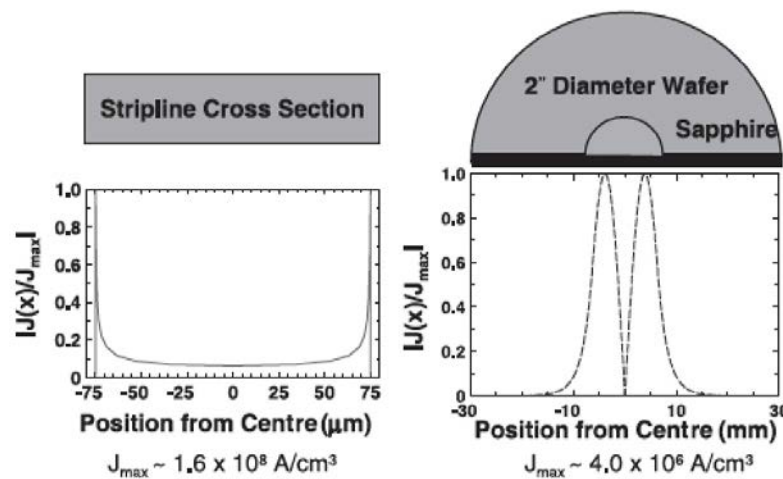
Fig. 2.2-13 Current distribution of both stripline resonator (left) and dielectric resonator (after [71]).

As can be observed from Fig. 2.2-13, the stripline resonator has microwave current spikes at the boundaries of the strip with minor values of current in the middle section, meaning that the patterning process could influence the measurement results. Otherwise, a circular spike of microwave current is detected near the disk centre, and practically no current observed near the disk edges. Results of the power dependence of R_S obtained with the two techniques at 10.7GHz and 75K are presented in Fig. 2.2-14.
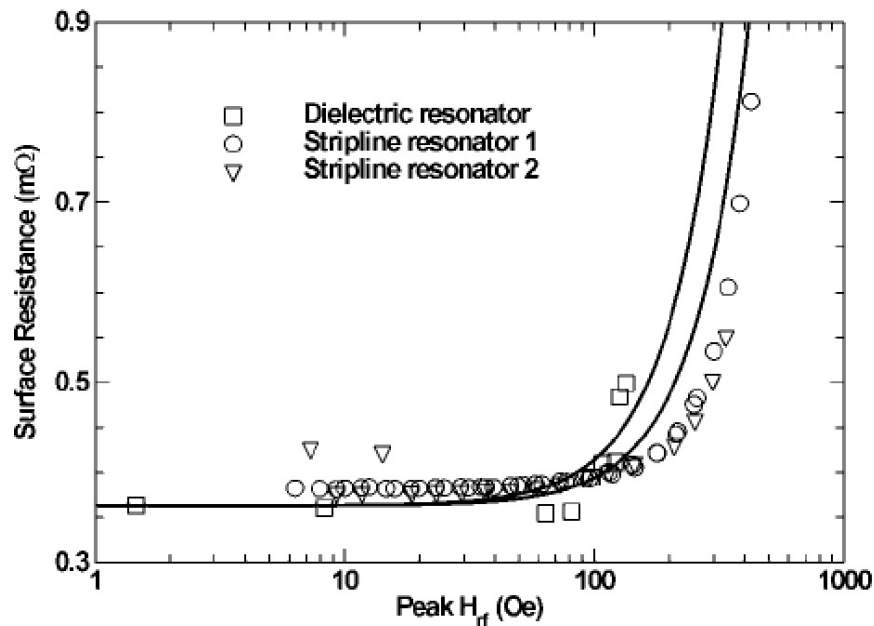
Fig. 2.2-14 R_S versus RF peak magnetic field H_{rf} measurements in the dielectric resonator and the stripline resonator using the same YBCO film on sapphire for both resonators at 75K and 10.7GHz. The solid curves are computed curves using the model presented in [71] (after [71]).

As can be seen, the both techniques provide qualitatively similar results, where the nonlinear onset occurring at approximately the same RF magnetic field for both resonators. Therefore, it was concluded by the authors that patterning process had little influence on the nonlinear characteristics of the film. It was also assumed that the nonlinearity was not caused by the vortex penetration in YBCO at low and intermediate (up to 100Oe) RF magnetic fields. The reason behind it was that H_{RF} is mainly perpendicular to the film surface in the sripline resonator, thus promoting the vortex penetration, while H_{RF} is typically parallel to the film in the dielectric resonator surface causing no or very small demagnetisation effect.

As far as the temperature dependence of the surface resistance of HTS thin films is concerned, Fig. 2.2-15 shows the surface resistance at 8GHz of some YBCO thin films on MgO substrate grown by different techniques (laser ablation, sputtering,

electron beam co-evaporation and MOCVD) compared with low-temperature superconducting materials at the same reduced temperature.
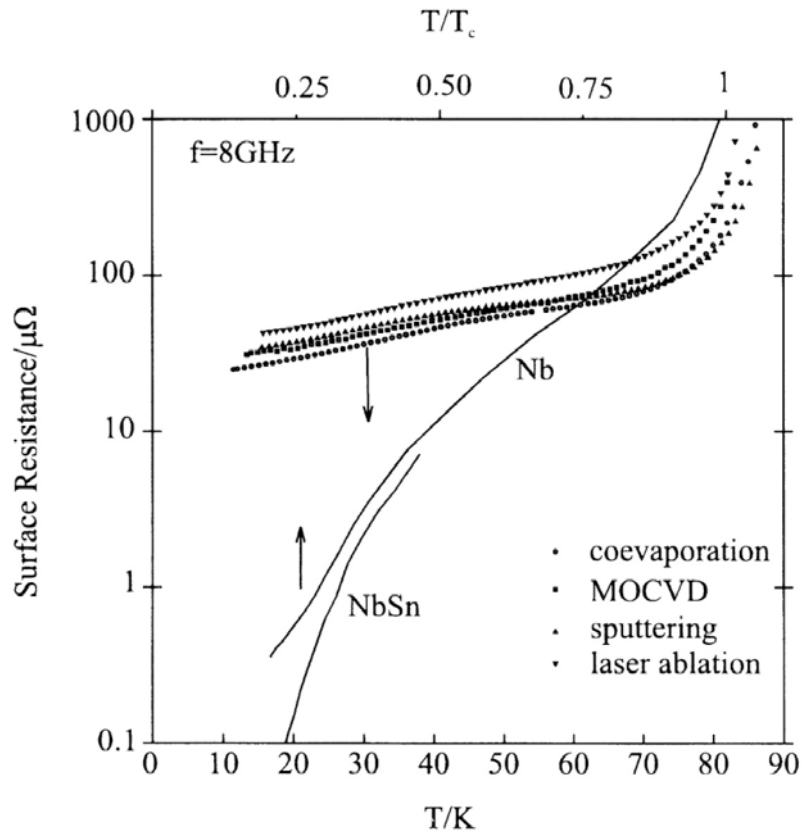
Fig. 2.2-15 Temperature dependence of the surface resistance of YBCO thin films on MgO substrate grown by a number of techniques compared with niobium and niobium-tin superconductors at the same reduced temperature. The scale on the upper axis refers to the reduced temperature for the Nb_3Sn and Nb, while the lower scale refers to the actual temperature of YBCO films. The T_C of the three materials coincides. (after [87]).

While it is difficult to distinguish individual films from the graph (Fig.2.2-15), the main point is that all these techniques can produce good quality epitaxial thin films with low surface resistance values. The thickness of the above films was 350nm for the laser ablated and co-evaporated films, 400nm for the sputtered film and 180nm for the MOCVD film. All the surface resistance values were calculated as though the

films were thick compared with the penetration depth. The films were measured using a coplanar resonator at 8GHz.

YBCO thin films grown by pulsed laser deposition technique on LaAlO$_3$ substrates with different deposition temperatures have been investigated by J. Booth et al. in [88] using a sapphire dielectric resonator. Fig. 2.2-16 shows the temperature dependence of the sapphire dielectric resonator Q-factor and R$_S$ for YBCO films obtained at deposition temperatures of 740C and 780C.
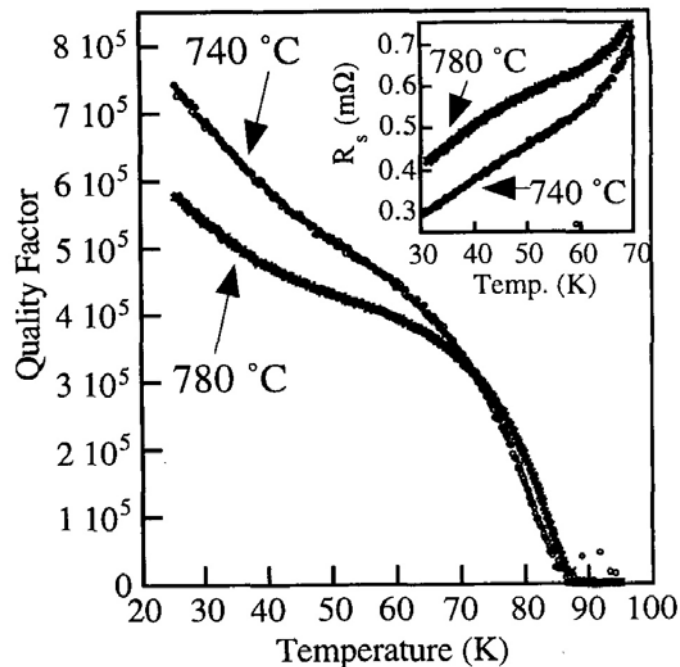
Fig. 2.2-16 Temperature dependence of sapphire dielectric resonator quality factor for pairs of YBCO films grown at deposition temperatures of 780C and 740C. The inset shows values for the surface resistance at 17.5GHz. (after [88]).

As can be observed from the obtained results, the HTS films at 740C show considerably smaller R$_S$ than 780C films, leading to a higher quality factor of the resonator, and lower corresponding R$_S$ (see inset). Films developed at lower deposition temperature display lower values of σ_1 (resulting from a higher quasiparticle scattering rate) and σ_2 (indicating a bigger penetration depth or a lower superconducting density). While the reduced σ_1 yields a smaller R$_S$ at low

temperature, by 76K the influence of the bigger λ made the surface resistance of the 740C sample to surge above the 780C samples.

The temperature results for TBCCO films on CeO_2 buffered sapphire measured in a dielectric resonator at 8.5GHz are presented in Fig. 2.2-17 [89]. A high quality YBCO film with small nonlinear effects up to 10mT was used as the reference film.
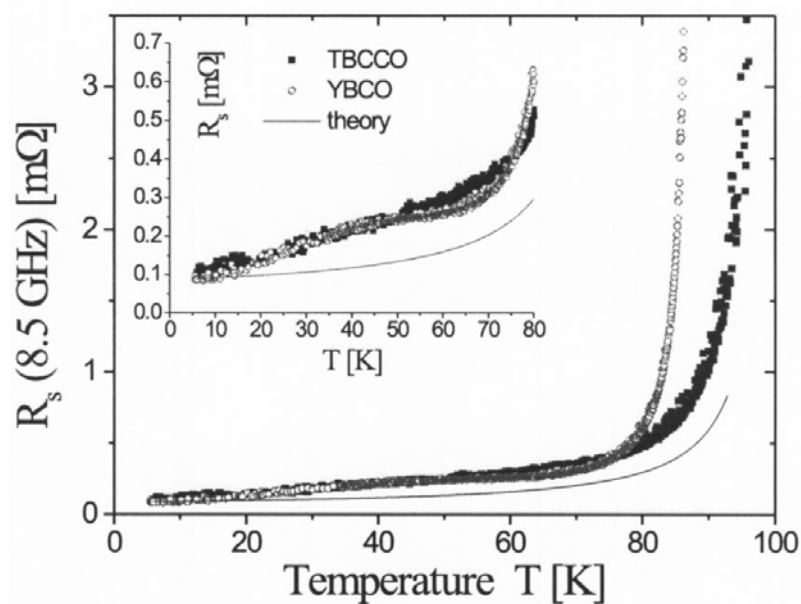
Fig. 2.2-17 Temperature dependence of surface resistance of TBCCO and YBCO thin films at 8.5GHz. The inset shows the same data on a different scale. A value 50$\mu\Omega$ was added to the theoretical curve to take into account the coupling losses (after [89]).

The dielectric resonator yielded average microwave properties of the two films, TBCCO and YBCO having a smaller T_C as shown in Fig. 2.2-17.

Measured dependence of the surface resistance R_S on frequency f obtained by various research groups for YBCO thin films are presented in Fig. 2.2-18. It can be observed that the superconducting films exhibit much lower values of the surface resistance than copper in the frequency range of up to 100GHz. Also, the results for a

traditional low temperature superconductor Nb are shown at the temperature of 77K for comparison.
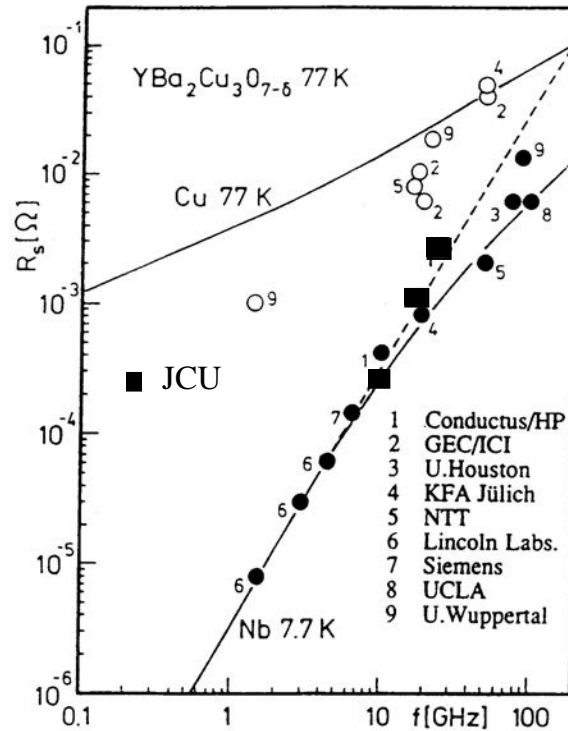
Fig. 2.2-18 Frequency dependence of the surface resistance of YBCO thin films and copper at 77K, as well as niobium at 7.7K (modified [72], with JCU results added).

As is well known, the frequency dependence of the surface resistance $R_S(f)$ is in the form of $f^{1/2}$ for normal metals and f^2 for superconductors.

Comments

As was mentioned before, several physical mechanisms are believed to be responsible for the nonlinear effects in superconductors. These mechanisms can be divided into two groups depending on their connection with either intrinsic or extrinsic nonlinearities. It is well known that a number of nonlinear effects appear due to defects in a crystal or a crystal-substrate interface. In good quality superconducting thin films the nonlinearities can be induced by a change in the superconducting

electron density due to the applied RF magnetic field H_{RF}. However, the effect is considerably small, and the nonlinear behaviour of superconductors cannot be fully explained by this phenomenon, even though it can explain the quadratic dependence of $R_S(H_{RF})$.

Superconductor thin films, which represent a system of superconducting grains linked by Josephson-junctions, can be characterised by a coupled-grain model, discussed in Chapter 3. As high quality superconductors have a small number of Josephson links, the intrinsic effects such as the microwave heating, local heating of weak links, weakly coupled grains, vortices, and mass vortex penetration become important for characterisation of the materials. Some intrinsic effects are induced by the flux penetration in a thin film at the increase of the magnetic field above H_{C1}. These effects are connected with a nonlinear change in a number of vortices in a superconductor due to the magnetic field H_{RF} and energy dissipation effects.

It also needs to be mentioned that the expertise in manufacturing HTS thin films has achieved a very progressive phase, where advanced HTS films with exceptional microwave characteristics, very reproducible with outstanding performance, can be regularly fabricated for widespread applications. However, the main restriction for microwave applications of HTS films still comes from microwave nonlinearity. As was mentioned before, the physical mechanisms responsible for nonlinearities are still not clear, although the leading causes of the microwave nonlinear effects have been investigated comprehensively and are well reported. For example, oxygen content and impurity doping are believed to be significantly responsible for nonlinearities of the HTS films. However, patterning and grain boundaries are found to be irrelevant to the power handling of high quality superconductors.

The problem of modelling the power dependent surface resistance of high-temperature superconductors is a complicated issue because the nonlinear dependence can arise due to the several physical phenomena. Proposed models usually assume that there is only one reason behind the nonlinear losses. Hence, more complex HTS

system models, or better models need to be developed to accurately simulate RF properties of HTS thin films at relatively high power levels. The next chapter reviews proposed lumped-element models by various research groups, and also paves the way for the development of the model used in this dissertation.

It also needs to be mentioned that the heat dissipation in the dielectric substrate of HTS thin films and HTS microstrip resonators at elevated power levels is not a crucial characteristic for investigations of nonlinear effects. This is due to the fact of high thermal conductivity of dielectric substrates at lower temperatures.

REFERENCES

[1]   Z. Kresin and S. Wolf, "Fundamentals of Superconductivity", *Plenum Press, New York,* 1990.

[2]   D. Cheng, "Field and Wave Electromagnetics", *Addison-Wesley Publishing Company*, 1989.

[3]   D. Pozar, "Microwave Engineering", *Addison-Wesley Publishing Company*, 1990.

[4]   H. Atwater, "Introduction to Microwave Theory", *McGraw Hill Book Company Inc.*, 1962.

[5]   H. London, *Proc. R. Soc. London, Ser. A*, v. 176, p. 522, 1940.

[6]   A. Pippard, *Proc. R. Soc. London Ser. A*, v. 191, p. 370, 1947.

[7]   A. Pippard, *Proc. R. Soc. London Ser. A,* v. 191, p. 385, 1947.

[8]   G. Reuter and E. Sondheimer, *Proc. R. Soc. London, Ser. A*, v. 195, p. 336, 1948.

[9]   M. Hein, "High-Temperature-Superconductor Thin Films at Microwave Frequencies", *Springer*, 1999.

[10] K. Zhang, et al., "Measurement of the ab plane anisotropy of microwave surface impedance of untwinned $YBa_2Cu_3O_{6.95}$ single crystals", *Phys. Rev. Lett.*, Vol. 73, No. 18, pp. 2484. 1994.

[11] R. Fletcher and J. Cook, "Measurement of surface impedance versus temperature using a generalized sapphire resonator technique", *Rev. Sci. Instrum*. Vol. 65, No. 8, pp. 2685, 1994.

[12] M. Tinkham, "Introduction to Superconductivity", *Dover Publications, 2nd edition,* 2004.

[13] T. Van Duzer and C. Turner, "Principles of Superconductive Devices and Circuits", *Prentice Hall*, *2nd edition*, 1998.

[14] J. Mazierska et al., "Influence of superconducting film thickness on resonant frequencies and Q-factor of the sapphire dielectric resonator and on resulting surface impedance of high T_c superconductors", *Proceedings of Asia-Pacific Microwave Conference*, 6-9 December, 1994, Tokyo, pp. 1069-1072. 1994.

[15] J. Mazierska, "Microwave Properties and Applications of HTS Materials: History and Progress", *Presentation at Yamagata University*, Nov, 2014.

[16] E. Rocas et al., "On the relation between the nonlinear surface impedance and the superfluid current density in High-Temperature Superconductors", *IEEE Trans Applied Superconductivity*, v. 21, no. 3, pp. 555-558, 2011.

[17] N. Klein et al., "The effective microwave surface impedance of high T_C thin films", *Journal of Applied Physics*, 67(11), pp. 6940-6945, 1990.

[18] N. Pompeo et al., "Measurements and removal of substrate effects on the microwave surface impedance of YBCO films on $SrTiO_3$", *Superc. Sci. Tech.*, 20(10), p. 1002, 2007.

[19] R. Glover and M. Tinkham, "Conductivity of superconducting films for photon ebnergies between 0.3 and $40kT_C$", *Phys. Rev.*, 108, pp. 243-256, 1957.

[20] P. Kobrin et al., *Physica C,* v. 176, p. 121, 1991.

[21] J. Ceremuga-Mazierska, "Trasmission of microwave signals through superconducting thin films in waveguides", *Supercond. Sci. Technol.*, v. 5, p. 371, 1992.

[22] E. Katawe et al., "Surface impedance measurements on high-T_C sup[erconductors using a far-infrared laser", *IEEE Trans Applied Superconductivity*, v. 7(2), pp. 1853-1856, 1997.

[23] A. Velichko et al., "Nonlinear microwave properties of high T_C thin films", *Superc. Sci. Technol.*, vol. 18, R24-R49, 2005.

[24] J. Mazierska, "Dielectric resonators as a possible standard for characterisation of high temperature superconducting films for microwave applications", *Journal of Supercond.*, vol. 10, no. 2, pp. 73-84, 1997.

[25] C.L. Bohn et al., "Radio frequency surface resistance of large-area bismuth strontium calcium copper oxide thick films on silver plates", *Appl. Phys. Lett.*, Vol. 55, No. 3, pp. 304. 1989.

[26] D. Kajfez and P. Guillon, "Dielectric Resonators", *Vector Fields*, 1990.

[27] Y. Kobayashi et al., "Microwave measurements of surface impedance of high-T_c superconductor", *IEEE MTT-S digest*, pp. 281-284, 1990.

[28] Z. Ma, "RF properties of high temperature superconducting materials", PhD thesis, G.L. Report No. 5298, *Edward L. Ginzton Laboratory, Stanford University*, May 1995.

[29] H. Piel et al., *Physica C*, v. 153, p. 1604, 1988.

[30] J. Carini et al., *Phys. Rev. B.*, v. 37, p. 9726, 1988.

[31] C. Wilker et al., "5GHz high-temperature superconductor resonators with high Q and low power dependence up to 90K", *Trans. Micr. Theory and Techn.*, v. 39(9), pp. 1462-1467, 1991.

[32] R. Taber, *Rev. Sci. Instrum*, v. 61, p. 2200, 1990.

[33] Y. Kobayashi and M. Katoh, *IEEE Trans MTT*, v. 33, p. 586, 1985.

[34] J. Krupka, *Proc. 5th Int. Conf. Dielectric Material and Appl.*, p. 322, 1980.

[35] B.W. Hakki and P.D. Coleman, "A dielectric resonator method of measuring inductive capacities in the millimetre range", *IEEE Trans. Microwave Theory Tech.*, Vol. MTT-8, pp. 402-410, July 1960.

[36] N. Klein et al, "Microwave surface resistance of epitaxial YBa$_2$Cu$_3$O$_7$ thin films at 18.7 GHz measured by a dielectric resonator technique", *Journal of Superconductivity*, Vol. 5, No. 2, pp. 195, April 1992.

[37] E. Ginzton, "Microwave measurements", *McGraw-Hill,* 1957.

[38] D. Kajfez, *IEEE Trans MTT,* v. 42, p. 1149, 1994.

[39] X. Ma, PhD Thesis, *Stanford University*, 1995.

[40] K. Leong, PhD Thesis, *James Cook University*, 2001.

[41] M. S. DiIorio et al., *Phys. Rev. B.*, v. 38, p. 7019, 1988.

[42] D. E. Oates et al., *J. Supercond.*, v. 3, p. 251, 1990.

[43] D.E. Oates et al, "Surface impedance measurements of superconducting NbN films", *Phys. Rev. B*, Vol. 43, No. 10, pp. 7655-7663, 1991.

[44] P. P. Nguyen et al., *Phys. Rev. B*, v. 48, p. 6400, 1993.

[45] N. Belk et al., *Phys. Rev. B*, v. 53, p. 3459, 1996.

[46] S. Angale, et al., *Appl. Phys. Lett.*, v. 54, p. 2710, 1989.

[47] S. Angale et al., *Phys Rev. B*, v. 44, p. 9764, 1991.

[48] B.W. Langley et al., "Magnetic penetration depth measurements of superconducting thin films by a microstrip resonator technique", *Rev. Sci. Instrum.*, Vol. 62, No. 6, pp. 1801, June 1991.

[49] A. Adreone et al., *J. Appl. Phys.*, v. 73, p. 4500, 1993.

[50] A. Adreone et al., *Phys. Rev. B*, v. 49, p. 6392, 1994.

[51] A. Porch et al., "Non-linear microwave surface impedance of patterned YBa$_2$Cu$_3$O$_7$ thin films", *Journal of Alloys and Compounds*, Vol. 195, No. 1-2, pp. 563-566, 1993.

[52] W. Rauch et al, *J. Appl. Phys.*, v. 73, p. 1866, 1993.

[53] C. Song, et al., *Phys. Rev. B,* v. 79, p. 174512, 2009.

[54] D. Oates et al., *IEEE Trans. Microw. Theory Tech.*, v. 39, p. 1522, 1991.

[55] K.C. Gupta et al., "Microstrip Lines and Slotlines", *Artech House*, 1979.

[56] K. Day et al., *Nature (London),* v. 425, p. 817, 2003.

[57] J. Zmuidzinas, *Annu. Rev. Condens. Matter Phys.,* v. 3, p. 169, 2012.

[58] A. Wallraff et al., *Nature (London),* v. 431, p. 162, 2004.

[59] M. Göppl et al., *J. Appl. Phys.*, v. 104, p. 113904, 2008.

[60] D. Oates, "Nonlinear befavior of superconducing devices", *Microwave superconductivity, edited by H. Weinstock and M. Nisenoff, Kluwert*, 2001.

[61] A. Portis et al., "Power and magnetic field-induced microwave absorption in Tl-based high Tc superconducting films", *Appl Phys Lett.,* v. 58, iss. 3, pp.307-09, 1991.

[62] T. Hylton et al., "Weakly coupled grain model of high-frequency losses in high Tc superconducting thin films", *Applied Physics Letters,* v. 53 pp.1343-1345, 1988.

[63] C. Attanassio et al., "Residual Surface Resistance of Polycrystalline Superconductors", *Phys Rev B,* v. 43, No. 7, pp. 6128-6131, 1991.

[64] J. Halbritter, "Rf residual losses, surface impedance, and granularity in superconducting cuprates", *J. Appl. Phys.,* v. 68, n. 12, pp. 6315-6326, 1990.

[65] J. Mazierska and M. Jacob, "High Temperature Superconducting Filters for Wireless Communication a chapter Novel Technologies for Microwave and Millimetre-Wave Applications", *edited by Jean-Fu Kiang, Kluwer Academic/Plenum Publishers*, pp. 123-152, 2003.

[66] W. Hackett et al., "Microwave flux-flow dissipation in paramagnetically-limited Ti-V alloys", *Phys. Lett.,* v. 24A, p.663, 1967.

[67] V. Berezin et al., "Magnetic-field dependence of the surface impedance in the mixed state of type-II superconductors", *Phys. Rev. B,* v. 49, no. 6, pp. 4331-4333, 1994.

[68] M. Tsindlekht et al., "Microwave properties of $YBa_2Cu_3O_{7-\delta}$ thin films in linear and nonlinear regime in a dc magnetic field", *Phys Rev B,* v. 61, pp. 1596-1604, 2000.

[69] A. Andreone et al., "Non-linear microwave properties of Nb_3Sn superconducting films", *J. Appl. Phys.*, v. 82, p. 1736, 1997.

[70] J. Delayen and C. Bohn, "Temperature, frequency, and rf field dependence of the surface resistance of polycrystalline $YBa_2Cu_3O_7$", *Phys Rev B,* v. 40, p. 5151, 1989.

[71] H. Xin et al., "Comparison of power dependence of microwave surface resistance of unpatterned and patterned YBCO thin films", *IEEE Trans Microwave Theory tech.*, 48, 1221, 2000.

[72] M. Hein, "Microwave properties of superconductors", *Microwave superconductivity, edited by H. Weinstock and M. Nisenoff, Kluwert*, 2001.

[73] D. Oates et al., "Nonlinear microwave surface impedance of YBCO films: latest results and present understanding", *Physica C: Superconductivity,* v. 372-376, Part 1, pp. 462-468, 2002.

[74] A. Velichko et al., "Non-linear Microwave Properties of High-Tc Thin Films - TOPICAL REVIEW", *Supercon. Sci. Technol.,* v. 18, pp. R24-R49, 2005.

[75] M. Hein, "High Temperature Superconductor thin films at microwave frequencies", *Springer*, 1999.

[76] J. Oates et al., "A nonlinear transmission line model for superconducting stripline resonators"", *IEEE Tran. Appl. Supercond.*, vol. 3, pp. 17-22, 1993.

[77] J. Delayen et al., *J. Superc.*, v. 3, p. 243, 1990.

[78] Y. Kobayashi et al., *IEEE Tran. Microwawe Theory Tech.*, v. 39, p. 1530, 1991.

[79] D. Cooke et al, *IEEE Tran. Mag.*, v. 27, p. 880, 1991.

[80] M. Hein et al, *J. Supercond.*, v. 3, p. 323, 1990.

[81] M. Hein, Dissertation, *University of Wuppertal*, 1992.

[82] H. Snortland, "Nonlinear surface impedance in superconductors", a dissertation, *Ginzton Laboratory Report,* no. 5552, pp. 1-159, 1997

[83] M. Jacob et al., "Modeling of nonlinear surface impedance of high Tc superconductors using an exponential vortex penetration model", *J. Supercond.*, v. 12, no. 2, p. 377, 1999.

[84] W. Fietz et al., *Phys. Rev. A*, v. 136, p. 335, 1964.

[85] P. Nguyen et al., *Phys. Rev. B*, v. 51, p. 6686, 1995.

[86] W. Diete et al., "Surface resistance and nonlinear dynamic microwave losses of epitaxial HTS films", *IEEE Trans Appl. Superc.*, v. 7, p. 1236, 1997.

[87] M. Lancaster, "Passive microwave device applications of HTS", *Cambridge*, 1997.

[88] J. Booth et al., "Simultaneous optimisation of the linear and nonlinear microwave resonse of YBCO films and devices", *IEEE Tran. Appl. Supercond.*, v. 9, no. 2, 1999.

[89] E. Gaganidze et al., "Nonlinear surface impedance of TBCCO thin films as a function of temperature, frequency, and magnetic field", *J. Appl. Phys.*, v. 93, no. 7, p. 4049, 2003.

CHAPTER 3

Review of lumped element modelling of microwave properties of HTS superconductors and superconducting resonators

As was discussed in Chapter 1, superconducting technologies have various applications in energy, transportation, and communication industries. The applications of HTS that are of interest in this thesis include microwave and high frequency filters for communication networks. As is known, the applications of HTS in this area have been limited so far to mobile base station networks affected by interference or specific purposes requiring ultimate performance. Additionally, applications have been limited to low RF power levels due to deterioration of performance caused by nonlinear effects as described in Chapter 2. Therefore, there is an obvious necessity for an enhanced CAD (computer-aided design) tool for simulations of HTS electronic circuits and systems that takes nonlinear HTS effects into account. To enable the CAD implementation, HTS lumped-element modelling is necessary that can be incorporated into existing software for simulations and design of HTS microwave filters.

Up to recently, the main progress in the development of CAD tools for superconducting electronics (SCE) has been achieved in enhancing calibration procedures for semiconductor instruments, instead of producing new technology specialised tools. The recent development in CAD field displays a preference for sizable and costly CAD applications, or instruments specifically designed for market based semiconductor CAD tools. Nevertheless, the momentum is also building for alternative open source or freeware circuit design tools to become widely available. Extensive research on the superconducting circuit design software, its accuracy and performance were conducted in the past in 1999 [1] and 2013 [2]. Following the

classifications used in [1] with some additions from [2] the SCE design software can be organised into several categories such as: circuit simulators, layout editors, circuit optimisers, inductance estimators, logic simulators, full–wave solvers, and layout synthesizers. Each listed category uses various design software packages, for example: *WRSpice*, *JSIM* and *JSPICE* for the circuit simulators; *MALT* and *COWBoy* for the circuit optimisers; *XIC*, *AutoCAD* and *Wavemaker* for the layout editors; *Sline* and *INDEX* for the inductance estimators, and others. As far as the scope of this dissertation is concerned, the full-wave solvers have been of interest, as they are needed for analog circuits and passive transmission lines where the investigation of scattering parameters of superconducting components is essential. Currently used commercial solvers are *FEKO* [3] – implemented for superconductor nanowire absorbance [4]; *HFSS* [5] – used for filters [6], microstrip lines [7, 8], and antennas [9]; *Sonnet* [10] – used for microstrip lines [8]; and *CST* [11] – implemented for antennas [9]. Most available applications implement special methods to simulate superconducting properties using the existing field solvers. However, this process makes computations very complicated, raising points regarding the suitability of used tools.

There is a substantial body of knowledge of circuit theory on analysis and design of resonators and filters. However, there are limited techniques as far as lumped element models of HTS and superconductors in general are concerned. Although certain methods listed above seem to be currently sufficient, purpose built superconducting models would enable better efficiency for the development for HTS circuits. The next subchapter provides a summary of existing body of knowledge in the field of modelling of superconducting phenomena.

3.1   Equivalent circuit representation of superconductors

An equivalent circuit for a superconductor can be determined based on its physical properties, as for any other type of material. As introduced in Chapter 2.1, a

simple way to describe the electrodynamics of superconductors was given by the London brothers in 1934, based on the phenomenological 'two-fluid' model of Gorter and Casimir [12]. According to the model, the charge carriers are divided into two subsystems – superconducting carriers of density n_s and normal electrons of density n_n. The superconducting carriers were associated later on with Cooper pairs of charge -2e and mass $2m_e$ [13]. The normal current J_n and the supercurrent J_S are assumed to flow in parallel, and the total current is the sum of J_S and J_n. J_S flows with no resistance and follows the London equations described in Chapter 2.1. In the two fluid model the conductivity of superconductor $\sigma_s = \sigma_1 - j\sigma_2$, and its impedance $Z_s = R_s + jX_s$, are complex values in the external electromagnetic field. Therefore, to represent a superconductor in the external field it is appropriate to model the superconductor as an equivalent electric network consisting of an active resistance and inductance connected in parallel [14], as shown in Fig. 3.1.
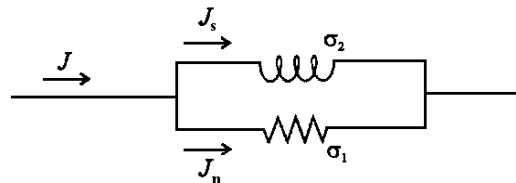
Fig. 3.1 Equivalent representation of the superconductor conductivity (after [14]).

Similarly, the surface impedance of a superconductor Z_S can be represented as a resistance and inductance connected in series [15], as illustrated in Fig. 3.2.

Fig. 3.2 Equivalent representation of the superconductor impedance (after [15]).

All electrons form Cooper pairs at zero temperature, while at finite temperatures - some pairs break into normal quasi-particles due to thermal effects. Cooper pairs produce an inductive channel, as shown in Fig. 3.1, while normal electrons create a resistive ohmic path for the electric current flow. The values of the

kinetic inductance and normal resistance of a superconductor are dependent on the density of Cooper pairs and normal electrons, defining the electromagnetic properties of the superconductor.

Other variation of the equivalent circuit model to represent a superconductor is illustrated in Fig 3.3 [16].
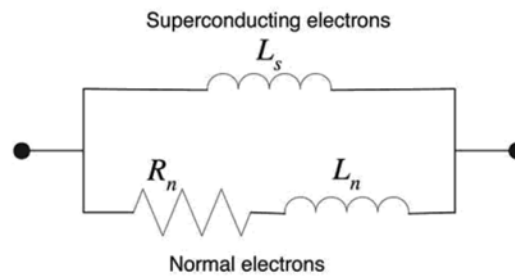
Fig. 3.3 Equivalent representation of the superconductor impedance (after [16])

The inductance L_S denotes the superconducting path, reflecting the flow of superconducting electrons. In more details - the resistance occurs due to the inertia of superconducting electrons, therefore when the electromagnetic field changes sign, the superconducting electrons are unable to adjust direction right away. Thus, the microwave current is modelled as an inductance L_S representing the current out of phase with the voltage.

The resistance R_n and inductance L_n represents the normal electron path. This path reflects the impedance of the normal electrons. The inductance produces a voltage across a superconductor causing the normal electrons to move, inducing currents in the normal channel and thereby generating dissipation. In case of a direct current and very low frequencies, the superconducting path shorts out the normal channel, leading to essentially zero resistance. It needs to be noted that the inductance L_n in the normal channel is often neglected which is similar to modelling the normal channel as nondispersive (frequency independent).

HTS materials have the extremely short coherence length ξ_0, making them very responsive to defects. When the defects get bigger than ξ_0 they are anticipated to become insulating or exhibit normal conductivity [14]. On the contrary, minor defects such as grain boundaries, were discovered to behave as Josephson junctions in High Temperature Superconductors [17], enabling the conduction of Cooper pairs past a boundary of thickness similar to ξ_0 [18]. The coupled-grain model was first presented in [19], postulating that the material was to be built of superconducting 'grains' linked by defects similar to Josephson junctions. This model, shown in Fig. 3.4, was implemented to analyse the surface impedance of polycrystalline YBCO thin films, where the magnetic field penetration at grain boundaries affected the inductance of weak links.
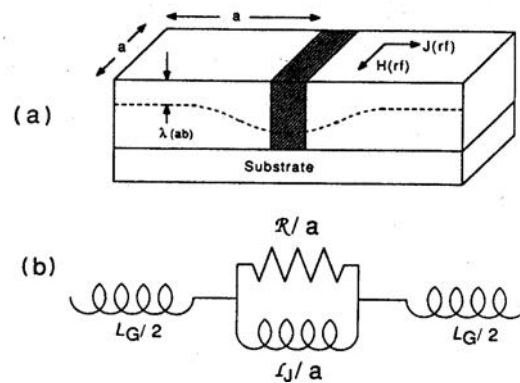
Fig. 3.4 (a) Superconducting film with grain boundary; (b) equivalent circuit of superconducting film with grain boundary structure (after [19]).

The weakly-coupled grain model has formed the basis for models which discussed specifically the nonlinear microwave losses of HTS films in RF fields. The adjusted coupled-grain model, that defines the initial raise of R_S and λ comparative to $H^2_{RF,}$ has been introduced in [20, 21] with the R_S dependence expressed as:

$$R_S(H) = R_S(0)\left[1 + b_r H^2_{rf}\right] \tag{3.1}$$

where $R_S(H)$ and $R_S(0)$ are the surface resistance at H_{RF} field and at zero field respectively, and b_r is the fitting parameter. Oates *et al.* [21] has modified the coupled-grain model to incorporate nonlinear effects via the junction dependence on the RF current. The model does not define the principle of the defects and the 'grains' are simply described as areas of defect free order. The authors further suggested that the YBCO thin films can be characterised by the grains in a series connection with Josephson junctions. Fig. 3.5 illustrates the simplified model and the equivalent circuit used for calculations of the nonlinear surface impedance.
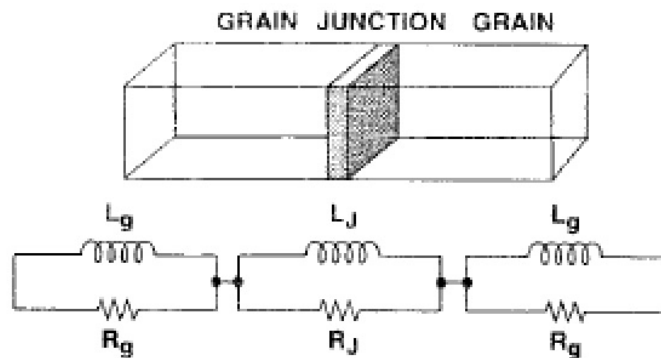
Fig. 3.5 Modified coupled-grain model (top) and equivalent circuit to calculate Z_S of the YBCO thin films (after [21]).

In this circuit, resistors in parallel combination with inductors model the grains. This coupled-grain equivalent circuit model represents in fact the usual two-fluid model for an ideal superconductor, where R_g and L_g are associated with the penetration depth and resistivity. The junctions are also modelled (the same as in Fig. 3.4) by a resistance in parallel with an inductance, however the physical nature of these elements is different from the grains. R_j is the shunting resistance and L_j is the junction inductance.

A hysteretic loss model was proposed in [22] and is based on calculations of Norris [23] derived from the Bean's critical state model [24]. The hysteresis model has been combined by Nguyen *et al.* [25] with the weakly coupled grain model. The model proposes that at certain value of H_{RF} the behaviour of the surface resistance varies, and losses start rising quicker than the primary quadratic rate. It is suggested that vortices begin to enter the superconductor in this high magnetic field, and the

expansion in losses occurs due to hysteresis losses, which become added to the coupled-grain model losses.

Halbritter [26, 27] explained the nonlinear phenomenon in superconducting materials by considering the formation of vortices in weak links with the vortex concentration determined by H_{RF}. The penetration of vortices into grains and fluxoid motion have been considered as possible factors contributing to the nonlinear effect.

Wosik *et al.* [28] and Hein *et al.* [29] attributed nonlinear losses to the global heating effects. The thermal power dissipated P_{diss} in YBCO superconducting films at high RF magnetic fields was given as [29]:

$$P_{diss} = 1/2\{R_{def}A_{def} + R_S(A - A_{def})\}B_S^2 \tag{3.2}$$

where R_{def} and A_{def} are the surface resistance and the area of defects respectively, B_S is the applied magnetic field, and A is the initial area.

Due to the improved quality of High Temperature Superconductors it was acknowledged that the model of granular HTS films might be unsuitable to describe the surface impedance. As a result, an alternative transmission line model was proposed by Portis and Cooke in [30], that accounts for microwave field penetration within the junctions and grains. The model regards the grain boundary junction being operational in the form of a stripline between the two superconducting grains, as illustrated in Fig. 3.6.
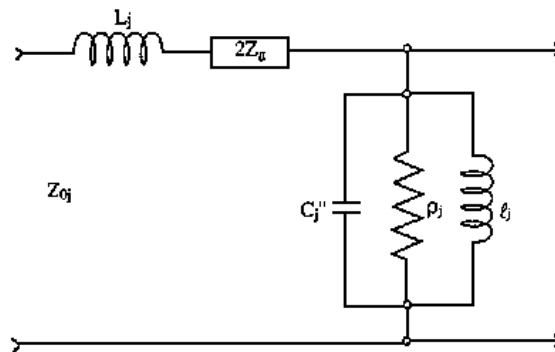

Fig. 3.6 Transmission line representation of an intergranular junction (after [30]).

In this model, the surface impedance Z_g characterises the granular region, and the inductance L_j denotes the flux within the junction. The capacitance C_j, inductivity l_j, and resistivity ρ_j characterise the current flow across the junction. This approach was able to describe the surface impedance $Z_S(T,H,f)$ in relation to parameters of the junction, as well as various levels of granularity.

In respect to applications of HTS films in microwave systems, as was stated in Chapter 2.2, the field dependence of the surface resistance has become a main question. As was shown before in this chapter, the quadratic field dependence of Z_S prevailed to be the main characteristic of the coupled-grain model. However, in view of the current understanding, which showed various mechanisms responsible for nonlinearities, the generalisation of using only the quadratic field dependence of R_S and L_S could not be justified. In this manuscript, the vortex penetration and vortex movement in a superconductor is considered as dominant factors causing the increase in losses in HTS films under the high RF magnetic fields ($H_{RF} > H_{C1}$). Thus, to model the nonlinear surface impedance of a superconductor, three types of RF field dependences have been analysed and assessed together, such as linear, quadratic and exponential. This approach enabled the development of a comprehensive lumped element model of HTS materials that takes into account dependence of nonlinear effects on elevated RF power levels. The results of this theoretical contribution are presented in Chapter 4.

Having discussed so far the equivalent circuit representation of a superconductor, the review of equivalent modelling of resonance circuits is presented in the next section.

3.2   RLC modelling of resonance systems

As is known, an ideal resonance circuit has infinite number of resonant frequencies which correspond to different wave modes excited in the network. In

systems with high quality factors, these resonant frequencies are located far enough from each other in relation to the width of the resonance curve. In this case, according to the known electromagnetic theory (see for example [31]), any resonator can be presented as either a series or a parallel equivalent RLC lumped element circuit. The frequency dependence of the normalised imaginary part $\overline{\mathbf{X}}$ (reactance) of the impedance (Z=R+jX), for an ideal resonance system without loses (R=0), can be presented as a graph shown in Fig. 3.7. [31].
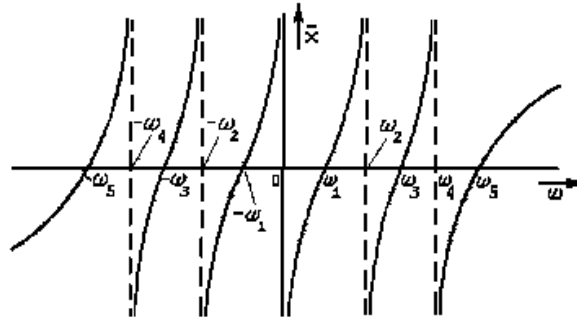
Fig. 3.7 Frequency dependence of microwave resonator reactance (after [31])

As illustrated, $X(-\omega) = -X(\omega)$.

The equation defining $\overline{\mathbf{X}}$ in a general format can be expressed as

$$\overline{\mathbf{X}} = \mathbf{A}\omega \frac{(\omega^2 - \omega_1^2)(\omega^2 - \omega_3^2)...(\omega^2 - \omega_{2n-1}^2)}{\omega^2(\omega^2 - \omega_2^2)(\omega^2 - \omega_4^2)...(\omega^2 - \omega_{2n-2}^2)} \tag{3.3}$$

where ω_2, ω_4, … ω_{2n-2} are the positive poles, $-\omega_2$, $-\omega_4$, … $-\omega_{2n-2}$ are the negative poles, ω_1, ω_2, … ω_{2n-1} are the positive zeros, $-\omega_1$, $-\omega_2$, … $-\omega_{2n-1}$ are the negative zeros, A is a constant.

On the basis of the theory of residues of complex functions [31], the equation (3.3) can be represented near the reactance poles when $X \rightarrow \infty$ as

$$\overline{\mathbf{X}} = \mathbf{L}\omega + \frac{\mathbf{a}_0}{\omega} + \frac{2\mathbf{a}_2\omega}{\omega^2 - \omega_2^2} + ... + \frac{2\mathbf{a}_{2n-2}\omega}{\omega^2 - \omega_{2n-2}^2} \tag{3.4}$$

where a_i denotes the residues of the given function near its corresponding poles.

An equivalent network of the equation (3.4) corresponds to a series representation of parallel L_iC_i circuits as shown in Fig. 3.12.
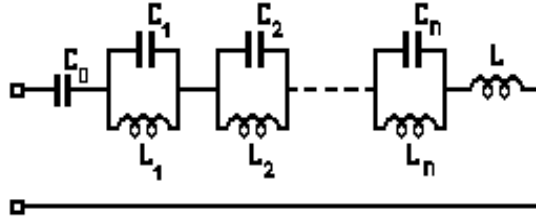
Fig. 3.8 Equivalent circuit for eqn. (3.4) (after [31])

The corresponding elements of the circuit in Fig. 3.8 can be expressed as:

$$C_0 = -1/a_0, \quad C_i = -1/2a_i, \quad \omega_{2i}^2 = 1/L_iC_i, \quad L = A.$$

The values of the inductance L_i and capacitance C_i are determined as a particular set for each resonant frequency.

The normalised reactive admittance, $\overline{b} = -1/\overline{X}$, has poles near zeros of the function $X(\omega)$. The equation for $\overline{b}$ can be written as

$$\overline{b} = -\frac{1}{A\omega} \frac{\omega^2(\omega^2 - \omega_2^2)(\omega^2 - \omega_4^2)...(\omega^2 - \omega_{2n-2}^2)}{(\omega^2 - \omega_1^2)(\omega^2 - \omega_3^2)...(\omega^2 - \omega_{2n-1}^2)} \tag{3.5}$$

Following the residue theory [31], the equation (3.5) can be represented as:

$$\overline{b} = C\omega + \frac{b_0}{\omega} + \frac{2b_1\omega}{\omega^2 - \omega_1^2} + ... + \frac{2b_{2n-1}\omega}{\omega^2 - \omega_{2n-1}^2} \tag{3.6}$$

where b_i is the residues of the given function near its corresponding poles.

An equivalent network of the eqn. (3.6) corresponds to a parallel representation of series L_iC_i circuits, as shown in Fig.3.9.
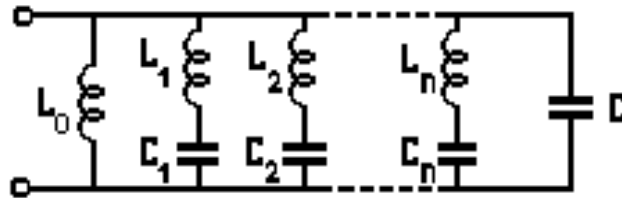

Fig. 3.9 Equivalent circuit for eqn. (3.6) (after [31])

The corresponding elements of the circuit (Fig.3.9) can be represented as:

$$L_0 = -1/b_0, \; L_i = -1/2b_i, \; \omega_{2i-1}^2 = 1/L_iC_i, \; C = -1/A.$$

The equivalent circuits presented above are the foundation for successful lumped element modelling of microwave resonant systems.

For conventional metallic circuits, when modes are separated and frequency range is limited, only one set of LC circuits is necessary. To take into account energy dissipation effects, equivalent networks for parallel and series models should involve a resistor representing losses, as shown in Fig. 3.10.
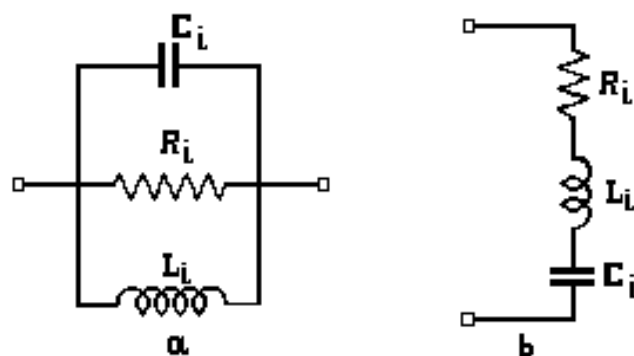
Fig. 3.10 Parallel (a) and series (b) equivalent lumped element networks for a resonator taking into account dissipation effects (after [31])

In this case, the quality factor of the parallel resonance circuit (Fig. 3.10 a) can be expressed as:

$$Q_i = \omega_{2i} C_i R_i \qquad (3.7)$$

and the quality factor of the series circuit (Fig.3.10 b) as:

$$Q_i = \omega_{2i-1} \frac{L_i}{R_i} \qquad (3.8)$$

It needs to be mentioned that conventional metallic and HTS microwave resonators are usually single mode for practical applications. However, for conventional resonators and filters, it has been sufficient for a while that the dissipation is modelled with a single resistor of constant value. Nevertheless, for HTS resonators and filters, the single resistor modelling approach is not adequate, thus, a more comprehensive model of HTS resonating system is required, as mentioned earlier in section 3.1.

In practical applications and microwave characterisation of HTS materials a resonator needs to be coupled to a source and to a load. As a result of incorporating the resonator into the loaded system, the measured loaded quality factor Q_L will differ from the unloaded Q_0-factor, as stated in Chapter 2, namely $Q_0 = Q_L(1+\beta_1+\beta_2)$, where β_1 and β_2 are coupling coefficients of the resonator system. The coupling coefficients are based on energy leakage through the input and output port respectively: $\beta = P_{ext}/P_0 = Q_0/Q_{ext}$, where P_{ext} is the external dissipated power and Q_{ext} is the Q-factor of the resonator circuitry.

In order to identify coupling of resonators in CAD microwave software simulations, a coupling matrix identification needs to be performed [32]. For this task, a full wave optimisation of the complete structure is required. The optimisation can include different functions, for example the scattering parameters computed at many

[33] or few [34] frequency points, an extracted coupling matrix [35, 36], as well as poles and zeros extracted from models of S_{11} and S_{21} [37].

Possibly the most capable method involves the identification of the coupling matrix after each separate full-wave investigations [32]. However, there are certain restrictions in application of this approach discussed in details in [32] with alternative solutions also discussed there. It needs to be mentioned that detailed consideration of coupling solutions involving CAD systems is outside of the scope of this thesis.

In relation to practical (not CAD) techniques developed in the past to determine the unloaded Q_0 factors of microwave resonance systems, they were not always applicable for microwave resonators placed in vacuum/cryogenic environments. The reasons for that were practical constraints of the cryogenic systems preventing measurements at locations appropriate for the Q_0-factor techniques, and also proper calibration of components inside a cryocooler using a Vector Network Analyser (VNA). As was stated in Chapter 2.2, the easiest method to get the loaded Q_L factor from S parameter measurements is using the 3dB method, that is implemented in VNA. However, in practical measurements of S parameters, the existence of noise and the fixed resolution of VNA result in a noisy S_{21} trace. This leads to inaccurate results if errors are not taken into account. It also needs to be mentioned, that most S-parameter techniques were developed for the presence of lossless coupling, leading to inaccuracies due to the always lossy coupling in practical measurements. There are also other practical effects that need to be accounted for, such as crosstalk effects and impedance mismatch [38]. To remove these uncertainties in obtaining the loaded Q_L-factor, multi-frequency measurements are required.

One of the most precise multi-frequency measurement methods is based on fitting a curve to measured Q-circles [38]. This technique enables to obtain accurate coupling coefficients and Q_L-factor. So far a number of methods have been developed such as the S_{11} reflection mode method [38], the S_{21} phase method for transmission mode resonators [39], and Transmission Mode Q-Factor (TMQF) technique [40].

In the phase technique, developed by Stanford University and Hewlett Packard [39], the loaded Q_L-factor is identified from the phase of S_{21} parameter and is founded on a transmission mode resonator with a series equivalent model pictured in Fig 3.11.
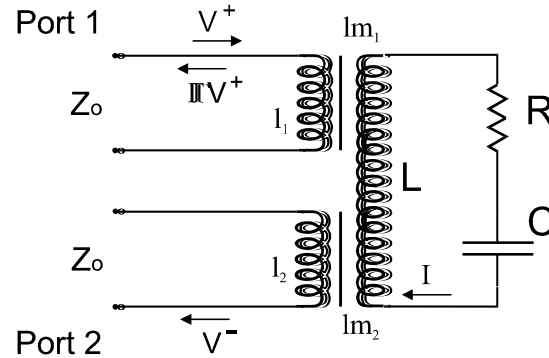
Fig. 3.11 A series RLC circuit of a microwave resonator (after [39])

However, the phase method has a substantial limitation, as it is only suitable for extremely weak coupling conditions, it was designed for S_{21} measurements only.

The technique described in [38], sometimes referred as the Kajfez technique, is based on measurements of S_{11} parameter and is suitable to reflection mode resonators. Using this technique the unloaded Q_0-factor can be obtained with very high precision of better than 1 percent. However, it was designed for reflection mode resonators only and is not applicable to measurements of S_{11} (or S_{22}) coefficients for transmission mode studies.

More precise method, called TMQF technique, was developed in [40] based on comparable circle fitting procedure and circuit theory implemented in the Kajfez technique. The TMQF technique enables to identify the loaded Q_L factor and the coupling coefficients for transmission mode resonators with lossy coupling. This technique has been implemented in this dissertation to accurately obtain unloaded Q_0 factor in the course of experimental investigations of microwave properties of YBCO and NdBCO superconductors, with obtained results presented in Chapter 5.

In relation to RLC circuits of loaded resonators, some examples of various model combinations are presented below. A review of cavities presented in the investigation [41] of microwave properties of HTS was followed by a lumped element study of transmission lines and resonators in terms of their coupling coefficients [41]. An example of the equivalent circuit of a two-port resonator coupled to input and output transmission lines is presented in Fig. 3.12.
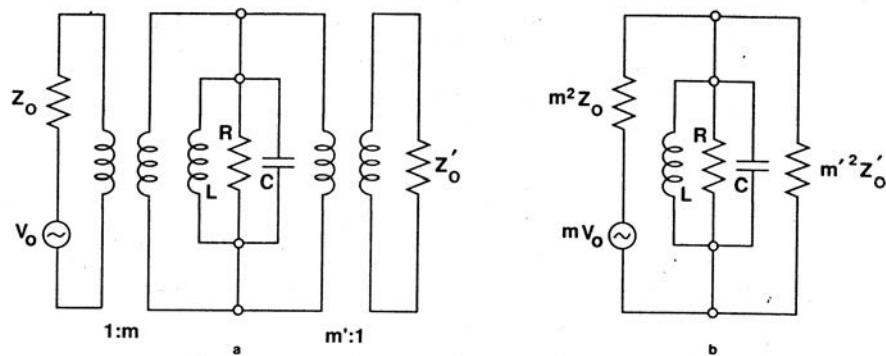
Fig. 3.12 (a) Equivalent circuit of a two-port resonator coupled to input and output transmission lines. (b) Transformation of the driving voltage and loads into shunt with the resonator (after [41])

The resistance R describes the dissipation of electromagnetic energy, the inductance L is related to the magnetic energy, and the capacitor C is linked with the electrical energy of the resonator. The microwave source is presented by the voltage V_0 matching to the input line. In parallel with the resistance R is the load resistances $m^2 Z_0$ and $m'^2 Z'_0$.

The following circuit representation of a practical dielectric resonator was proposed in [42] and shown in Fig. 3.13. This circuit is based on the TMQF technique introduced before in this Chapter.
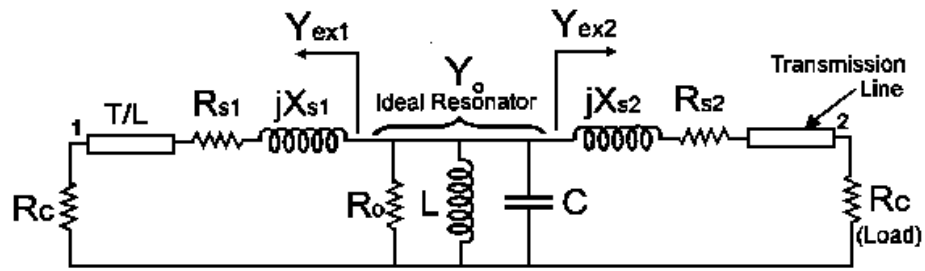
Fig. 3.13 Equivalent model of transmission resonator system (after [42])

A resonator is presented by the parallel RLC network. The coupling losses of each port are represented by resistances R_{S1} and R_{S2}, and the coupling reactances are simulated by X_{S1} and X_{S2}. The transmission lines of each port have characteristic impedances equal to the load R_C.

Calculations of equivalent series network for a resonator utilised in investigations of the electron spin resonance effect were presented in [43]. Two variations of the equivalent resonant circuit are illustrated in Fig. 3.14 and Fig. 3.15. The first case involves the series circuit connected to the input and output coupling networks through the transformer representation, while in other case the coupling parts are integrated into the series circuit itself as shown in Fig. 3.15.
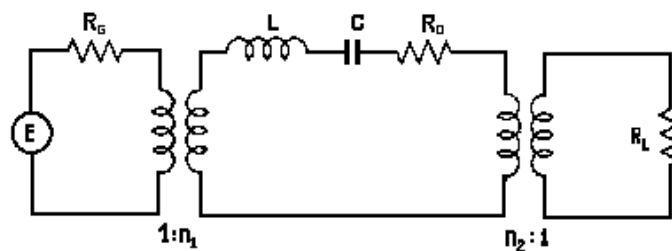
Fig. 3.14 Equivalent series circuit of resonator connected to the input and output coupling networks (after [43])
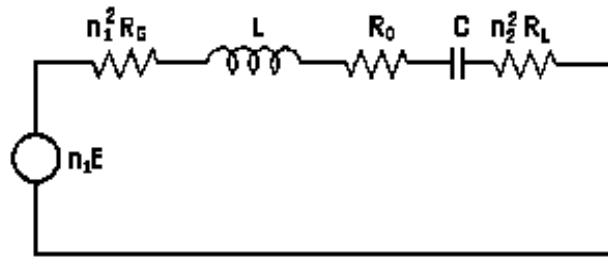
Fig. 3.15 Equivalent series circuit with integrated coupling parts (after [43])

A simplified series equivalent circuit for analysis of transmission microstrip resonators was used in [44], where nonlinearities occurring in a half-wavelength resonator based on a superconducting microstrip line were discussed (Fig. 3.16 and 3.17).
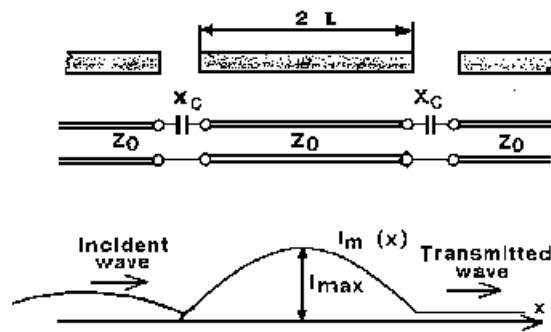
Fig. 3.16 Transmission line with current distribution (after [44])
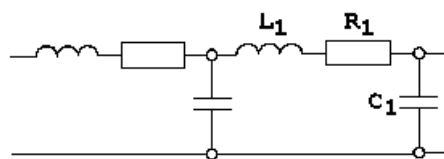
Fig. 3.17 Equivalent circuit of transmission line (after [44])

A series equivalent circuit was employed in the application to harmonic balance algorithms for the nonlinear modelling of HTS devices [45]. Fig. 3.18 shows an equivalent circuit of a transmission line section with incorporated nonlinear elements that account for nonlinearities in HTS.
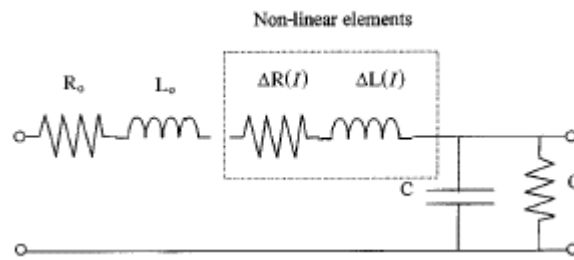
Fig. 3.18 Equivalent circuit of a transmission line section (after [45])

A complete network suggested in [45] to analyse the response of a High Temperature Superconducting nonlinear transmission line to a signal source is shown in Fig. 3.19.
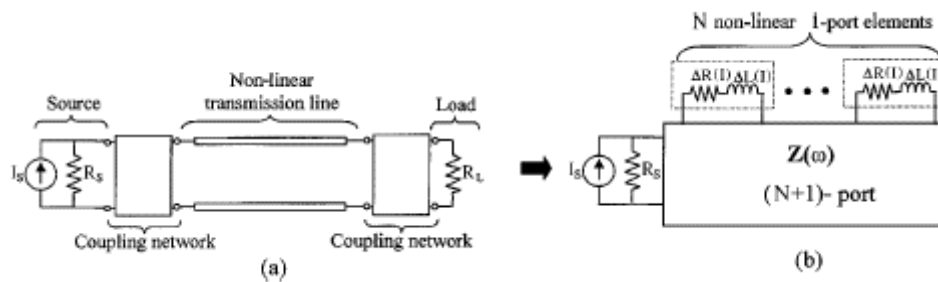
Fig. 3.19 Equivalent circuit of HTS (nonlinear) transmission line consisting of linear network with N+1 ports loaded with N nonlinear 1-ports (after [45])

Nonlinear effects in HTS using an equivalent circuit of HTS line resonators shown in Fig. 3.20 were analysed in [46]. The equivalent network was simulated to investigate intermodulation distortion effects in resonators. $\Delta R(i)$ and $\Delta L(i)$ are nonlinear functions of the current i.
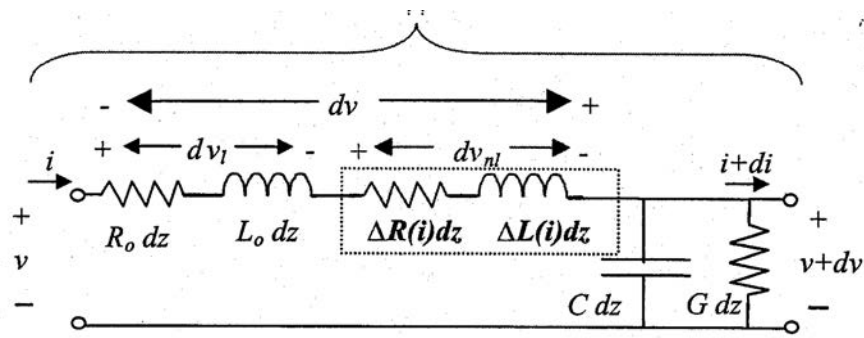
Fig. 3.20 Equivalent circuit to research Inter Modulation Distortion (IMD) in resonators (after [46]).

As can be seen from the review presented in this chapter, all elements of resonators and superconducting samples under test can be represented using resonant lump element circuits. Very basic equivalent circuit models of resonators and superconductors, as often presented in fundamental books on microwave engineering, are normally inadequate for the development of precise RLC model to represent nonlinearities in HTS. This is because they do not sufficiently describe the behaviour of superconductors under high RF currents. Modelling of the nonlinear properties of the resonators and superconducting samples can be achieved when the equivalent circuit parameters R, L and C are represented as nonlinearly dependent on either the superconducting current I_S or the magnetic field H_{RF}. As was presented in this Chapter, the increase in RF losses in HTS films can be attributed to several mechanisms which can occur under high RF currents, for example weak link losses, microwave heating, vortices in weak links and a bulk vortex penetration. Opinions among research community remain divided on which phenomenon can be considered as the major factor. As a result, there is a difference in presentation of nonlinear dependences of the resistance and inductance in equivalent circuits by various scientific groups. It was shown that linear, quadratic and exponential dependences can be used to model nonlinearities. Those dependences have been investigated separately and no unified comparable analysis was proposed in the past. In addition, there is a lack of an adequate RLC model to simulate nonlinear responses accurately at elevated power levels. Therefore, an accurate RLC equivalent circuit model to represent nonlinearities in HTS at high RF currents is necessary.

The development of accurate techniques to model nonlinear effects at elevated power levels of microwave resonators demands skilled methodologies and tactics in measurement procedures, circuit analysis and mathematical techniques. In addition, an advanced understanding of physical mechanisms responsible for nonlinear effects is essential. In the next Chapter a development of an advanced lumped element model of HTS materials reflecting dependence of nonlinear effects on RF power is presented.

In addition, it needs to be mentioned that there is also a distributed element model approach which assumes that circuit elements are distributed continuously throughout the material of the circuit. This approach is mostly used in circuits where the wavelengths of the signals are comparable with dimensions of the components. However, the distributed models are not fully suitable for microwave characterisation of materials, especially superconductors, embedded in a resonator structure, as radiation losses are high and the quality factor is small in the distributed model approach. One of the scientific goals of this thesis was to investigate/simulate microwave properties of superconducting materials, while the distributed model is more appropriate for modelling of actual devices, for example microwave planar filters.

REFERENCES

[1]   K. Gaj et al., "Tools for the computer-aided design of multigigahertz superconducting digital circuits," *IEEE Trans. Appl. Supercond*., vol. 9, no. 1, pp. 18–38, 1999.

[2]   C. Fourie and M. H. Volkmann, "Status of superconductor electronic circuit design software," *IEEE Trans. Appl. Supercond*., vol. 23, no. 3, 2013.

[3]   EMSS, 3 Meson Street, Technopark, Stellenbosch, 7600, RSA.

[4]   A. D. Semenov et al., "An energy-resolving superconducting nanowire photon counter," *Supercond. Sci Technol*., vol. 20, pp. 919-924, 2007.

[5]   ANSYS, Inc., 275 Technology Drive, Canonsburg, PA 15317, USA.

[6]   N. Takeuchi et. al., "3D simulation of superconducting microwave devices with an electro-magnetic field simulator," *Physica C*, vol. 469, pp. 1662-1665, 2009.

[7]   V. Belitsky, et. al., "Superconducting microstrip line model studies at millimetre and sub-millimetre waves," *Int. J. Infrared Milli*., vol. 27, pp. 809-834, 2006.

[8]   M. Rafique et. al., "Optmization of superconducting microstrip interconnects for rapid single-flux-quantum circuits," *Supercond. Sci. Technol*., vol. 18, pp. 1065-1072, 2005.

[9]   D. Rauly et. al., "Design of two-band 150-220 GHz superconducting bolometric detection structure," *PIERS Online*, vol. 4, pp. 671-675, 2008.

[10]   Sonnet Software, 100 Elwood Davis Rd., N.Syracuse, NY 13212, USA.

[11]   CST, 492 Old Connecticut Path, Framingham, MA 01701, USA.

[12]   C. Gorter and H. Casimir, "On superconductivity I", *Physica 1*, no. 4, pp. 306-320, 1934.

[13]   L. N. Cooper, Bound Electron Pairs in a Degenerate Fermi Gas, *Phys. Rev.,* vol. **104**, pp. 1189-1190, 1956.

[14]   M. Lancaster, "Fundamental Consideration of Superconductors at Microwave Frequencies", Microwave Superconductivity edited by H. Weinstock and M. Nisenoff, *NATO Science Series E: Applied Science, Kluwer Academic Press,* v. 375, pp. 1-20, 2001.

[15]   M. Trunin, "Microwave Frequency Surface Impedance of High-T$_C$ Single Crystals", *Uspekhi Fiz Nauk,* v. 168, no. 9, pp. 931-952, 1998.

[16]   D. Oates, "Microwave measurements of fundamental properties of superconductors", *Chapter 8 in "100 Yeas of Superconductivity", edited by H. Rogalla and P. Kes*, 2011.

[17]   P. Chaudhari et al., Direct measurement of the superconducting properties of single grain boundaries in Y$_1$Ba$_2$Cu$_3$O$_{7-\delta}$, Phys. Rev. Lett. V. 60, iss. 16, pp. 1653-1656, 1988.

[18]   A. Barone and G. Paterno, "Physics and Applications of the Josephson Effect", *Wiley, New York*, 1982.

[19]   T. Hylton et. al., "Weakly Coupled Grain Model of High-Frequency Losses in High T$_C$ Superconducting Thin Films", *Appl Phys Lett,* v. 53, no. 14, pp. 1343-1345, 1988.

[20]   P. Nguyen et al., "Nonlinear Surface Impedance for YBa$_2$Cu$_3$O$_{7-x}$ Thin Films: Measurements and Coupled-Grain Model", *Phys. Re. B.,* v. 48, p. 6400, 1993.

[21]   D. Oates et al., "Nonlinear surface imperdance of YBCO thin films: Measurements, Modeling, and Effects in devices", *J of Supercond.*, v. 8., no. 6, p. 725, 1995.

[22]   S. Sridhar, Nonlinear microwave impedance of superconductors and ac response of the critical state, *Appl. Phys. Lett.,* vol. **65,** no. 8, pp. 1054-1056, 1994.

[23]   W. Norris, Calculation of hysteresis losses in hard superconductors carrying ac: isolated conductors and edges of thin sheets, *J. Phys D*, v. 3, p. 489, 1967.

[24]   C. Bean, Magnetization of hard superconductors, *Phys. Rev. Lett*, v. 8, p. 250, 1962.

[25]   P. Nguyen et. al., "Microwave hysteretic losses in YBCO and NbN thin films", *Phys. Rev. B,* v. 50, p. 6686, 1995.

[26]   J. Halbritter, RF residual losses, surface impedance, and granularity in superconducting cuprates, *Appl. Phys.*, v. 68, p. 6315, 1990.

[27]   J. Halbritter, On extrinsic effects in the surface impedance of cuprate superconductors by weak links, *Appl. Phys.*, v. 71, p. 339, 1992.

[28]   J. Wosik et al., Thermally induced nonlinearities in the surface impedance of superconducting YBCO thin films, *IEEE Trans. Appl. Supercond.*, v. 7, p. 1470, 1997.

[29]   M. Hein, Progress, properties and prospects of passive high-temperature superconductive microwave devices in Europe, *J. Supercond.*, v. 10, p. 109, 1997.

[30]   A. Portis and D. Cooke, "Superconducting stripline model of integranular flux penetration", *Supercond. Sci. Technol.*, v. 5, p. 395, 1995.

[31]   J. Altman, "Microwave Circuits", *Van Nostrand Princeton*, 1964.

[32]   P. Kozakowski, "Quadratic programming approach to coupled resonator filter CAD", *IEEE Trans. On Microwave. Theory and Tech.*, v. 54, no.11,p. 3906, 2006.

[33]   F. Arndt et al., "Automated design of waveguide components using hybrid mode-matching/numerical EM building-blocks in optimization-oriented CAD frameworks-state of the art and recent advances", IEEE Trans. Microw. Theory Tech., vol. 45, no. 5, pp. 747-760, 1997.

[34]   S. Tao et al., "Full-wave design of canonical waveguide filters by optimization", IEEE Trans. Microw. Theory Tech., vol. 51, no. 2, pp. 504-511, 2003.

[35]   S. Bila et al., "Direct electromagnetic optimization of microwave filters", IEEE Micro, vol. 2, pp. 46 – 51, 2001.

[36]   M. Ismail et al., "EM-based design of large-scale dielectric-resonator filters and multiplexers by space mapping", IEEE Trans. Microw. Theory Tech., vol. 52, no. 1, pp. 386 – 392, 2004.

[37]   A. Lamperez et al., "Efficient electromagnetic optimization of microwave filters and multiplexers using rational models", IEEE Trans. Microw. Theory Tech., vol. 52, no. 2, pp. 508 – 521, 2004.

[38]   D. Kajfez, "Q Factor", Vector Fields, 1994.

[39]   Z. Ma, "RF properties of high temperature superconducting materials", PhD thesis, G.L. Report No. 5298, Edward L. Ginzton Laboratory, Stanford University, May 1995.

[40]   K. Leong. "Precise measurements of surface resistance of high temperature superconducting thin films using a novel method of Q-factor computations for sapphire dielectric resonators in the transmission mode", PhD thesis, James Cook University, 2000.

[41]   A. Portis et al., "RF Properties of High-Temperature Superconductors: Cavity Methods", *Journal of Superconductivit,* v. 3, no. 3, pp. 297-304, 1990.

[42]   K. Leong and J. Mazierska, "Accurate Measurements of Surface Resistance of HTS Films Using a Novel Transmission Mode Q-Factor Technique", *Journal of Superconductivity,* v. 14, no. 1, pp. 93-103, 2001.

[43]   C. Poole, "Electron spin resonance", *John Wiley & Sons NY*, 1967.

[44]   O. Vendik et al., "Modeling, simulation, and measurement of nonlinearities in superconducting lines and resonators", *Journal of Superconductivity,* v. 10, no. 2, pp. 63-71, 1997.

[45]   C. Collado C et al., "Harmonic Balance Algorithms for the Nonlinear Simulation of HTS Devices", *Journal of Superconductivity: Incorporating Novel Magnetism*, v. 14, no. 1, pp. 57-64, 2001.

[46]   J. Mateu et al., "Nonlinear performance characterization in a 8-pole quasi-elliptic bandpass HTS filter", *Proceedings of HTSHFF-2004 Spain*, 2004.

CHAPTER 4

Development of a lumped element model describing nonlinear properties of HTS materials for Computer Aided Design (CAD)

The main subject considered in this chapter is the development of a lumped element model of superconducting resonator, which takes nonlinear properties of HTS materials into consideration. This model needed to be relatively simple, so it could be implemented within a CAD tool that can be used for design of superconducting devices with more precise characteristics. To the author's knowledge, there is currently no commercial CAD tool available that takes into account nonlinear effects.

During the model development, there were two separate topics to consider. The first topic was relatively simple - the modelling of a resonator. The second topic was more complex – the modelling of high temperature superconductors exhibiting nonlinear properties that depend on RF power. The basic model of HTS – the two fluid model [1] and its lumped element equivalent circuit [2], as well as a modified circuit [3], are not able to reflect the nonlinear properties of HTS materials due to constant values of their elements.

As discussed in Chapter 3, nonlinear power effects result in nonlinear surface impedance, harmonic generation and two tone intermodulation distortion. Different RF power dependences (linear, quadratic, exponential) of surface resistance R_S on RF magnetic field based on observed characteristics have been proposed by separate research groups [4-9], as described in chapter 3. In this chapter, all three dependences (linear, quadratic, exponential) have been applied to the superconducting circuit elements of the equivalent models for more complete analysis. A comparative analysis

of three functional dependences and an identification of model parameters are also presented. This chapter also describes one of the possible approaches to extend an advanced lumped element model of a superconducting resonator to represent nonlinear effects applicable for wide range of RF power level.

4.1 Equivalent lumped element models of superconducting resonators

As it is well known from the circuit theory (also discussed in Chapter 3), two basic lumped element RLC circuit representations can be used for modelling of microwave electromagnetic responses of any resonator [10]. Therefore, microwave resonators, including the Hakki-Coleman dielectric resonator, considered in this thesis, can be represented as either a parallel or a series RLC network (see Fig. 4.1), where L and C are inductance and capacitance of the resonator, and the resistance R represents losses of the resonator related to cavity walls, dielectric (if any), and top/bottom plates.
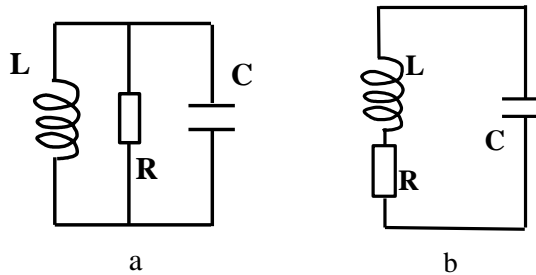


Fig. 4.1 Parallel (a) and series (b) circuits representing a microwave resonator.

The series RLC circuit has been selected for the work described in this thesis, so the lower the resistance of the resonator, the higher Q-factor (4.1) of the resonator.

$$Q_{0(ser)} = \frac{\omega_0 L}{R} = \frac{\omega_0}{2\alpha}; \quad \omega_0 = \frac{1}{\sqrt{LC}}; \quad \alpha = \frac{R}{2L} \tag{4.1}$$

where $Q_{0(ser)}$ is the quality factor of a series circuit, ω_0 – resonant frequency, and α - attenuation coefficient.

The quality factor Q of the Hakki-Coleman dielectric resonator with HTS plates, used in this thesis, is determined by the surface resistance of superconducting plates, surface resistance of metallic walls R_{met} and loss tangent of the dielectric $\tan\delta$, as repeated below after eq. (2.2.18):

$$\frac{1}{Q_0} = \frac{R_S}{A_S} + \frac{R_{met}}{A_{met}} + \frac{\tan\delta}{A_{diel}}$$ (4.2)

As discussed in Chapter 3, the basic model of High Temperature Superconductor is the two-fluid model, as shown in Fig. 4.2. The inductive part of the circuit denotes superconducting electrons and the resistive part is responsible for normal electrons in HTS materials.
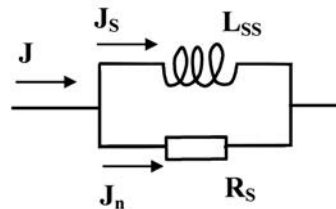
Fig. 4.2 Equivalent representation of a superconductor based on the two-fluid model (after [11] with element notations changed for clarity).

However, this equivalent circuit (Fig. 4.2) has a number of drawbacks such as that the reactance ωL_{SS} can be short-circuited by surface resistance R_S at T=0 due to the fact that the at temperatures close to absolute zero, the losses in a superconductor are very small and the resistance of normal electrons R_S is close to zero. It also needs to be mentioned that the equivalent diagram in Fig. 4.2 models the normal current flow path as nondispersive (frequency independent). Hence, the author of this dissertation proposed that an additional element L_{Sn} to be added to the parallel combination of L_{SS} and R_S. The inductance L_{Sn} can be seen as related to the frequency

dependent flow of normal electrons under the influence of applied external RF magnetic field.

As reported in chapter 3, the inductance L_{Sn} can be incorporated in series to the normal electron path surface resistance R_S as shown in Fig. 4.3. In this model, the superconducting current path with no resistance is represented by the inductance L_{SS}, and the normal current path is modelled by impedance with the inductance L_{Sn} and resistance R_S in series.
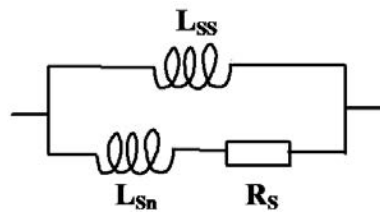
Fig. 4.3 Equivalent lumped element model of a superconductor, with L_{Sn} in series to R_S (after [3] with element notations changed for clarity).

In addition, from the point of view of conceptual possible circuit variations, the inductance L_{Sn} can be placed in series to the parallel combination of L_{SS} and R_S as shown in Fig. 4.4. However, this circuit representation needs to be considered as a 'Black Box' modelling approach due to the element L_{Sn} circuitry position.
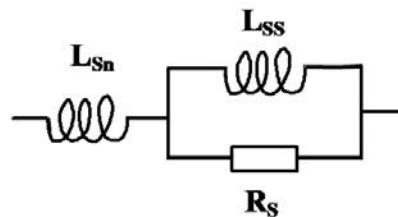

Fig. 4.4 Equivalent lumped element model of a superconductor, with L_{Sn} in series to the parallel combination of $L_{SS}R_S$.

By connecting the three lumped element models of HTS materials: the basic two fluid model and two modifications proposed (shown in Fig. 4.2, Fig. 4.3 and Fig. 4.4 respectively) in series with the RLC model of a microwave resonator (Fig. 4.1b),

three configurations of the superconducting resonator models are obtained. These three configurations are presented below in Figs. 4.5 – 4.7.

The model 'A', shown in Fig. 4.5, is the simplest representation of a superconducting resonator, when a resonator itself, is represented by a series RLC network with a parallel combination of inductance L_{SS} and surface resistance R_S only to model a superconductor.
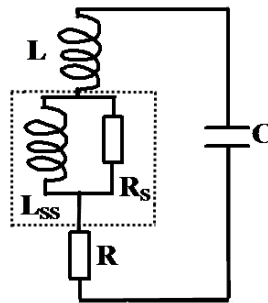
Fig. 4.5 Circuit representation of a superconducting resonator using the two-fluid model (model 'A').

Fig. 4.6 shows the second model (model 'B') with the inductance L_{Sn} in series to the surface resistance R_S of the superconducting sample.
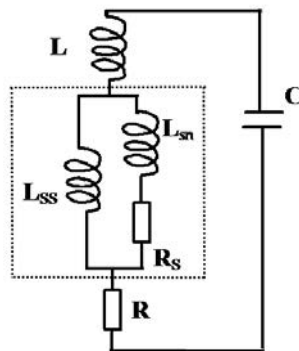
Fig. 4.6 Circuit representation of a superconducting resonator (model 'B').

The third model of the superconducting resonator with the inductance L_{Sn}, in series to a parallel combination of inductance L_{SS} and surface resistance R_S is illustrated in Fig. 4.7 (model 'C').
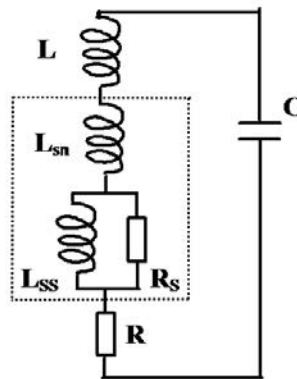
Fig. 4.7 Circuit representation of a superconducting resonator (model 'C')

From this point forward, only two models 'B' and 'C' are considered further in this thesis due to the mentioned earlier model 'A' superconducting circuit limitations.

The resonance frequency of the models is determined mostly by the inductance L with a very small contribution from the inductances L_{SS} and $L_{Sn,}$ because of their relatively small values. The element R represents EM losses in normal metal walls of the dielectric resonator.

In order to simulate and investigate the transmitted RF power responses of the two equivalent lumped element models 'B' and 'C', corresponding power equations were derived by the author of this thesis (using the circuit theory and mathematical algorithms created in the Maple software [11]). Obtained RF power equations model resonant curves of the superconducting resonator that can be measured using appropriate equipment.

The equation derived for the model 'B' and 'C' of Figs. 4.6 and 4.7 are given below as eqns. (4.3) and (4.4) respectively:

$$P = \frac{1}{2} \frac{\omega^2 C^2 V^2 (L_{SS}^2 \omega^2 R_S + R R_S^2 + R \omega^2 L_{SS}^2 + 2 R \omega^2 L_{SS} L_{Sn} + R \omega^2 L_{Sn}^2)}{2 \omega^2 L_{SS} L_{Sn} + R^2 \omega^4 C^2 L_{SS}^2 + R_S^2 + \omega^2 L_{SS}^2 + \omega^2 L_{Sn}^2 + 2 \omega^6 L C^2 L_{Sn}^2 L_{SS} + \omega^4 L_{SS}^2 C^2 R_S^2 +}$$

$$\frac{}{+ 2 \omega^4 L C^2 R_S^2 L_{SS} + 2 \omega^6 L^2 C^2 L_{SS} L_{Sn} + 2 \omega^6 L C^2 L_{SS}^2 L_{Sn} + 2 R \omega^4 C^2 L_{SS}^2 R_S + R^2 \omega^4 C^2 L_{Sn}^2}$$

$$\frac{}{+ \omega^4 L^2 C^2 R_S^2 - 4 \omega^4 L_{SS} L_{Sn} C L_{Sn} + 2 R^2 \omega^4 C^2 L_{SS} L_{Sn} - 2 \omega^4 L_{SS}^2 L C - 2 \omega^4 L_{SS}^2 C L_{Sn} - 2 \omega^4 L_{Sn}^2 L C}$$

$$\frac{}{- 2 \omega^4 L_{Sn}^2 L_{SS} C + R^2 \omega^2 C^2 R_S^2 + \omega^6 L^2 C^2 L_{SS}^2 + \omega^6 L^2 C^2 L_{Sn}^2 + \omega^6 L_{SS}^2 C^2 L_{Sn}^2 - 2 R_S^2 \omega^2 L C - 2 R_S^2 \omega^2 L_{SS} C}$$

$$(4.3)$$

$$P = \frac{1}{2} \frac{V^2 \omega^2 C^2 (R \omega^2 L_{SS}^2 + R R_S^2 + L_{SS}^2 \omega^2 R_S)}{R_S^2 - 2 \omega^2 (L + L_{Sn}) C R_S^2 - 2 R_S^2 \omega^2 L_{SS} C + R^2 \omega^4 C^2 L_{SS}^2 + \omega^4 (L + L_{Sn})^2 C^2 R_S^2 + R_S^2 \omega^4 L_{SS}^2 C^2 -}$$

$$\frac{}{- 2 \omega^4 L_{SS}^2 L C + \omega^2 L_{SS}^2 + 2 R \omega^4 C^2 L_{SS}^2 R_S + R^2 \omega^2 C^2 R_S^2 + \omega^6 (L + L_{Sn})^2 C^2 L_{SS}^2 + 2 \omega^4 (L + L_{Sn}) C^2 R_S^2 L_{SS}}$$

$$(4.4)$$

where R, L, C are microwave resonator model parameters; L_{SS}, L_{Sn}, R_S are superconductor model parameters; ω is the circular frequency ($\omega = 2\pi f = 1/(LC)^{-1/2}$); and V is the voltage across the capacitor C, assumed to equal 1 (one) here, and other elements as described before.

These circuit solutions (4.3 and 4.4) were found to be stable in a wide range of R_S, L_{SS}, and L_{Sn} parameters deviations.

As discussed before in this chapter, in order to model the nonlinear behaviour of HTS resonators, the circuit elements R_{SS}, L_{SS}, and L_{Sn} of the equivalent lumped element models 'B' and 'C' need to be presented as a function of RF magnetic field H_{RF}, or RF power P. As described in Chapter 3, linear, quadratic and exponential mathematical dependences of the surface resistance R_S on the magnetic field H_{RF} have

been proposed in literature [7-9] to fit observed characteristics depending on RF power levels and physical phenomena behind the nonlinear effects.

Hence, the physical phenomena responsible for partial transition of superconducting electrons into normal electrons at low power levels can be described through the linear dependence on the circuit elements L_{SS}, L_{Sn}, and R_S on RF magnetic field H_{RF} (see eq. 4.5). The nonlinearity contributing causes in terms of energy losses such as weak links losses at low power levels, microwave heating effects, weakly coupled grains with magnetic field penetration at grain boundaries, and partial vortex penetration in weak links can be included in the model with the quadratic dependence of the circuit elements on the RF magnetic field H_{RF}, as presented in equation (4.6). The vortex penetration into superconducting grains and the fluxoid motion can be modelled by the exponential dependence of circuit elements on RF magnetic field, as formulated in (4.7).

In this thesis, all three types of RF field dependences known in literature (linear, quadratic and exponential) have been applied to all superconducting circuit elements R_S, L_{SS}, and L_{Sn}, as presented below in eq. (4.5 – 4.7).

For ***Linear*** dependence on RF magnetic field H:

$$
\begin{aligned}
R_S &= R_{S0}(1 + \rho H(i-1)); \\
L_{SS} &= L_{SS0}(1 + lH(i-1)); \\
L_{Sn} &= L_{Sn0}(1 + lH(i-1));
\end{aligned}
\tag{4.5}
$$

For ***Quadratic*** dependence on RF magnetic field:

$$
\begin{aligned}
R_S &= R_{S0}(1 + \rho_1 H(i-1) + \rho_2 H^2(i-1)); \\
L_{SS} &= L_{SS0}(1 + l_1 H(i-1) + l_2 H^2(i-1)); \\
L_{Sn} &= L_{Sn0}(1 + l_1 H(i-1) + l_2 H^2(i-1));
\end{aligned}
\tag{4.6}
$$

For ***Exponential*** dependence on RF magnetic field:

$$R_S = R_{S0}(1 + a\exp(bH(i-1)));$$
$$L_{SS} = L_{SS0}(1 + c\exp(dH(i-1)));$$
$$L_{Sn} = L_{Sn0}(1 + c\exp(dH(i-1)));$$

(4.7)

where ρ, ρ_1, ρ_2, l, l_1, l_2, a, b, c, d are fitting constants; R_{S0} is the value of superconducting surface resistance, L_{SS0} is the value of superconducting surface inductance, and L_{Sn0} is the value of normal electron surface inductance for H=0; (i-1) describes an iterative approach for calculations, where i is a corresponding point at given frequency.

The expressions (4.5 – 4.7) were integrated into the derived transmitted RF power equations, namely into eq. (4.3) and (4.4), so the resulting equations have capabilities to model superconducting properties and nonlinear effects in the superconducting dielectric resonator.

4.2   Computations of transmitted RF power of superconducting resonators using models 'B' and 'C'

Computations of the transmitted power and sensitivity investigation of the model fitting coefficients are necessary for complete model analysis. Hence, simulations of the transmitted RF power of the superconducting microwave resonator, using the two proposed models 'B' and 'C' (Fig. 4.6 , Fig. 4.7), along with the derived equations (4.3, 4.4), applying three different function dependences (4.5 – 4.7), have been performed using the Matlab software. An iterative computational method has been applied to obtain the transmitted RF power P on frequency dependence. At each frequency point ω_i, the values of the complex inductances and resistance were computed using the magnitude of power P taken at the previous frequency point, $P(\omega_{i-1})$.

In order to investigate any model, its corresponding model parameters relevant to the measurement system, need to be determined. For the simulations conducted in this chapter, the following values of models' parameters have been identified:

1) <u>For the resonator</u>: The resonant frequency of the microwave dielectric resonator was assumed to be 10GHz and hence the values of parameters C and L were taken as the following: $C=10^{-12}F$, $L=2.5\times10^{-10}H$. The surface resistance R of the resonator metal walls was assumed to be $R=3\times10^{-4}\Omega$.

2) <u>For the Superconductor</u>: Typical parameters of the HTS thin film – $YBa_2Cu_3O_7$ has been used in the computations, namely $\lambda =1.4\times10^{-7}m$ and $R_{S0}=5\times10^{-4}\Omega$. Hence, $L_{SS0}=L_{Sn0}$ ($L_{SS}=L_{Sn0}=\mu_0\lambda$, where $\mu_0=1.25\times10^{-6}H/m$), thus $L_{SS0}=L_{Sn0}=1.8\times10^{-13}H$. The values for the fitting coefficients ρ, ρ_1, ρ_2, l, l_1, l_2, a, b, c and d have been selected in a way to fit the data of measured P(f) dependences of YBCO thin films at 10GHz using the "Black box" modelling approach: $\rho=1.6\times10^{-2}$, $l=1.1\times10^{-3}$, $\rho_1=4.1\times10^{-2}$, $l_1=1.8\times10^{-3}$, $\rho_2=3.2\times10^{-7}$, $l_2=2\times10^{-8}$, $a=9.5\times10^{-1}$, $b=2\times10^{-2}$, $c=3.2\times10^{-2}$, $d=2.5\times10^{-2}$, $f_0=10GHz$.

Results of the simulations for the models 'B' and 'C' for all types of nonlinear dependences on H_{RF}, with parameters assumed as described earlier, are shown in Fig. 4.8 and Fig. 4.9 respectively.
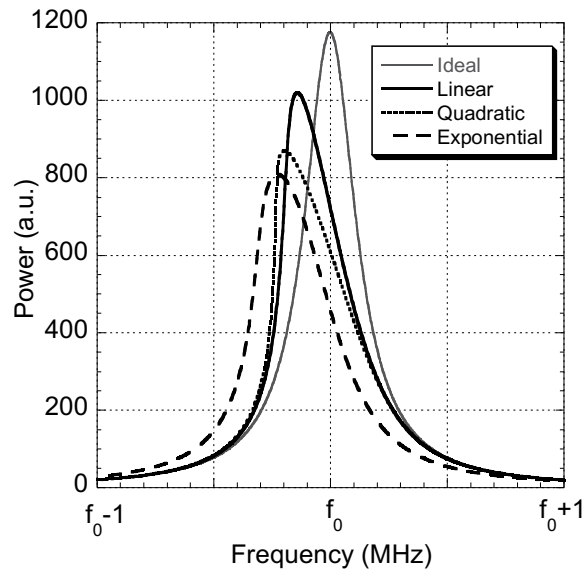
Fig. 4.8 Simulated RF power for the network illustrated in Fig. 4.6 - model 'B'

(f_0=10GHz)
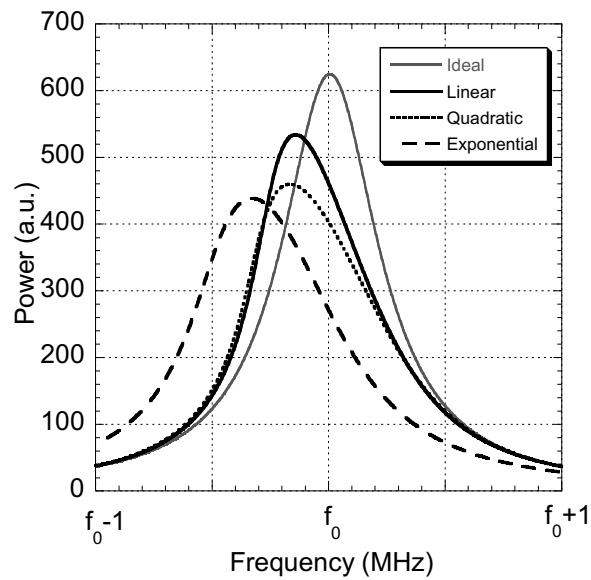
Fig. 4.9 Simulated RF power for the network shown in Fig. 4.7 - model 'C'

(f_0 = 10GHz)

Due to the differences in equivalent circuits for the models 'B' and 'C', the corresponding effective R_S and effective L_{SS}, L_{Sn} elements are different, leading to the

different maximum power and Q-factor values of the corresponding resonance curves. For the model 'B', R_S was calculated as $1.25 \times 10^{-4} \Omega$, and for the model 'C' R_S was $5 \times 10^{-4} \Omega$, four times higher than for the model 'B'. The reactance X for the model 'B' was $5.65 \times 10^{-3} \Omega$, and for the model 'C' $X = 1.13 \times 10^{-2} \Omega$. Thus, the impedance Z for the model 'B' was $5.63 \times 10^{-3} \Omega$ and for the model 'C' Z equalled $1.13 \times 10^{-2} \Omega$, leading to the differences in P_{max} values of the two models and higher Q-factor of the model 'B'.

In order to examine the sensitivity of the fitting parameters of the models, simulations with varying values of the corresponding fitting coefficients in related mathematical dependences: ρ, ρ_1, ρ_2, l, l_1, l_2, a, b, c and d have been performed for the two models ('B' and 'C'). Each parameter was changed at a time for the linear, quadratic and exponential dependences. The ideal curve in all graphs presented in this chapter denotes the case when corresponding fitting parameters equal zero.

The following Fig. 4.10, Fig. 4.11 and Fig. 4.12 illustrate computed responses for the linear (4.5), quadratic (4.6), and exponential (4.7) dependences respectively for the model 'C' (Fig. 4.7), computed using eq. (4.4).
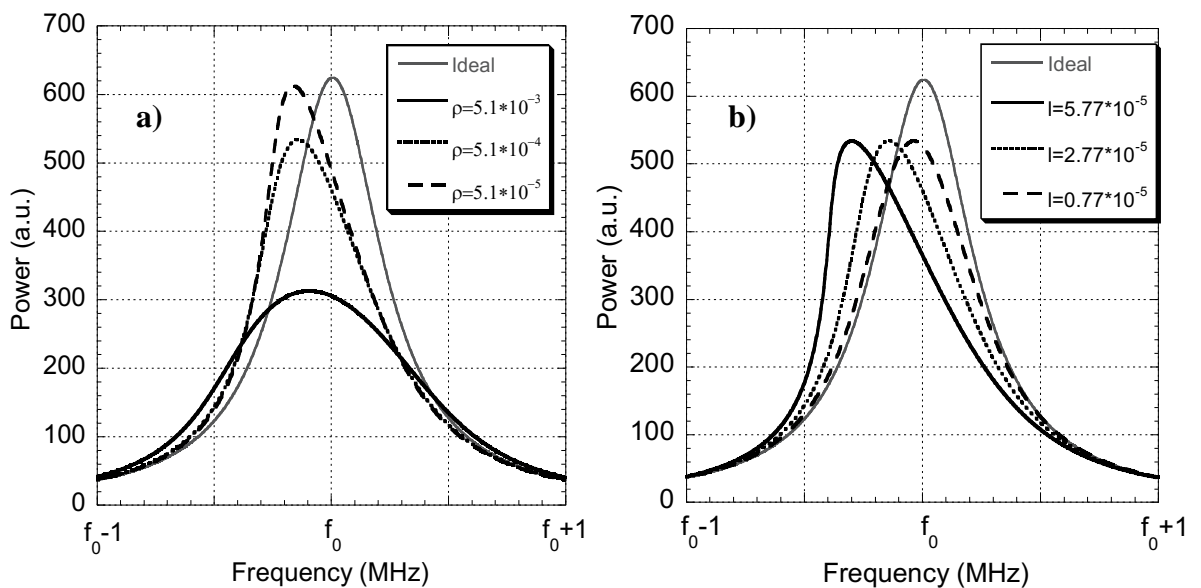

Fig. 4.10 Simulated RF power for varying fitting coefficients ρ (a) and l (b) for linear dependence of model 'C'.

As can be observed in Fig. 4.10 (a) the fitting parameter ρ related to R_S affects the maximum power values of the system, with the higher values of ρ the response function becomes smaller and wider, lowering Q values of the resonator. The values of l for results of Fig. 4.10 (a) were the same: $l=2.77\text{x}10^{-5}$. The sensitivity of the change in Q with variations in ρ ($\Delta Q/\Delta \rho$) was calculated as $2.53\text{x}10^{6}$, while the sensitivity of the change in maximum power with change in ρ ($\Delta P_{max}/\Delta \rho$) equalled $6\text{x}10^{4}$.

The Fig. 4.10 (b) shows the case of varying l parameter related to both L_{SS} and L_{Sn}. The value of ρ for this case were the same: $\rho=5.1\text{x}10^{-4}$. As can be seen, parameter l affects only the frequency change of the resonant curves, showing that the higher values of l the higher nonlinear effects. The sensitivity of the change in resonance frequency f_0 with the change in fitting parameter l ($\Delta f_0/\Delta l$) was calculated as $5.2\text{x}10^{6}$.

Fig. 4.11 shows simulation results for varying nonlinear parameters of the quadratic complex dependence for the circuit 'C' (Fig. 4.7):
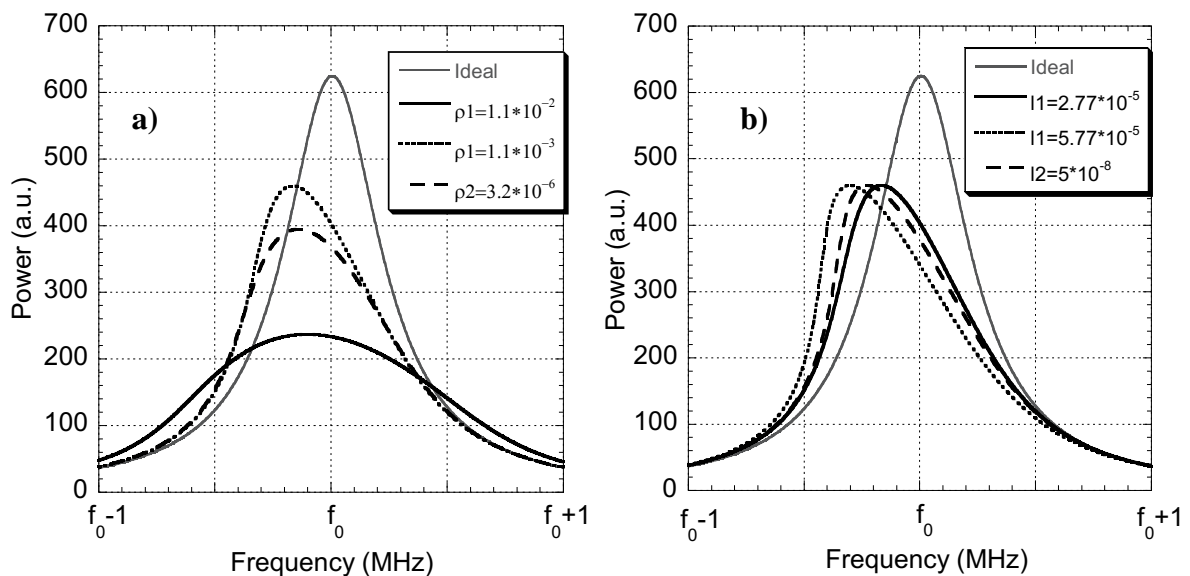

Fig. 4.11 Simulated RF power for varying fitting coefficients for quadratic dependence for model 'C' in Fig. 4.7.

Fig. 4.11 (a) reflects the case where the parameters ρ_1 and ρ_2 related to the complex R_S of the quadratic case were manipulated. When the parameter ρ_1 was changing, the value of the coefficient ρ_2 was as defined earlier 3.2×10^{-7}, and when ρ_2 was varied, ρ_1 was 4.1×10^{-2} The sensitivity values were $\Delta P_{max}/\Delta\rho = 2.475\times10^4$ and $\Delta Q/\Delta\rho = 1.29\times10^6$.

Components of the nonlinear inductances (L_{SS} and L_{Sn}) such as l_1 and l_2 were investigated in Fig. 4.11 (b). Similarly, the results illustrate a comparative behaviour of the fitting coefficients with the linear case, where the resonant frequency is only affected. The sensitivity of the change in resonance frequency f_0 with the change in fitting parameter l ($\Delta f_0/\Delta l$) was 2.67×10^6.

Fig. 4.12 illustrates two cases where the fitting parameters a, b, c, and d of the exponential dependence (eq. 4.7) were varied in relation to the nonlinear network elements R_S and L_{SS}, L_{Sn} respectively.
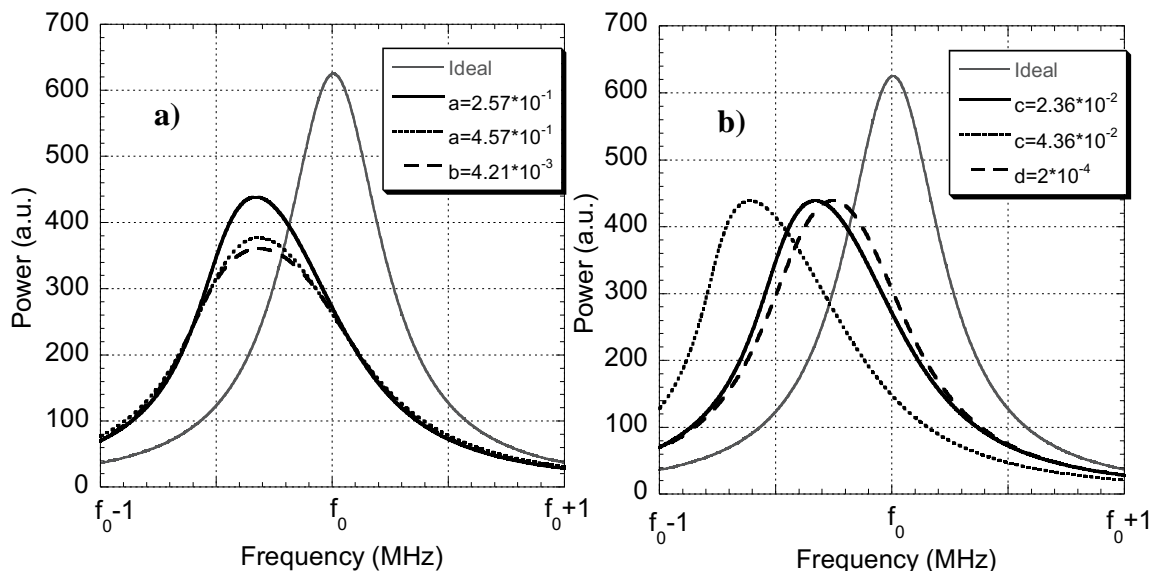

Fig.4.12 Simulated RF power for varying fitting coefficients for exponential dependence of model 'C'.

As can be observed in Fig. 4.12 (a), varying the parameters *a* and *b* of the nonlinear surface resistance affects the magnitude of the resonance curve, similar to the corresponding parameters of the linear and quadratic dependences. The sensitivity of the change in Q with variations in *a* ($\Delta Q/\Delta a$) had the value of 5.74×10^4, while the sensitivity of the change in the maximum power with change in *a* ($\Delta P_{max}/\Delta a$) was 3×10^2.

Fig. 4.12 (b) illustrates value variations of parameters *c* and *d* linked to nonlinear inductance elements of a superconductor L_{SS} and L_{Sn}. As expected, simulated results demonstrate that changing the parameters *c* and *d* tilts the resonance curves towards either higher or lower frequencies. The sensitivity value of the change in frequency with the change in c ($\Delta f_0 /\Delta c$) was 1.5×10^4.

Simulated results for the model 'B' (presented in Fig. 4.6) are shown below (Figs. 4.13 – 4.15). Fig. 4.13 illustrates results of simulated Power versus frequency for the linear dependence of the superconducting surface resistance R_S and inductances L_{SS} and L_{Sn}.
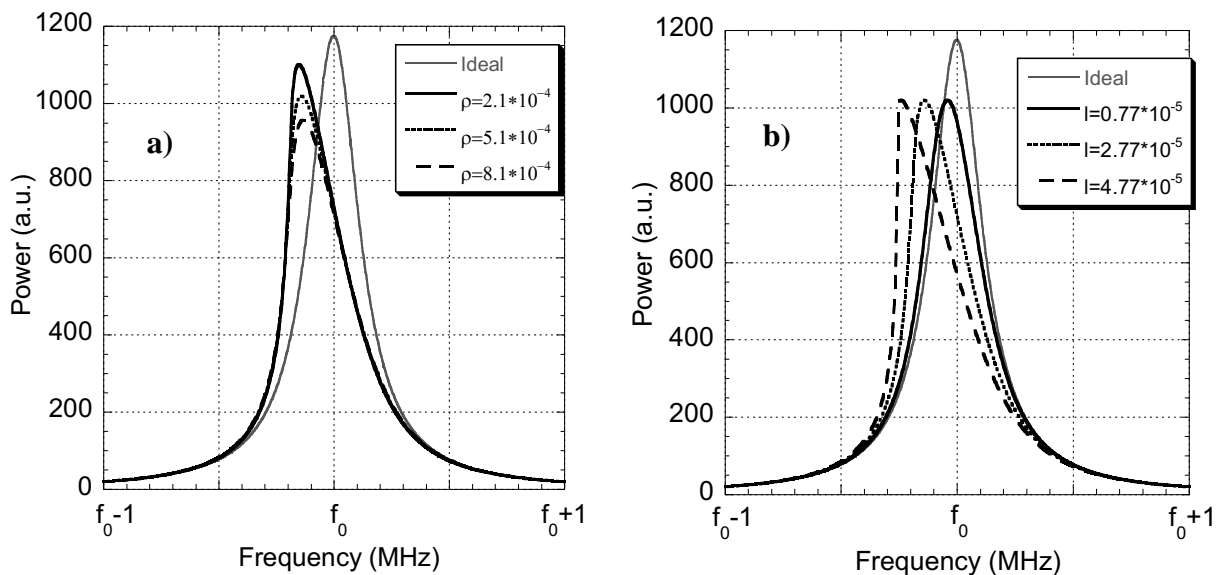

Fig. 4.13 Simulated RF power for varying fitting coefficients for linear dependence for model 'B' in Fig. 4.6.

Similar to the results of the model 'C' in Fig. 4.7, the change in the parameter ρ, shown in Fig. 4.13 (a), affects the magnitude of the resonance curves, while the variation of the parameter l (Fig. 4.13 (b), linked to the superconductor inductances, tilts the resonance responses towards nonlinear forms with increased values of l. The sensitivity of the change in quality factor with the change in ρ $(\Delta Q/\Delta\rho)$ was calculated as 2.19×10^7, being approximately one order of magnitude higher if comparing to the reported earlier value of 2.53×10^6 for the model 'C'. The sensitivity of the change in the maximum power with the variations in ρ $(\Delta P_{max}/\Delta\rho)$ was 2.5×10^5, also almost one order of magnitude higher comparing to stated earlier value of 6×10^4 for the model 'C'. The calculations of the sensitivity for the resonance frequency with dependence on the l parameter produced a value of 4.6×10^6, similar to the model 'C' value of 5.2×10^6 reported earlier.

The simulated responses depicted in Fig. 4.14 reflect the case of small variations of the fitting parameters in terms of the nonlinear quadratic components R_S and L_{SS}/L_{Sn}. The parameters ρ_1 and ρ_2 are linked to the surface resistance R_S, and the parameters l_1 and l_2 are related to the inductances L_{SS} and L_{Sn}.
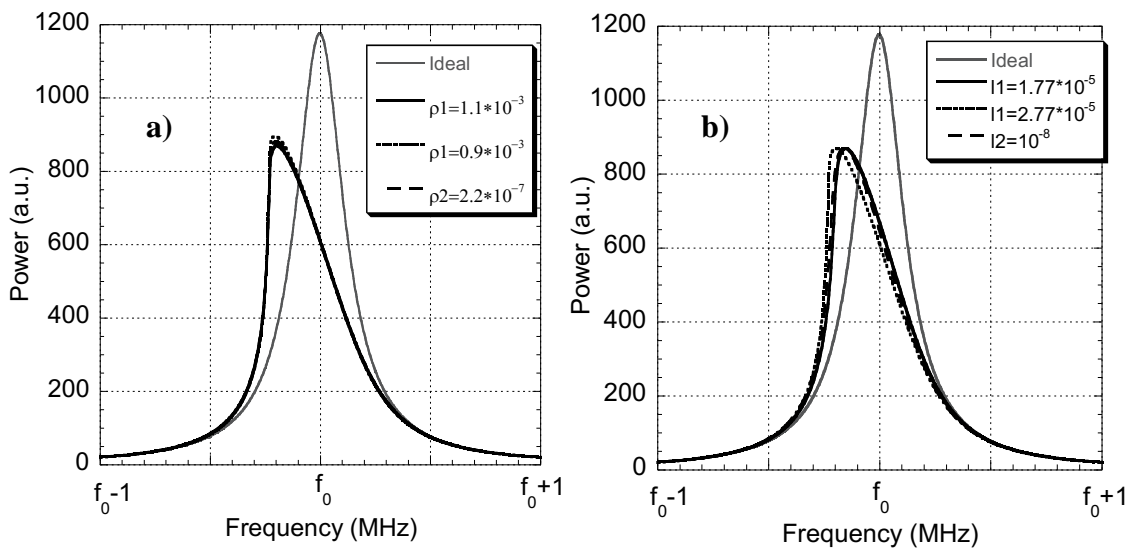

Fig. 4.14 Simulated RF power for varying coefficients for quadratic dependence for model 'B' in Fig. 4.6.

Both graphs (Fig. 4.14a and 4.14b) illustrate that small changes in the corresponding fitting coefficients barely bring any charges to the resonance curves, resulting in no system sensitivity.

Simulations of the exponential nonlinear dependence for the model 'B' are illustrated in Fig. 4.15, which again includes two pairs of fitting parameters such as a, b and d, c related to the R_S and L_{SS}/L_{Sn} components respectively.
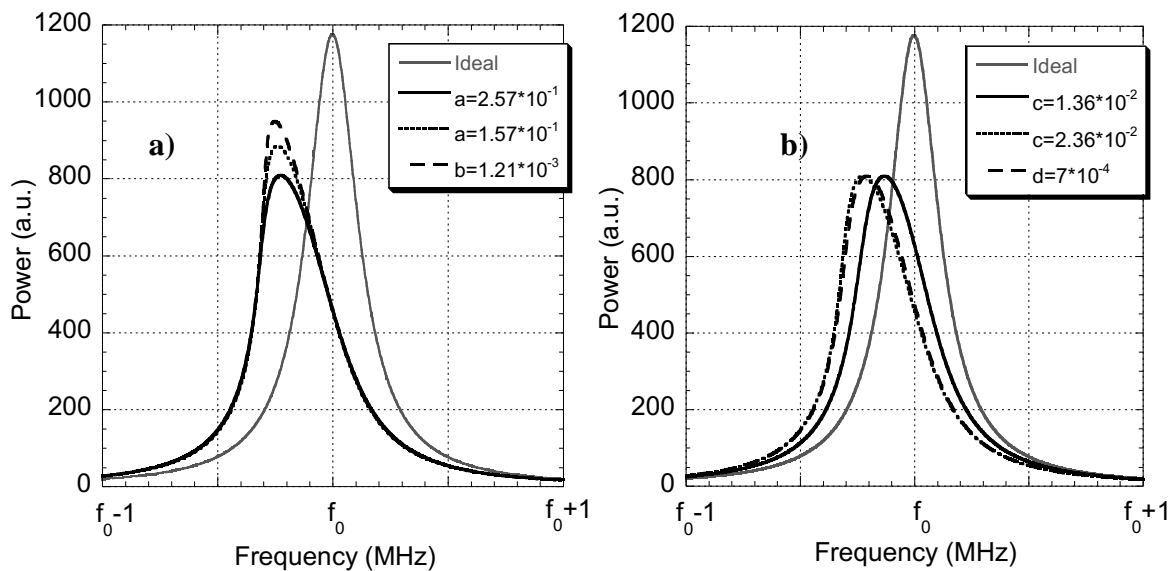
Fig. 4.15 Simulated change of RF power magnitude for varying fitting coefficients for exponential nonlinear dependences of RF power P vs frequency f of the model 'B' in Fig. 4.6.

The similar behaviour to model 'C' in terms of the shift in the resonance amplitude (Fig. 4.15 (a)), and the change of the resonance frequency (Fig. 4.15 (b)) is observed here. The sensitivity values of the maximum power P_{max}, quality factor Q and frequency f were: $\Delta P_{max}/\Delta a = 6.95 \times 10^2$ (higher than for the model 'C' with the value of 3×10^2; $\Delta Q/\Delta a = 2.179 \times 10^4$ (lower than for the model 'C': 5.735×10^4); and $\Delta f_0/\Delta c = 1.3 \times 10^4$ (almost identical with the model 'C': 1.5×10^4).

In summary, obtained results show that varying of the coefficients, related to surface resistance R_S, mostly affects the amplitude of the resonance responses, as expected; while changing the coefficients referred to inductances tilts the resonance curves towards either higher or lower frequencies. The outlined behaviour based on the coefficients variations confirms the application of proper physical approach engineered for the proposed models.

All numerical values of fitting coefficients were selected in a way that enabled observation of the changes in shapes of resonance curves at frequency deviation limits of $\pm$ 1MHz at the resonance frequency f_0 of 10GHz. It needs to be mentioned that the strong increase in values of the fitting coefficients in equations (4.5 – 4.7) may lead to the simulated 'overload' responses of the systems, where highly unstable behaviour of the power curve can be observed.

In terms of the parameters identification, the model-fitting parameters used in the calculations are temperature and frequency dependent constants. To identify the circuit fitting parameters ρ, ρ_1, ρ_2, l, l_1, l_2, a, b, c and d, first a resonator with a superconductor needs to be measured at low RF power levels when values of the fitting parameters are negligible. This enables to identify the values of the surface resistance R_{S0} and inductances L_{SS0} and L_{Sn0}. Thus, from the equations (4.5 – 4.7) the fitting parameters can be identified for all three nonlinear dependences.

The selected models 'B' and 'C' (presented in Fig. 4.6 and 4.7) could be used for simulations of nonlinear effects of HTS films in resonant structures at wide range of power. It is believed that the developed lumped element models can also contribute towards development of dedicated CAD tools for electronic circuits analysis. Having discussed the potentials of the selected models, it also needs to be mentioned that the main problem with precise modelling of nonlinear effects at elevated power levels is that the physical phenomena in superconductors cannot always be closely approximated by linear, quadratic or even exponential dependencies in the process of simulations, because the nature of nonlinearities is not clearly understood and may require further research. However, as was shown in this chapter, it is possible to model

the nonlinear properties of HTS thin films with a good approximation and identify appropriate fitting coefficients for simulated nonlinear dependences.

It also needs to be mentioned that the exponential model can also be considered in investigations of intermodulation distortion (IMD) and harmonic generation of superconducting resonators. However, one needs to keep in mind that certain physical mechanisms responsible for nonlinearities, like excitation of vortices at higher power levels, could play more dominant role at different stages of the modelling.

REFERENCES

[1]   C. Gorter and H. Casimir, "On superconductivity I", *Physica 1*, no. 4, pp. 306-320, 1934.

[2]   M. Lancaster, "Fundamental Consideration of Superconductors at Microwave Frequencies", Microwave Superconductivity edited by H. Weinstock and M. Nisenoff, *NATO Science Series E: Applied Science, Kluwer Academic Press,* v. 375, pp. 1-20, 2001.

[3]   D. Oates, "Microwave measurements of fundamental properties of superconductors", *Chapter 8 in "100 Yeas of Superconductivity", edited by H. Rogalla and P. Kes*, 2011.

[4]   J. Halbritter, RF residual losses, surface impedance, and granularity in superconducting cuprates, *Appl. Phys.*, v. 68, p. 6315, 1990

[5]   P. Nguyen et al., "Nonlinear Surface Impedance for $YBa_2Cu_3O_{7-x}$ Thin Films: Measurements and Coupled-Grain Model", *Phys. Re. B.,* v. 48, p. 6400, 1993.

[6]   S. Sridhar, Nonlinear microwave impedance of superconductors and ac response of the critical state, *Appl. Phys. Lett.,* vol. **65,** no. 8, pp. 1054-1056,1994.

[7]   D. Oates et al., "Nonlinear surface imperdance of YBCO thin films: Measurements, Modeling, and Effects in devices", *J of Supercond.*, v. 8., no. 6, p. 725, 1995.

[8]   P. Nguyen et. al., "Microwave hysteretic losses in YBCO and NbN thin films", *Phys. Rev. B,* v. 50, p. 6686, 1995.

[9]   J. Halbritter, RF residual losses, surface impedance, and granularity in superconducting cuprates, *Appl. Phys.*, v. 68, p. 6315, 1990

[10]   C. Desoer, "Basic circuit theory", *McGraw-Hill*, 1969.

[11]   Maple software, www.maplesoft.com

CHAPTER 5

Experimental investigation of microwave properties of YBa$_2$Cu$_3$O$_7$ and NdBa$_2$Cu$_3$O$_7$ thin films and microstrip resonators

As was stated before in Chapter 1 of this manuscript, the second goal of this thesis (after lumped element modelling presented in Chapter 4) was to investigate if there is any other HTS material that exhibits smaller nonlinear effects than found in the widely used YBCO superconductor that could be used in microwave superconducting circuits. As is known, YBCO superconductors exhibit much lower surface resistance than conventional conductors at high frequencies, and this property enabled them to dominate the market of superconducting microwave devices. However, as was shown in Chapter 2.2, superconducting YBCO materials are susceptible to nonlinear effects at elevated power levels. Thus, as discussed earlier, the NdBCO superconductor was considered as a material of choice and a top HTS candidate for investigation to determine if it is able to yield smaller surface resistance and less nonlinearity than YBCO at higher power levels.

As was presented in Chapter 1, the NdBa$_2$Cu$_3$O$_7$ cuprates demonstrated a few key benefits in comparison to YBa$_2$Cu$_3$O$_7$, namely a higher critical temperature T$_C$ recorded at 94K [1-2], and a higher critical current density J$_C$ with maximum values of 10^6A/cm^2 [3-4]. The surface resistance (R$_S$) of NdBCO films on MgO substrate was listed as 230$\mu\Omega$ at 10GHz and 77K [2], lower than of YBCO films, approximately 300-400$\mu\Omega$ at 10GHz and 77K [3]. In the author's earlier work (co-authored with others) [5], NdBCO films with different thickness (50nm and 700/800nm) deposited on MgO substrates without and with a 25nm YBCO buffer layer showed excellent values of intrinsic R$_{Sint}$ of 0.52mΩ and 4.48mΩ at 25GHz and 19K, J$_C$ of approximately 0.75MA/cm^2 and 5.8MA/cm^2 at 77K, with T$_C$ of 88K and 93.9K respectively. However, the 700/800nm NdBCO films, reported in [5] exhibited

effective measured R_S of 750µΩ at 10GHz, almost twice the values of equivalent morphological quality commercial YBCO films, making those samples unsuitable for microwave applications. Nevertheless, it needs to be mentioned that there has been only very limited research conducted on microwave properties of NdBCO material [6-11], in part due to the wide commercial availability of high quality YBCO films on large area substrates. Also, to the author's knowledge, no investigations of the nonlinear properties of NdBCO cuprates have been conducted in the past, thus creating a gap of knowledge of the potential of this material for microwave applications.

In this chapter, a comparison of microwave properties of $YBa_2Cu_3O_7$ (YBCO) and $NdBa_2Cu_3O_7$ (NdBCO) thin films on MgO substrates is presented. The microwave measurements of the thin films were performed at a frequency of 25 GHz, as a function of temperature as well as RF input power, using a Hakki-Coleman sapphire dielectric resonator. The YBCO and NdBCO films were deposited on MgO substrates of 0.5mm using the thermal co-evaporation technique [1]. The NdBCO films incorporated 25nm YBCO buffer layers deposited on MgO. Other parameters of the films were:

YBCO: T_C = 87.4K; J_C = 2.6MA/cm^2; 700nm film thickness.

NdBCO: T_C = 93.8K; J_C = 5.8MA/cm^2; 600nm film thickness.

Both sets of films were manufactured at Ceraco, Germany [6].

To investigate microwave properties of the YBCO and NdBCO thin films, the unloaded Q_0 factor and the surface resistance R_S of the films have been calculated from values of loaded Q and coupling coefficients computed from S_{21}, S_{11} and S_{22} measurements with the dependence on temperature, with results presented in section 5.2 below. More detailed analysis of the measurement system and calculation procedures is presented in the following subchapter.

As discussed in Chapter 2.2, the surface resistance increases very little in the low field region (H_{rf} < 10Oe), with the normally quadratic increase in the intermediate fields (10Oe < H_{rf} < 50Oe), and at high fields (H_{rf} > 50-300Oe) R_S rises faster than the

quadratic increase. As a consequence, the elevated levels of nonlinear R_S at higher power levels lead to performance limitations of microwave devices. Therefore, to investigate nonlinear microwave properties of YBCO and NdBCO films, a separate set of measurements has been performed at various power levels (-5dBm to 25dBm), with the results of the power investigation provided later in this chapter. The onset of nonlinear effects in YBCO and NdBCO films has also been identified and presented.

In order to conduct a more complete analysis and comparison of YBCO and NdBCO materials not only in superconducting thin films, but also in microwave devices, three NdBCO (R1N, R2N, R3N) and two YBCO (R1Y, R2Y) microstrip resonators, manufactured in Tsinghua University, China in cooperation with Professor Bin Wei, have been investigated. The films for the resonators were purchased by the James Cook University from Ceraco, Germany. In this chapter, the measured results of the transmission coefficient S_{21} dependence on power and temperature, along with the computed dependence of quality factor Q_0 and surface resistance R_S on temperature and RF signal power for YBCO and NdBCO resonators are presented and evaluated. Similar to the thin film nonlinear properties evaluation, the onset of nonlinearities in the YBCO and NdBCO resonators has also been examined in this chapter.

5.1 Measurement system for microwave characterisation of YBCO and NdBCO films

In order to measure the surface resistance R_S of the YBCO and NdBCO thin films, a Hakki-Coleman silver plated sapphire resonator working at the TE_{011} mode at 25GHz was used. The sapphire rod was manufactured from a very high purity crystal with losses ($\tan\delta$) assessed not to exceed 5×10^{-8}. Fig. 5.1 shows the diagram of the Hakki-Coleman resonator. The parameters of the resonator were: sapphire rod diameter = 3.98mm, height = 3.975mm, cavity diameter = 9.25mm, cavity height =

4mm, geometrical factors $A_S = 561.3$, $A_{met} = 12,162.3$, $p_d = 0.9464$, surface resistance of the lateral copper wall $R_m = 25m\Omega$, permittivity of the sapphire, $\varepsilon_{r\perp} = 9.38$.
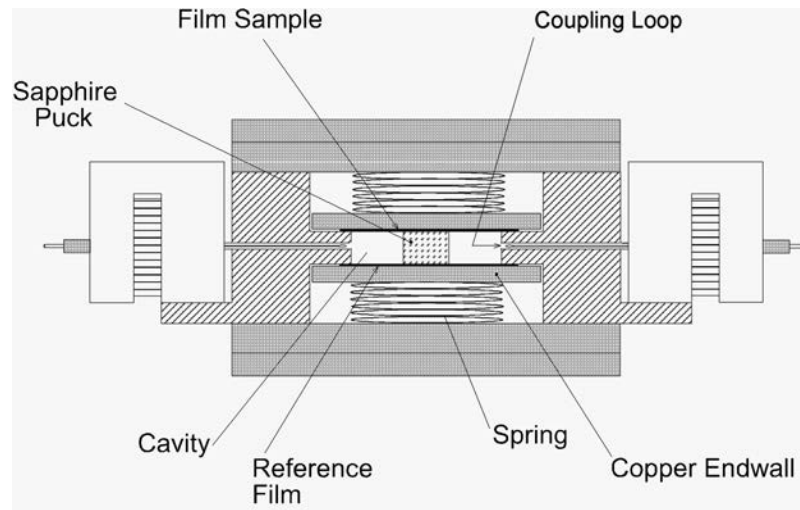

Fig. 5.1 Schematic diagram of Hakki-Coleman test resonator (after [13]).

The resonator was designed to have a high concentration of EM energy in the top and bottom HTS plates, and was manufactured with high precision (tolerance of $0.1\mu m$). The Hakki-Coleman resonator technique requires two HTS films for measurements of R_S. The average R_S of the two HTS thin films is obtained from the loss equation (2.2.20) introduced in Chapter 2.2. The Fig. 5.2 shows the inner structure of the sapphire resonator used in this dissertation.

Fig. 5.2 Inner structure of a 25GHz Hakki-Coleman resonator used in this thesis, with one of the endplates removed (photo by the author).

A Hakki-Coleman dielectric resonator with films under test was inserted into a dewar as shown in Fig. 5.3 The resonator is tightly secured to the brass plate using a solid brass strip and screws.
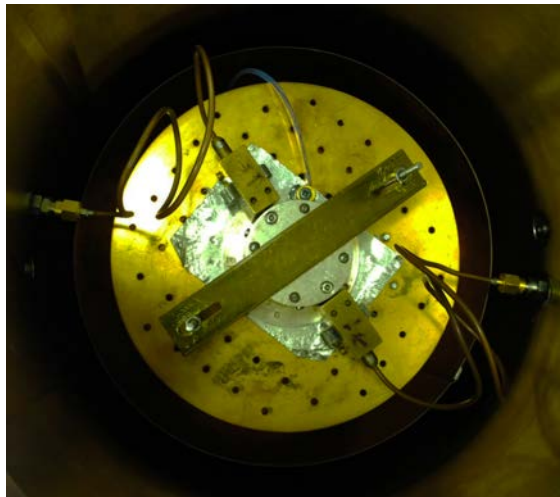

Fig. 5.3 25GHz Hakki-Coleman resonator inside a vacuum dewar (photo by the author).

The microwave characterisation of the YBCO and NdBCO films was conducted implementing a two-stage closed cycle Stirling cryocooler, Agilent PNA

E8364B, a temperature controller LTC-10 and a desktop computer, as shown in Fig. 5.4. A purposely designed software specifically written for data login and temperature controls, with implementation of the LabView program, was used in all measurements.
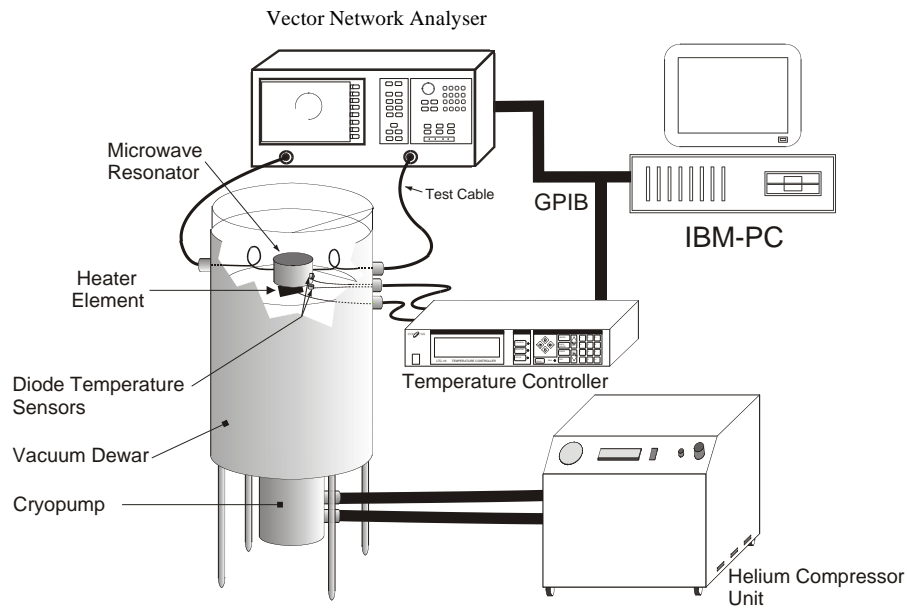

Fig. 5.4 Cryogenic microwave measurement system (after [14]).

To ensure the highest possible accuracy in computed values, the loaded Q_L-factor and coupling coefficients β_1 and β_2 of the resonator were determined from multi-frequency measurements of S_{21}, S_{11} and S_{22} parameters obtained around the resonance using the Transmission Mode Quality Factor (TMQF) Technique, mentioned in Chapter 3, for data processing. The TMQF method enables to obtain accurate values of surface resistance accounting for factors such as noise, delays due to uncompensated transmission lines, and crosstalk occurring in measured data. The unloaded Q_0-factor was calculated from the exact equation $Q_0 = Q_L(1 + \beta_1 + \beta_2)$, using the TMQF method for all temperatures. For each temperature, 1601 points of S_{21}, S_{11} and S_{22} parameters around the resonance were logged and the measured valued fitted to circles on the complex plane to compute coupling coefficients, loaded Q_L and unloaded Q_0 factors.

The dielectric resonator with embedded superconducting samples, mounted inside the vacuum dewar, was cooled down to around 18K, and the S parameters were measured around the resonant frequency up to 89K for YBCO films and 95K for NdBCO samples. The RF signal power was 0dBm for non-power dependent measurements. The surface resistance R_S of YBCO and NdBCO thin films on MgO substrates was computed using the software SUPER [15], based on the equation (2.2.20). The following sections show microwave measurements results obtained by the author during the course of work on this thesis.

5.2 Results of microwave characterisation of YBCO and NdBCO thin films on MgO substrates

Measurements of YBCO and NdBCO thin films have been performed for a temperature range of 18K – 89K for YBCO films and 18K – 95K for NdBCO films. The critical temperature of the manufactured samples was $T_C = 87.4$K for YBCO films; and $T_C = 93.8$K for NdBCO films. As was stated earlier, the power was set to 0dBm for all non-power dependent measurements. The calculated values of Q_0, obtained from values of loaded Q and coupling coefficients computed from S_{21}, S_{11} and S_{22}, as a function of temperature are presented in Fig. 5.5 and 5.6.
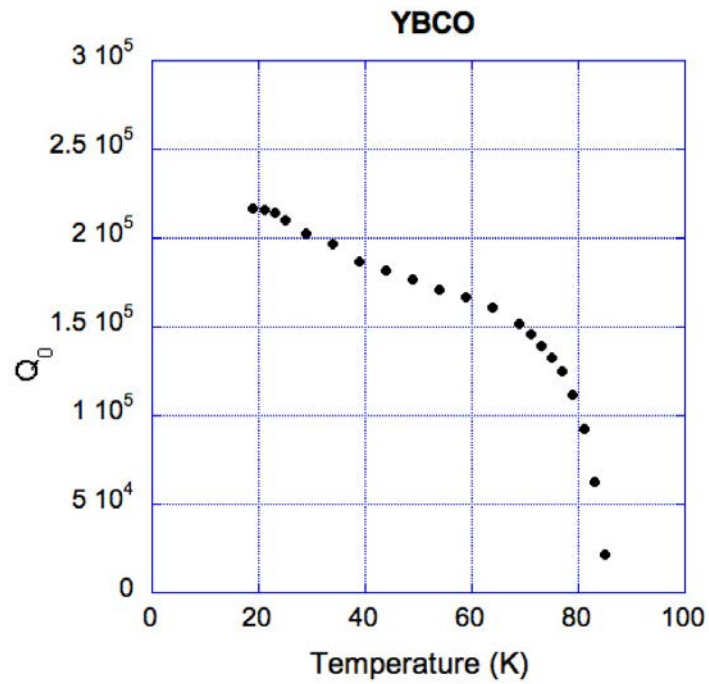
Fig. 5.5 Temperature dependence on unloaded quality factor of
YBCO thin films (1-2) at 25GHz and 0dBm.
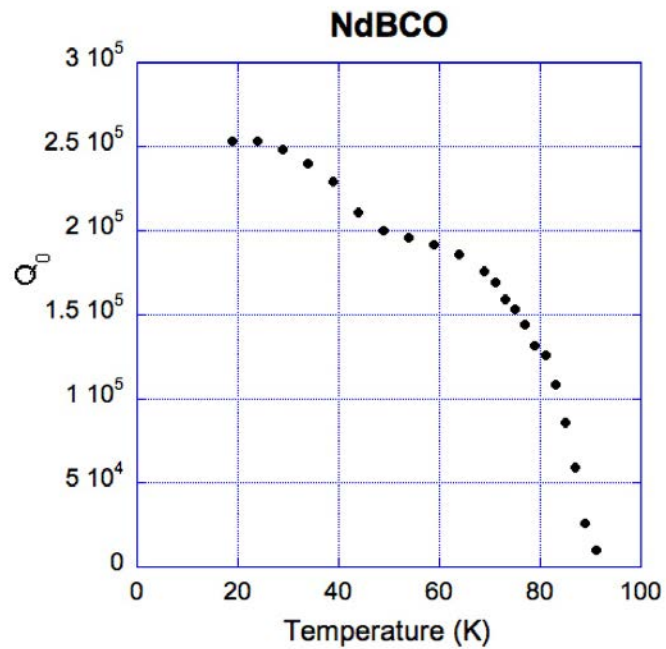
Fig. 5.6 Temperature dependence on unloaded quality factor of
NdBCO thin films (1-2) at 25GHz and 0dBm.

As can be observed from Fig. 5.5 and Fig. 5.6, NdBCO films show higher Q_0 factor and higher critical temperature than YBCO films, as was expected.

The temperature dependences of the surface resistance R_S of YBCO (films 1-2) and NdBCO (films 1-2) measured at input RF Power of 0dBm at frequency of 25GHz is presented in Fig. 5.7.
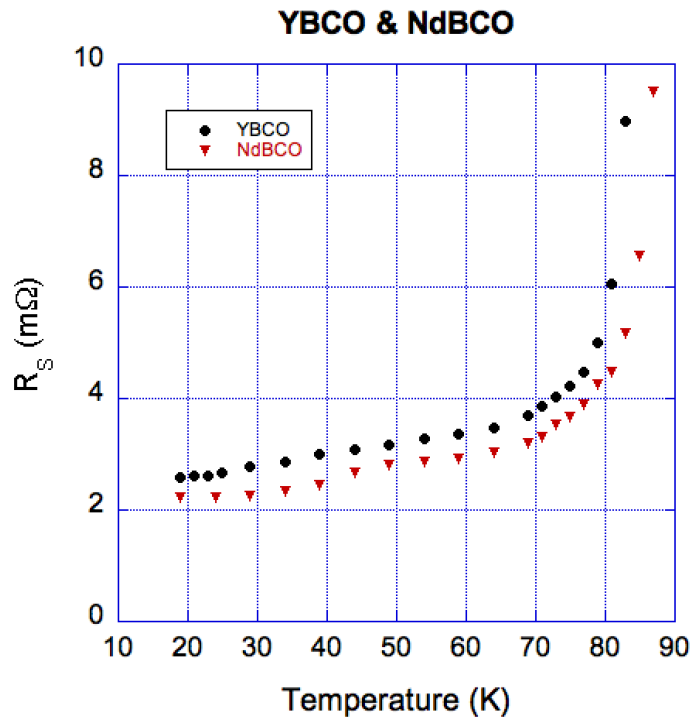

Fig. 5.7 Surface resistance R_S of YBCO thin films (1-2) and NdBCO thin films (1-2) on MgO substrate at 25GHz and 0dBm versus temperature.

As can be observed in Fig. 5.7, measured temperature characteristics of the surface resistance for the YBCO buffered NdBCO films under test exhibited lower dependence on temperature as commercially available YBCO films. Obtained results illustrate that the bigger difference in R_S occurred at high temperatures close to YBCO critical temperature where at 81K the surface resistance of YBCO was 6.06mΩ, while NdBCO samples showed 4.46mΩ, and at 83K with YBCO films demonstrating 8.98mΩ and NdBCO films displaying lower R_S of 5.18mΩ. At the temperature of

85K the R_S of YBCO was 26.06mΩ while NdBCO was 6.55mΩ, the big difference explained by the temperature shift due to higher T_C, as expected. However, the smaller R_S change of approximately 0.3-0.6mΩ is observed for the remaining temperature range of 19-79K.

The error analysis in the measurement results of the surface resistance R_S can be conducted knowing the accuracy of the unloaded Q-factor, as well as the uncertainty in the remaining constants presented in equation (2.2.20) [16]. Thus, the most probable relative errors in measured values of the surface resistance R_S in the 25GHz resonator were computed as [16]:

$$\Delta_r R_S = \left| \frac{\Delta R_S}{R_S} \right| = \left\{ \left(1 + \frac{R_m A_S}{R_S A_m} + \frac{A_S}{R_S Q_d} \right)^2 \left| \frac{\Delta Q_o}{Q_o} \right|^2 + \left(\frac{R_m A_S}{R_S A_m} \right) \left| \frac{\Delta R_m}{R_m} \right|^2 + \left| \frac{\Delta A_S}{A_S} \right|^2 \right.$$
$$\left. + \left(\frac{A_S}{R_S Q_d} \right)^2 \left| \frac{\Delta Q_d}{Q_d} \right|^2 + \left(\frac{R_m A_S}{R_S A_m} \right)^2 \left| \frac{\Delta A_m}{A_m} \right|^2 \right\}^{0.5} \tag{5.1}$$

where $1/Q_d = p_d \tan\delta$.

The following values of individual errors in (5.1) were assumed as:

$\left| \frac{\Delta Q_o}{Q_o} \right|^2 = \pm 2\%, \frac{\Delta A}{A} = \pm 0.5\%, \frac{\Delta R_m}{R_m} = \pm 2\%,$

where values of relative errors in the Q_0-factor, geometrical factors A and in the surface resistance of the resonator's walls R_m were assessed in [16], taking into consideration, as mentioned before, the accuracy in resonator's manufacturing and how the unloaded Q-factor was computed. Values of errors in R_S measurements were computed against NdBCO film data and are presented in Fig. 5.8 on a right-hand side bar.
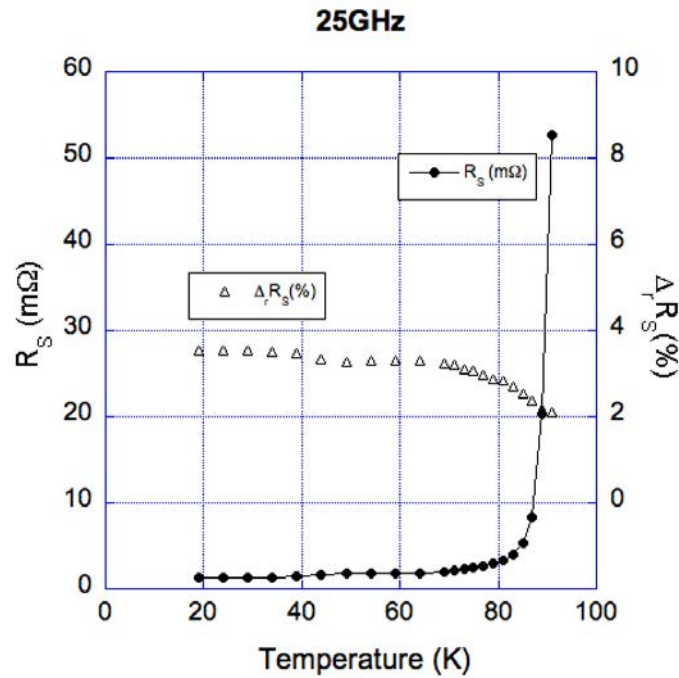
Fig. 5.8 Surface resistance of NdBCO films (1-2) and most probable error vs temperature at 25GHz.

As can be observed, the computed most probable errors in R_S measurements based on (5.1) were in the range from 2% to 3.8% for 25GHz resonator. The most probable error range for the YBCO thin film data is similar.

5.2.1 Results of microwave power characterisation of YBCO and NdBCO thin films on MgO substrates at different power levels

To enable investigation of microwave properties of YBCO and NdBCO films under varying RF input power P_{RF}, a 20dB microwave amplifier was employed between the VNA and the 25GHz resonator. The power range varied from -5dBm to +25dBm with a 5 dBm step. In this configuration, an attenuator was not required due to the VNA high power capabilities handling up to +40dBm. With this setup, it was

not possible to measure S_{11} parameter at the input of the resonator, and hence the computations of R_S were performed using the conventional 3dB method.

The influence of RF power from -5dBm to +25dBm on the surface resistance of YBCO and NdBCO films is shown in detail in Fig 5.9 and 5.10 for various temperatures.
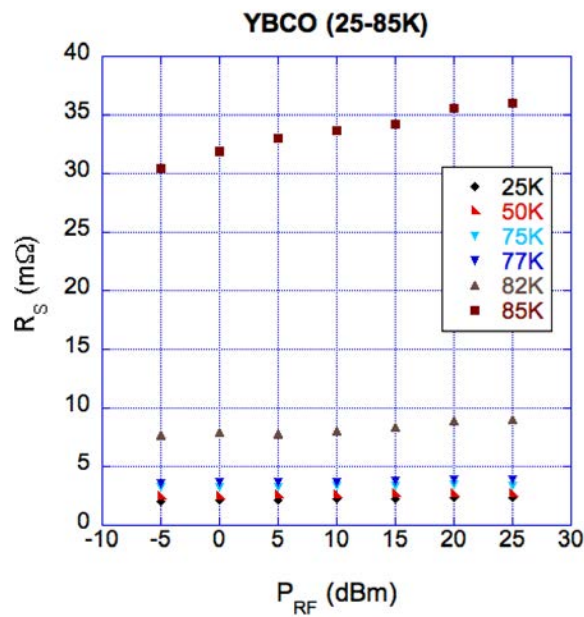

Fig. 5.9 Surface resistance versus RF power for YBCO films (1-2)

for various temperatures.
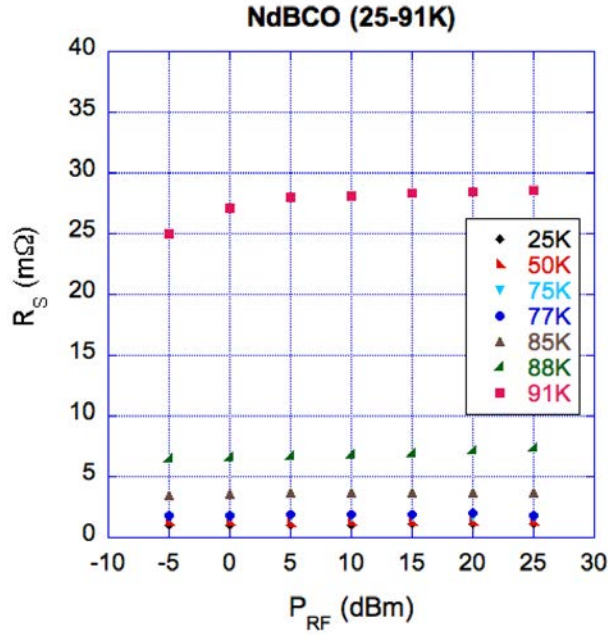
Fig. 5.10 Surface resistance versus RF power for NdBCO films (1-2)

for various temperatures.

From the above results, it is clearly visible that the increase of R_S for YBCO films starts approximately at temperature of 82K, and in NdBCO films under test the increase is observable at 88K and higher.

To identify the onset of nonlinear effects in the YBCO and NdBCO films, a two segment piecewise linear approximation of measurement results was performed. The change in R_S for the 30dBm increase (from -5dBm to 25dBm) in RF input power normalised to the value of surface resistance at 77K and 0dBm, $\Delta_P R_S$, is shown in Fig. 5.11 and 5.12 for YBCO and NdBCO films respectively. $\Delta_P R_S$ was computed as:

$$\Delta_P R_S = \frac{R_S(25dBm) - R_S(-5dBm)|_{T=const}}{R_S(0dBm)|_{T=77K}} \tag{5.2}$$
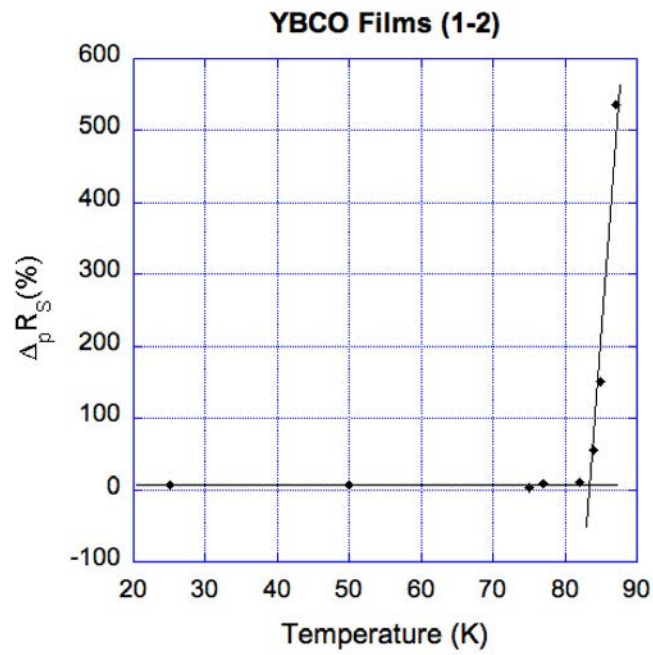
Fig. 5.11 Normalised change in R_S of YBCO films (1-2) for ΔP_{RF} from -5dBm to
+25dBm at 25GHz.
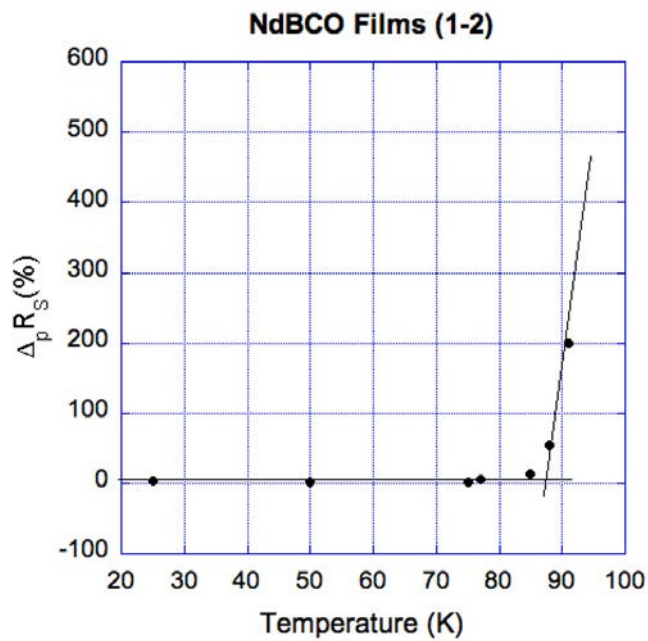
Fig. 5.12 Normalised change in R_S of NdBCO films (1-2) versus temperature for
ΔP_{RF} from -5dBm to +25dBm at 25GHz.

The average value of the linear regression of $\Delta_p R_S$ below 80K for YBCO films (Fig. 5.11) was 6.7%, and for the NdBCO films (Fig. 5.12) was 3.2%.

Applying a two segment piecewise linear approximation of measurement results, the onset of nonlinear effects can be defined in the YBCO films at temperature of approximately 84K, and in the NdBCO films at approximately 88K. Hence, it is possible to assume that the NdBCO films exhibit better power handling capabilities than YBCO films. As far as the accuracy of the two segment piecewise linear fitting technique is concerned, it depends on the number of points obtained. As visible from Fig. 5.11 and 5.12, there is only a small number of points available for higher temperatures, thus the accuracy of the results lacks certain precision at higher temperatures. The results of this investigation have been submitted for publication in the Advances in Science and Technology journal.

In summary, smaller nonlinear effects of NdBCO films could give them an advantage over YBCO films for microwave applications to microwave filters. In order to conduct a more complete and comprehensive investigation, YBCO and NdBCO microstrip resonators and filters were manufactured in cooperation with the Tsinghua University, China. The microwave characterisation of the resonators was conducted by the author of this thesis with results presented in the next few sections.

5.3   Design of YBCO and NdBCO microstrip resonators

As shown in the previous section, NdBCO superconducting films exhibit better power handling capabilities than YBCO superconducting films in terms of nonlinearities at higher power levels. Thus, smaller nonlinear effects of NdBCO films might give them an advantage over YBCO films in mobile network applications. In this regards, for the purpose of more complete research and analysis of YBCO and NdBCO materials and microwave devices, microstrip resonators were designed, manufactured, and investigated. As was stated before, the films for the resonators were purchased by the James Cook University (JCU) from Ceraco, Germany. The

original design of the resonators was provided by the author of this thesis to Tsinghua University, China, where in cooperation with Professor Bin Wei, three NdBCO (R1N, R2N, R3N) and two YBCO (R1Y, R2Y) microstrip resonators were manufactured with slight modifications in the original design.

The Ceraco YBCO and NdBCO films on MgO substrates were double sided (covered with a superconducting layer on both sides), hence the thermal co-evaporation process had to be repeated. An additional layer of gold with thickness of 200nm was co-evaporated for contacts. As stated before in this chapter, the NdBCO films also had a 25nm YBCO buffer layer.

The films characteristics were as following:

- YBCO films: 10x10mm, 500nm YBCO double sided, with 200nm Au double sided, 0.5mm MgO substrate, both sides polished.
- NdBCO films: 10x10mm, YBCO buffered NdBCO films, 600nm double sided, 0.5mm MgO substrate, 200nm Au double sided, both sides polished.

YBCO and NdBCO thin films in preparation for manufacturing of microstrip resonators are shown in Fig. 5.13.

a)   b)

Fig. 5.13 YBCO (a) and NdBCO (b) thin films fabricated at Ceraco, Germany.

Both YBCO and NdBCO resonators had the same layout, presented in Fig. 5.14 (a). The precise etching technique was applied in resonator manufacturing. The center frequency of the resonator was 2.171GHz. The loaded Q factor of the resonator was 1552.7, and the unloaded Q-factor of the resonator can be calculated according to the eq. (2.2.22) given in Chapter 2. It was assumed that $S_{11} = S_{22} = -39.9$dB, hence the calculated unloaded Q factor can be computed as 1.53×10^5.

a)   b)
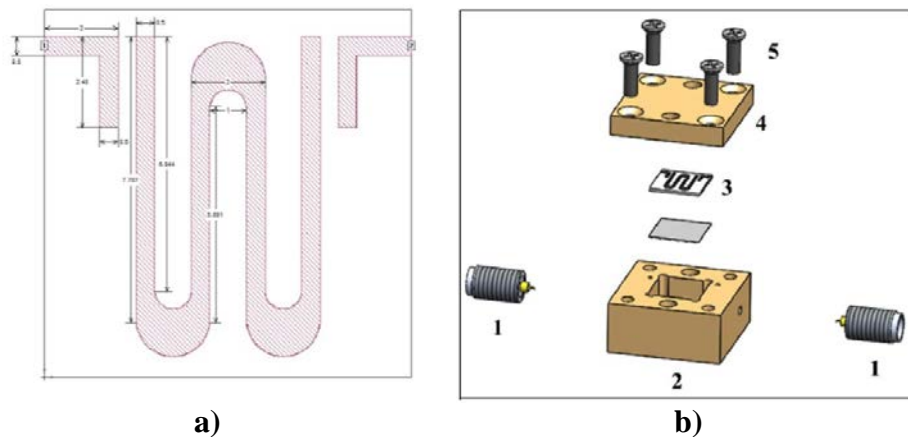
Fig. 5.14 Layout (a) of the YBCO and NdBCO resonators, and (b) components of a resonator package.

Fig 5.14 (b) illustrates the main components of the resonator package, namely:

1. A pair of SMA connectors;
2. Au coated main body of the package, including the bottom plate and the shield walls;
3. HTS resonator;
4. Au coated cover plate;
5. Screws

The top view of the HTS microstrip resonator is illustrated in Fig. 5.15 (a), with the actual pictures of the fabricated resonators shown in Fig. 5.15 (b).

a)   b)
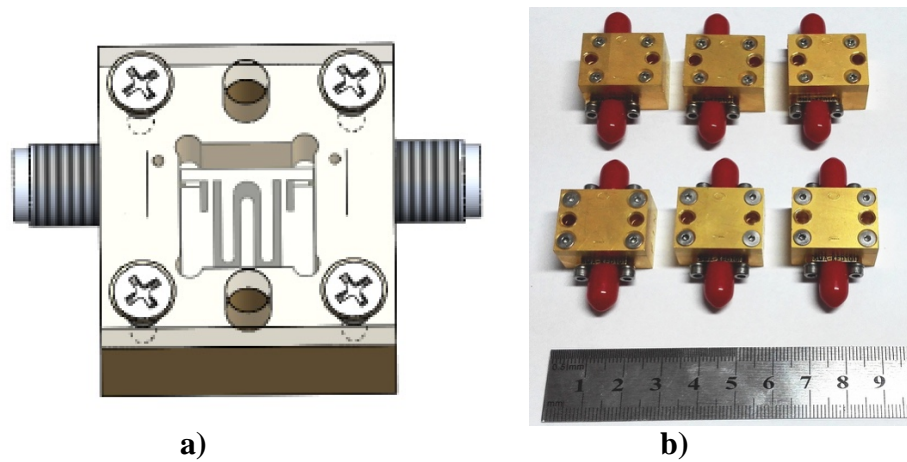
Fig. 5.15 (a) HTS microstrip resonator package; (b) HTS microstrip resonators.

The simulated response of the resonator, computed at the Tsinghua University, is shown in Fig 5.16 with the resonant frequency of 1963.5MHz.
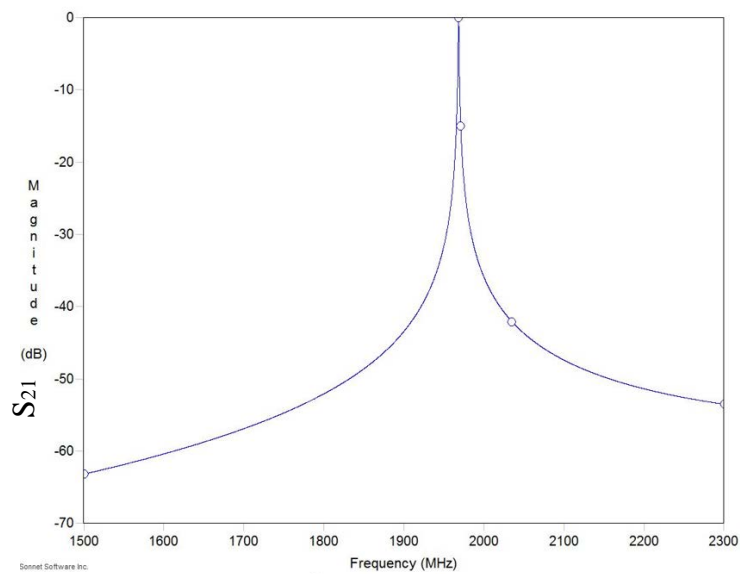

Fig. 5.16 Simulated response of HTS microstrip resonators (Y-axis: S21 (dB)).

5.4 Measured transmission coefficient S_{21} dependence on power and temperature of YBCO and NdBCO microstrip resonators

In order to investigate the influence of RF input power on the surface resistance of both types of resonators, a similar power measurement setup was implemented as described in section 5.1 for superconducting films. In this section, measured results for YBCO and NdBCO resonators at temperatures of 25K, 77K and 87K (YBCO), 90K (NdBCO) are presented. The power levels were varied from -5dBm to +30dBm with a 5dBm step increase.

Figs. 5.17 and 5.18 show the resonance dependences of transmission coefficient S_{21} on frequency for YBCO (R3Y) and NdBCO (R1N) resonators respectively at 25K at various applied power levels. Other measured resonators showed similar behaviour, therefore they are not presented in this chapter for a concise account.
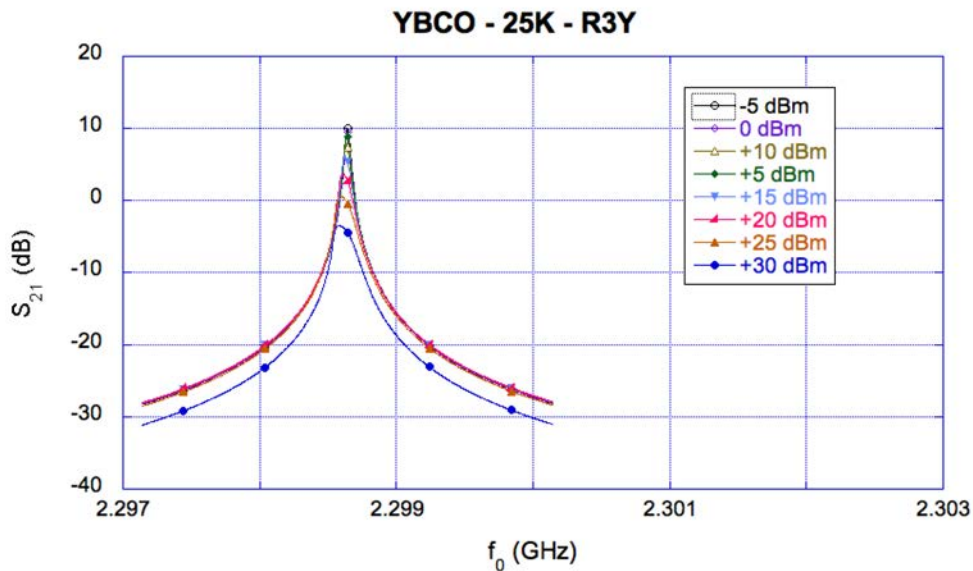

Fig. 5.17 Transmission coefficient of YBCO resonator R3Y at 25K at varying power levels.
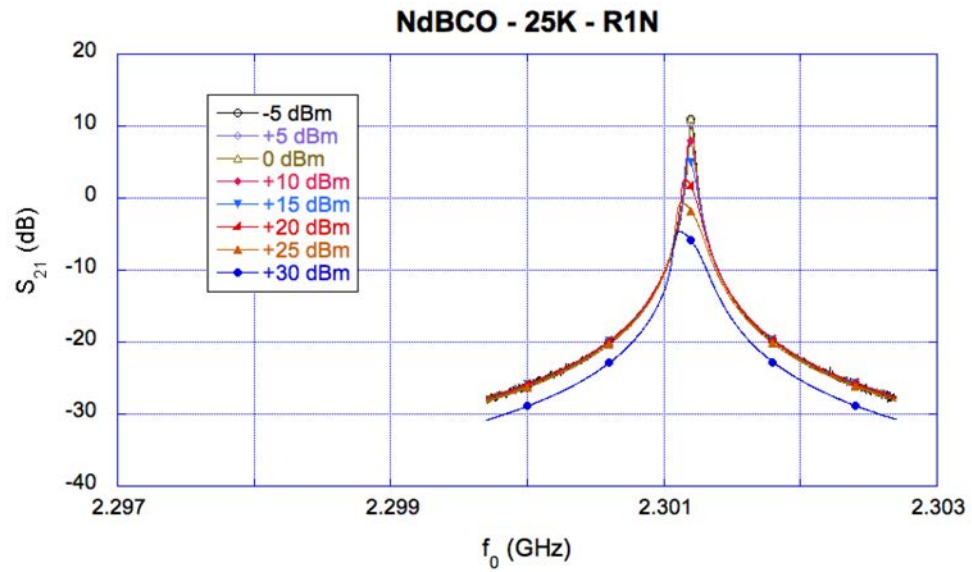
Fig. 5.18 Transmission coefficient of NdBCO (R1N) resonator at 25K for varying power levels.

The same frequency scale was applied to both graphs. From Figs. 5.17 and 5.18 it is visible that the microwave signal strength has a relatively little influence on the value of the transmission coefficient S_{21} at lower power levels for both resonators, with some nonlinear effects appearing at +15dBm and above, with the strongest one detected at +30dBm as expected.

Fig. 5.19 and 5.20 show measured S_{21} results for YBCO (R3Y) and NdBCO (R1N) resonators at 77K.
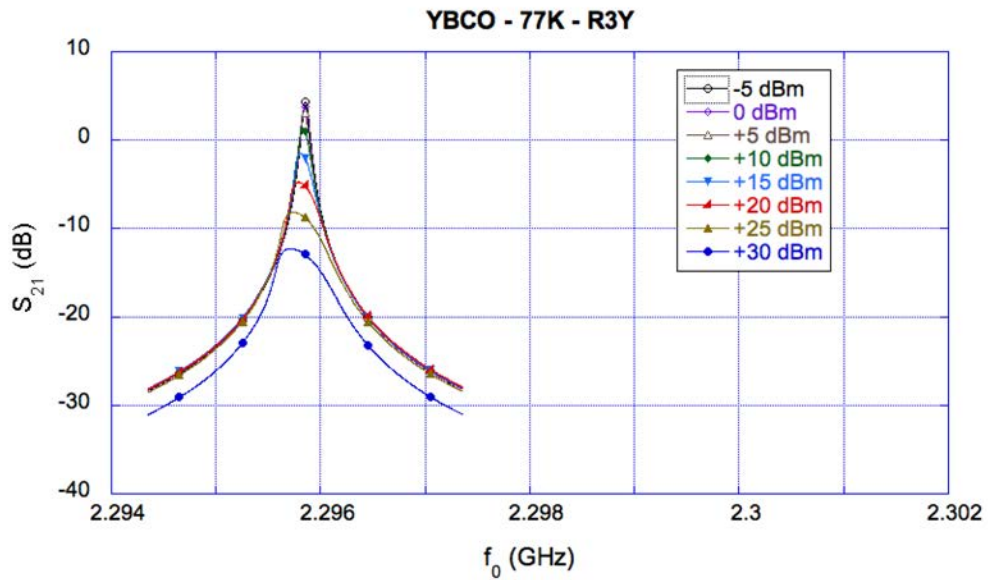
Fig. 5.19 S_{21} of YBCO (R3Y) resonator at 77K for varying power levels.
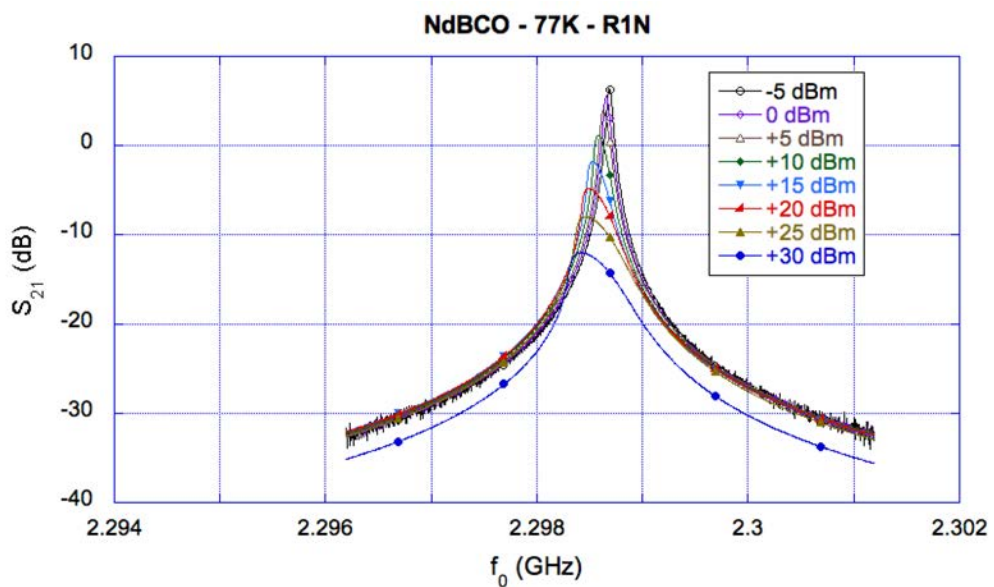
Fig. 5.20 S_{21} of NdBCO (R1N) resonator at 77K for varying power levels.

The results presented in Figs. 5.19 and 5.20 show visible nonlinear effects at +30dBm for both resonators. Starting from +15dBm and higher, YBCO films illustrate more visible widening effect of the resonance curves, meaning the corresponding influence on Q factor.

Figs. 5.21 and 5.22 display S_{21} characteristics for temperatures of 87K and 90K for YBCO and NdBCO resonators respectively.
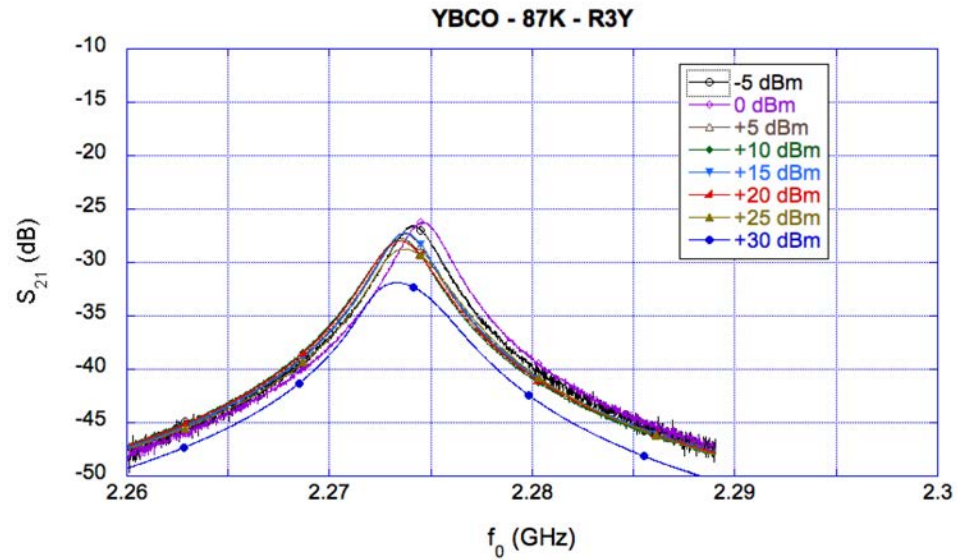

Fig. 5.21 S_{21} of YBCO (R3Y) resonator at 87K for varying power levels.
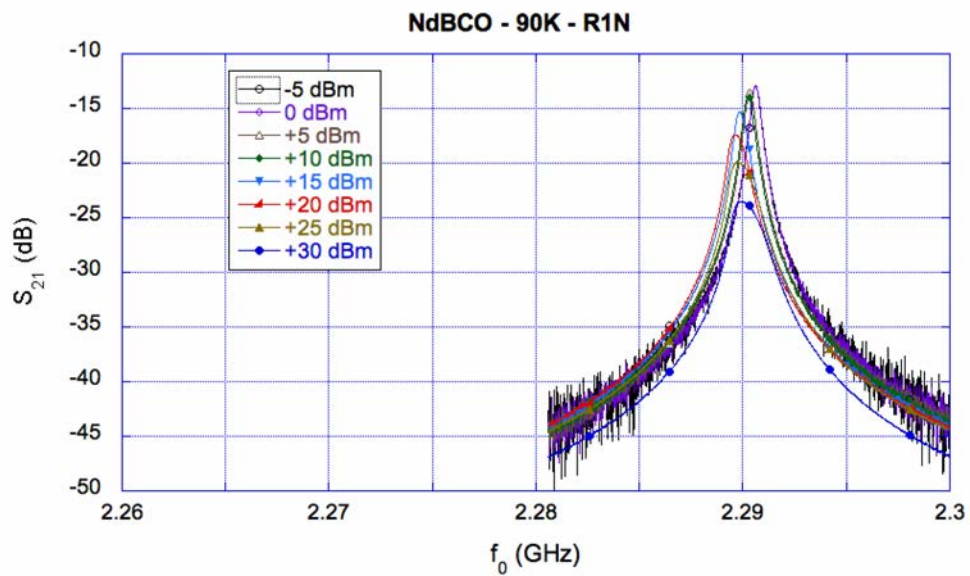
Fig. 5.22 S_{21} of NBCO (R1N) resonator at 90K for varying power levels.

A visible widening and a slight shift of the S_{21} curve at 87K for the YBCO resonator under RF power of +30dBm indicates the presence of nonlinear effects. The NdBCO resonator shows higher Q values and less visible nonlinearities at temperature

of 90K, comparing to the YBCO resonator at 87K. Obviously, the power effects at + 30dBm are still present, shifting the top of the curves towards smaller frequencies for both resonators. The power effect of shifting the curves is also noticeable for levels starting from +15dBm and higher, but not with the degree observed at +30dBm for both resonators.

5.5   Computed dependence of quality factor Q_0 and surface resistance R_S on temperature and RF signal power for YBCO and NdBCO resonators.

As stated earlier in Chapter 3 and this chapter, to obtain the unloaded Q_0 a sophisticated Transmission Mode Quality Factor (TMQF) technique for data processing was applied. For each temperature, 1601 points of S_{21}, S_{11} and S_{22} parameters around the resonance were recorded and the measured values fitted to circles on the complex plane to compute coupling coefficients, loaded Q_L and unloaded Q_0 factor. As was defined before, the TMQF technique enabled to eliminate or reduce noise, impedance mismatch and phase delay from measured results. Fig. 5.23 shows the comparison of the unloaded quality factor Q_0 dependence on temperature for YBCO (R3Y) and two NdBCO (R1N and R2N) resonators computed as an average value at 0dBm.
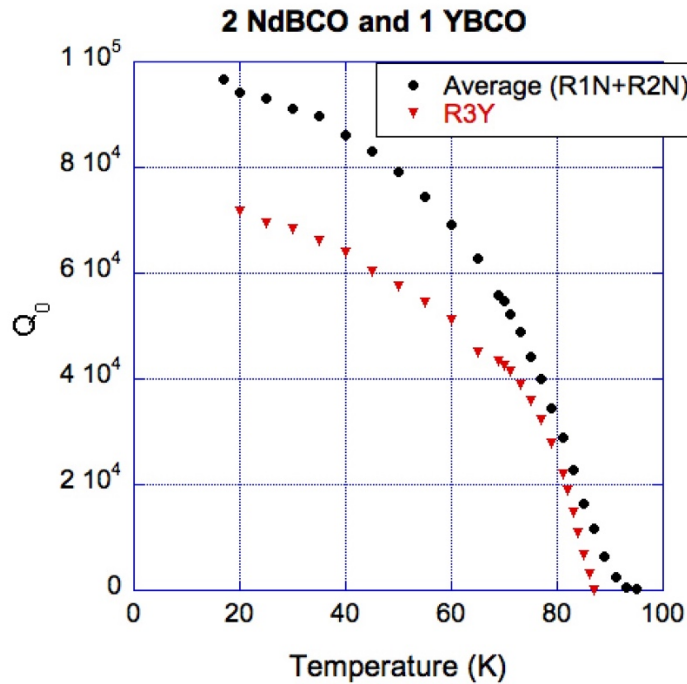
Fig. 5.23 Quality factor for two NdBCO (R1N and R2N) resonators computed as an average value, and YBCO (R3Y) resonator at 0dBm.

For comparison, results of the two NdBCO resonators have been presented as an average. As illustrated, the NdBCO resonator has much higher Q_0 than YBCO resonator at lower temperatures, with the difference of almost 30% at 20K: NdBCO Q_0 of 92198, YBCO Q_0 of 71600. The difference becomes smaller closer to 80K (NdBCO Q_0 of 28965 at 81K, YBCO Q_0 of 21946 at 81K), with the behaviour becoming more consistent towards T_C of corresponding superconductors.

As far as the uncertainty of the measurement results is concerned, it can be caused by instrument limitations; by unequal coupling; or by coupling losses [17]. In the conducted measurements it was assumed that the instrument limitations were less than 1%, taking into account the TMQF technique for data processing that reduces noise, impedance mismatch and phase delay. The coupling was assumed equal and coupling losses negligible.

Fig 5.24 illustrates the dependence of the effective surface resistance, computed according to eq. (2.2.21), on power for YBCO resonator at various temperatures.
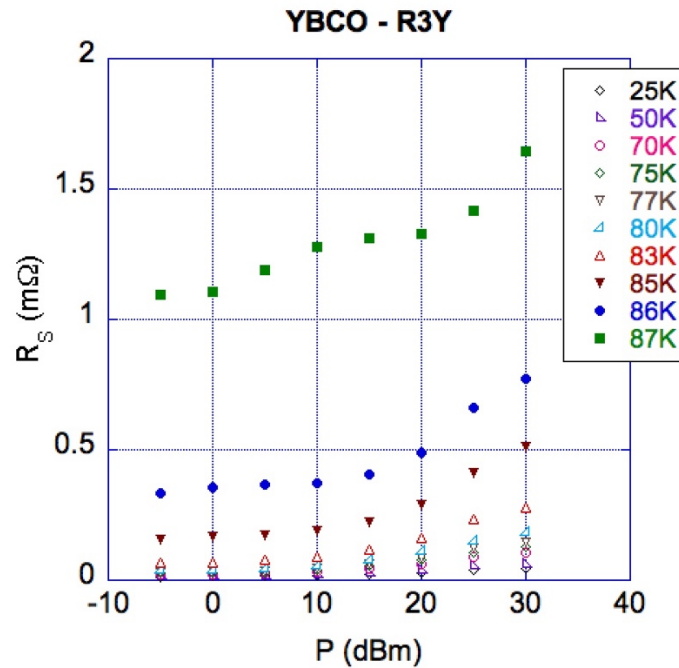
Fig. 5.24 Surface resistance vs RF power for different temperatures for YBCO (R3Y) microstrip resonator.

As can be seen, the R_S values become higher with the temperature increase, with the biggest increase detected from 86K to 87K, near the critical temperature. The surface resistance also rises with higher power levels, increasing steeper in the range from +15dBm to +30dBm.

Similar investigations of R_S vs Power were conducted for NdBCO resonators, with results for R1N resonator shown in Fig. 5.25 and R2N resonator in Fig. 5.26.
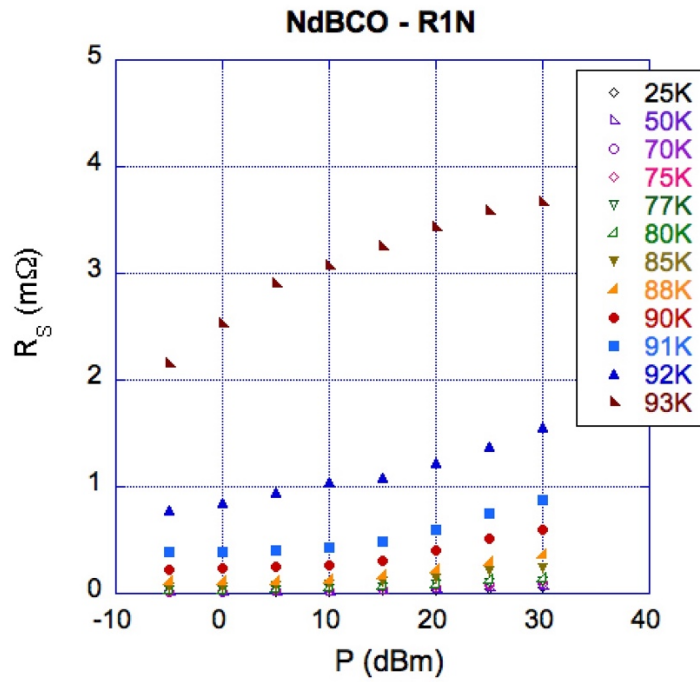
Fig. 5.25 Surface resistance vs RF power for different temperatures for NdBCO (R1N) microstrip resonator.
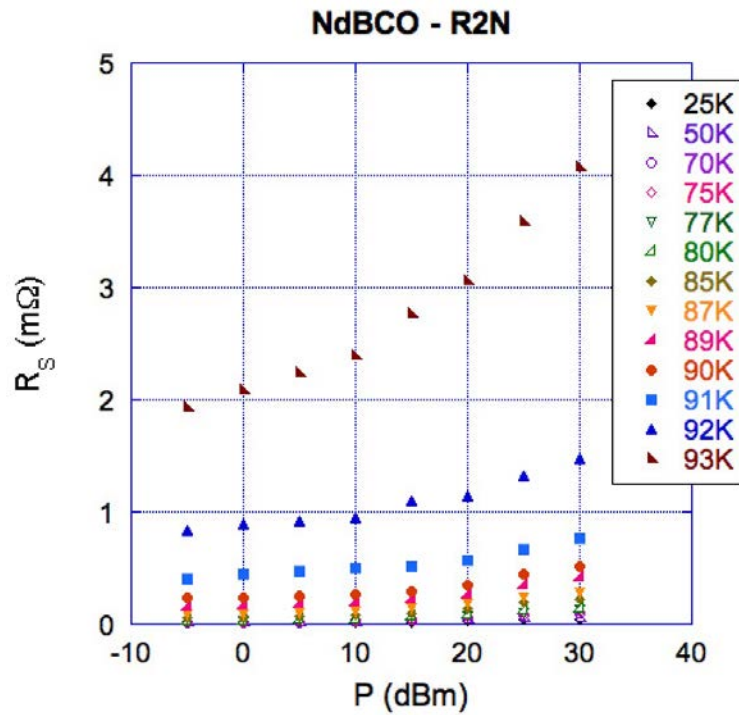

Fig. 5.26 Surface resistance vs RF power for different temperatures for NdBCO (R2N) microstrip resonator.

As can be observed from Fig. 5.25 and 5.26, both NdBCO resonators show similar behaviour of R_S with varying power levels, with the only difference visible at 93K where R_S is higher for R1N resonator at middle power ranges between +5dBm to +20dBm, while showing slightly lower value at +30dBm. In general, the behaviour of $R_S(P)$ lies within an expected pattern of R_S rising with the increase of power.

Comparing the two types of resonators, YBCO and NdBCO, it is visible that both resonators show similar rise of R_S with increased power, but NdBCO resonators have higher critical temperatures and lower R_S at corresponding temperatures, for example:

YBCO R3Y resonator at **77K**: $R_S = 0.144$mΩ;

NdBCO R1N resonator at **77K**: $R_S = 0.119$mΩ;

NdBCO R2N resonator at **77K**: $R_S = 0.12$mΩ;

Closer to critical temperatures of corresponding materials the following R_S values were detected:

YBCO R3Y resonator at **87K**: $R_S = 1.64$mΩ;

NdBCO R1N resonator at **93K**: $R_S = 3.66$mΩ;

NdBCO R2N resonator at **93K**: $R_S = 4.06$mΩ;

For the highest value of temperature at **87**K for YBCO resonator ($R_S = 1.64$mΩ) the following values of R_S were measured for NdBCO resonators:

NdBCO R1N resonator at **88K**: $R_S = 0.359$mΩ;

NdBCO R2N resonator at **87K**: $R_S = 0.282$mΩ;

As can be seen and as was expected, NdBCO resonators showed smaller surface resistance values at elevated power levels at corresponding temperatures, than YBCO resonators. Their power handling capabilities also extended to higher temperatures due to higher T_C of NdBCO resonators.

In order to identify nonlinear effects with the onset of nonlinearities in the YBCO and NdBCO resonators, a two segment piecewise linear approximation was used as described earlier in this chapter. The change in R_S for 35dBm increase in RF input power normalised to R_S at 77K and 0dBm is presented in Fig. 5.27 and 5.28 for YBCO and NdBCO resonators respectively. It was computed as (5.2):

$$\Delta_P R_S = \frac{R_S(30dBm) - R_S(-5dBm)|_{T=const}}{R_S(0dBm)|_{T=77K}} \qquad (5.2)$$
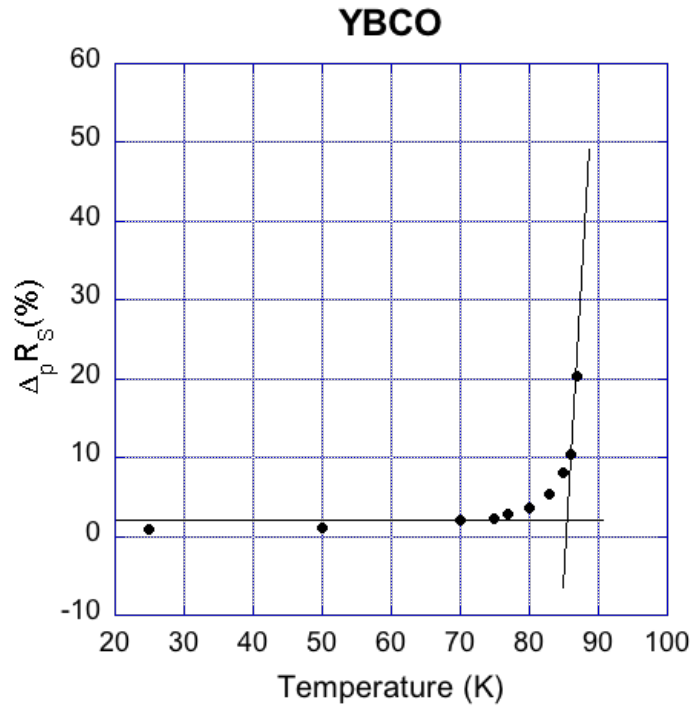
Fig. 5.27 Measured change in R_S of YBCO (R3Y) resonator for ΔP_{RF} from -5dBm to 30dBm.

As visible, the measurements of nonlinear effects under varying RF power from -5dBm to +30dBm showed that the onset of nonlinearities occurs approximately at 85K for YBCO resonator.

The same approach was applied to calculate the measured change in R_S for NdBCO resonator for varying power from -5dBm to +30dBm, with results shown in Fig. 5.28.
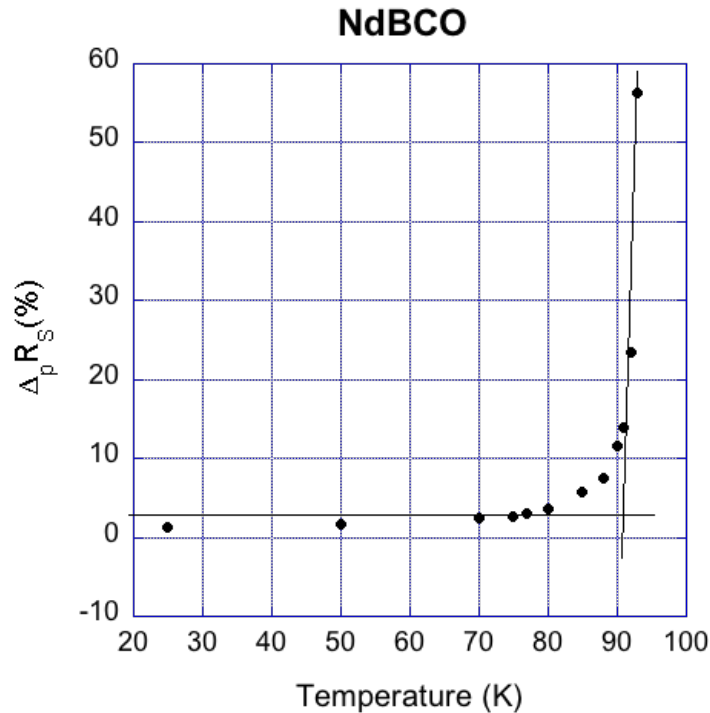
Fig. 5.28 Measured change in R_S of NdBCO (R1N) resonator for ΔP_{RF} from -5dBm to 30dBm.

As can be observed in Fig. 5.28, the onset of nonlinearities occurs approximately at 91K for NdBCO resonator.

In summary, the experimental investigation of microwave properties of $YBa_2Cu_3O_7$ and $NdBa_2Cu_3O_7$ thin films and microstrip resonators, presented in this chapter under varying RF power levels, showed that the onset of nonlinearities occurred at approximately 88K for NdBCO films and 91K for NdBCO resonators, while the onset values were approximately 84K for YBCO films and 85K for YBCO resonators. Therefore, it is possible to conclude that the NdBCO thin films and NdBCO microstrip resonators showed better power handling capabilities than the YBCO thin films and YBCO microstrip resonator.

The microwave investigation also showed that the corresponding surface resistance of both NdBCO films and resonators was lower than R_S of YBCO films and resonators with the most probable error calculated between 2% to 3.8%.

REFERENCES

[1]   C. Cantoni et al., "Structural and transport properties of epitaxial NdBCO thin films on single crystal and Ni metal substrates", *Physica C*, v. 324, p. 177, 1999.

[2]   R. Semerad et al., "RE-123 thin films for microwave applications", Physica C, v. 378, pp. 1414-1418, 2002.

[3]   B. Utz et al., "Deposition of YBCO and NBCO films on areas of 9 inches in diameter", *IEEE Trans. Appl. Supercond.*, v. 7, no. 2, pp. 1272-1277, 1997.

[4]   Z. Mori et al., "In-situ annealing effect of sputter-deposited NdBCO thin films", *Thin Solid Films*, v. 354, pp. 195-200, 1999.

[5]   J. Mazierska et al., "Microwave measurements of surface resistance and complex conductivity in NdBaCuO films", *Advances in Science and Technology*, v. 95, pp. 162-168, 2014.

[6]   M. Badaye et al., "Superior properties of NdBCO over YBCO thin films", Superc. Science and Technol., v. 10, pp. 825-830, 1997

[7]   K. Muranaka, "Microwave properties of Nd-Ba-Cu-O film characterized by dielectric resonator", Advances in Supercond. X, Springer, pp. 1061-1064, 1998.

[8]   M. Salluzo et.al., "Superconducting properties of YBaCuO and NdBaCuO thin films deposited by dc sputtering", IEEE Trans. on Applied Superconductivity, v. 11, pp. 3201-3204, 2001.

[9]   M. Boffa et al., "Realization of highly epitazial (Y, Nd, Sm) $Ba_2Cu_3O_7$ films for microwave applications", Physica C: Superconductivity, v. 384, pp. 419-424, 2003.

[10]   N. Zuchowski, "Microwave properties of NdBaCuO HTS films", B.Eng. thesis, James Cook University, 2014.

[11]   A. Rains, " Micrwoave characterisation of NdBaCuO HTS thin films and comparison of measurement techniques in terms of uncertainty in quality factor and surface resistance", B.Eng thesis, James Cook University, 2014.

[12]   Ceraco, Germany, www.ceraco.de.

[13]   J. Mazierska and C. Wilker, "Accuracy issues in surface resistance measurements of high temperature superconductors using dielectric resonators", *IEEE Trans Appl. Supercond.*, v. 11, pp. 4140-4147, 2001.

[14]   K. Leong and J. Mazierska, "Precise Measurements of the Q-factor of Dielectric Resonators in the Transmission Mode: Accounting for Noise, Crosstalk, Uncalibrated Lines, Coupling Loss and Coupling Reactance", *IEEE Trans. MTT,* 50 pp. 2115-2127, 2002.

[15]   J. Krupka, Software *"SUPER", Warsaw University of Technology*, 2002.

[16]   J. Mazierska, "Dielectric resonator as a possible standard for characterisation of high temperature superconducting films for microwave applications", *J. Supercond.*, v. 10, no. 2, pp.73-85, 1997.

[17]   D. Kajfez et al., "Uncertainty Analysis of the Transmission-Type Measurement of Q–Factor", IEEE Trans. on Micro. Theory and Techn., v. 47, p. 367, 1999.

CHAPTER 6

Discussions and conclusions

This dissertation focused on two hypotheses: the theoretical development of an advanced lumped element model of microwave properties of superconducting materials to include nonlinear effects for the purpose of application of the model to analysis of performance of HTS circuits; and the experimental investigation of microwave properties of $YBa_2Cu_3O_7$ (YBCO) and $NdBa_2Cu_3O_7$ (NdBCO) thin films and microstrip resonators in order to establish if there is any other material that exhibits smaller nonlinear effects than found in the widely utilised YBCO superconductor.

As mentioned throughout the course of this thesis, nonlinear effects arising at elevated power levels in High Temperature Superconductors (HTS) can significantly limit HTS superior microwave characteristics. The phenomena behind nonlinearities is still not completely understood by the scientific community. The increase in RF losses in HTS can be attributed to various mechanisms occurring under high powers, sometimes simultaneously, such as weak links, microwave heating, local heating effects, vortices in weak links and vortex motion penetration. Understanding the extent of nonlinear limitations and possibly predicting them can be a substantial advantage in early stages of design electronic circuits. Currently, CAD models do not account for superconducting nonlinear effects. In addition, the development of HTS films with better power handling capabilities than widely accepted YBCO materials, would be very useful for microwave devices. In the course of this thesis a number of theoretical and experimental contributions have been achieved - they are:

- A novel advanced lumped element circuit model to account for nonlinear effects in a superconductor has been developed and analysed. In the process

of development, three lumped element models for describing a Hakki-Coleman dielectric resonator with integrated superconductor, represented as a two-fluid model, have been proposed. One superconductor model included a novel approach proposed by the author of this thesis to represent lumped elements of superconductor (R_S, L_{SS} and L_{Sn}) as L_{Sn} series and L_{SS}, R_S parallel circuit combination. Complex equations to describe transmitted RF power for each circuit have been derived by the author using the circuit theory and rigorous mathematical algorithms (see Chapter 4).

- To investigate the modelling of nonlinear effects of superconductors, three nonlinear dependencies (linear, quadratic and exponential) have been applied to nonlinear elements (R_S, L_{SS} and L_{Sn}) of the above described circuits and examined together for the first time. To analyse all three dependencies together is important as it is believed they describe various mechanism responsible for nonlinearities. The *linear* dependence can be attributed to microwave heating effects and weak link losses at low power levels. The *quadratic* nonlinear dependence can describe a weakly coupled grain model with magnetic field penetration at grain boundaries, and partial vortex penetration in weak links. The *exponential* dependence can be associated with vortex penetration into superconducting grains and the fluxoid motion as possible factors contributing to the nonlinear effect. Simulations of all three nonlinear dependencies incorporated into three RLC equivalent lumped element models have been conducted using Matlab software. Based on simulated results, the selected models 'B' and 'C' (Figs. 4.6 and 4.7) could be used for simulations of nonlinear effects of HTS films in resonant structures at wide range of power levels. It is believed that the developed lumped element models can also contribute towards development of dedicated CAD tools for electronic circuit analysis.

- Thermally co-evaporated $NdBa_2Cu_3O_7$ (NdBCO) thin films and resonators have been investigated in the course of this thesis to identify if they can exhibit

smaller nonlinear effects than found in YBa$_2$Cu$_3$O$_7$ (YBCO) thin films deposited with the same technique. While NdBCO films are known to have higher T$_C$ and J$_C$ than YBCO films, the latter have been almost exclusively implemented in HTS microwave applications and research due to availability of high quality YBCO films and their relatively low prices. Also, a valuable factor of the investigation in this thesis was that films and resonators of two materials were deposited in the same laboratory (Ceraco, Germany) using the same thermal co-evaporation technique. For investigation of microwave properties of NdBCO and YBCO thin films a Hakki-Coleman 25GHz dielectric resonator operating at the TE$_{011}$ mode was implemented. To ensure the highest possible accuracy in computed values, the loaded Q$_L$-factor and coupling coefficients β_1 and β_2 of the resonator were obtained from multi-frequency measurements of S$_{21}$, S$_{11}$ and S$_{22}$ parameters measured around the resonance using the Transmission Mode Quality Factor (TMQF) Technique, mentioned in Chapter 3. The unloaded Q$_0$-factor was calculated from the exact equation $Q_0 = Q_L(1 + \beta_1 + \beta_2)$, using the TMQF method for all temperatures. For each temperature, 1601 points of S$_{21}$, S$_{11}$ and S$_{22}$ parameters around the resonance were obtained and the measured values fitted to circles on the complex plane to compute coupling coefficients, loaded Q$_L$ and unloaded Q$_0$ factors. Obtained results for the surface resistance of YBCO and NdBCO films illustrated that NdBCO films showed lower dependence on temperature as commercially available YBCO films. The biggest difference occurred at higher temperatures close to the YBCO critical temperature, with R$_S$ of YBCO: 26.06mΩ at 85K and R$_S$ of NdBCO: 6.55mΩ at 85K. At 81K the surface resistance of YBCO was 6.06mΩ, while NdBCO samples showed 4.46mΩ, and at 83K - YBCO films demonstrated 8.98mΩ and NdBCO films exhibited R$_S$ of 5.18mΩ. At lower temperatures between 19-79K, the difference of R$_S$ was within 0.3-0.6mΩ throughout the whole stated temperature range. Computed most probable errors in R$_S$ measurements at 25GHz (based on eq. (5.1)) were in the range from +3.2% to +3.8%.

- Power measurements have been conducted in the range from -5dBm to +30dBm to investigate the effect of applied RF power on YBCO and NdBCO thin film microwave properties. To identify the onset of nonlinear effects in the films, a two segment piecewise linear approximation of measurement results was performed. The change in R_S for the 30dBm increase in RF input power normalised to R_S at 77K and 0dBm as calculated in (5.2) was analysed. To the author's knowledge, it is the first time that such a comparison of the onset of nonlinear effects of YBCO and NdBCO films is presented. Obtained results showed that the onset of nonlinear effects can be defined in the YBCO films at a temperature of approximately 84K and in the NdBCO films at approximately 88K.

- In order to investigate YBCO and NdBCO materials for microwave applications, YBCO and NdBCO stripline resonators and filters were manufactured in cooperation with Professor Bin Wei of the Tsinghua University, China. A comprehensive microwave investigation and comparison of NdBCO and YBCO resonators was conducted by the author of this dissertation under varying RF power conditions (-5dBm to +30dBm). The centre frequency of the designed resonator was 2.171GHz. Obtained results for the measured dependence of quality factor Q_0 and surface resistance R_S on temperature and RF signal power for YBCO and NdBCO resonators showed that NdBCO resonator had much higher Q_0 than YBCO resonator at lower temperatures, with the difference of almost 30% at 20K: NdBCO Q_0 of 92198, YBCO Q_0 of 71600. The difference gets smaller closer to 80K (NdBCO Q_0 of 28965 at 81K, YBCO Q_0 of 21946 at 81K), with the behaviour becoming more consistent towards T_C of corresponding superconductors. Comparing two types of resonators, YBCO and NdBCO, it was observed that both resonators showed similar rise of R_S with increased power, but NdBCO resonators had higher critical temperatures and lower R_S at corresponding temperatures.

-   In order to identify nonlinear effects with the onset of nonlinearities in the YBCO and NdBCO resonators, a two segment piecewise linear approximation was used as described in Chapter 5. The change in R_S for 35dBm increase in RF input power normalised to R_S at 77K and 0dBm is presented in Fig. 6.1 for both YBCO and NdBCO resonators.
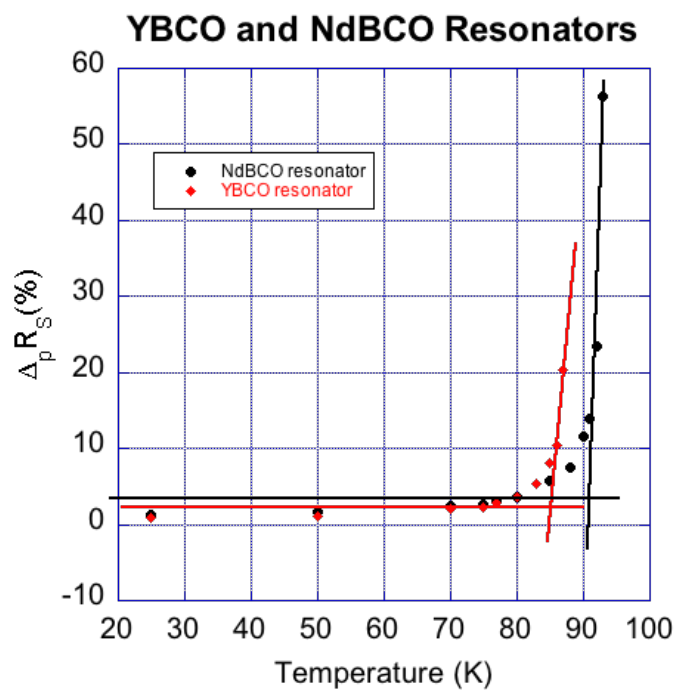

Fig. 6.1 Measured change in R_S of YBCO and NBCO resonators for ΔP_{RFInp} from -5dBm to +30dBm.

It was observed that the onset of nonlinear effects occurred approximately at 91K for the NdBCO resonator and approximately at 85K for the YBCO resonator. Therefore, it can be assumed that the NdBCO resonators under test had better power handling capabilities than the YBCO resonator.

6.1 Summary and recommendations

In summary, the developed novel equivalent circuit lumped element RLC model is a step forward over other RLC and LC models. The applied nonlinear exponential dependence accounts for vortex penetration into superconducting grains and vortex motion as dominant factors causing the increase in losses in HTS films under high RF magnetic fields. The proposed models can be made more accurate with more complex functions of H_{RF}, not just one function. It needs to be mentioned that the main problem with precise modelling of nonlinear effects at elevated power levels is that the physical phenomena in superconductors cannot always be closely approximated by linear, quadratic or even exponential dependencies in process of simulation, due to the nature of nonlinearities not clearly understood and may require further research. A mathematical model that consists of several terms representing various basic possible physical phenomena that engage at relevant temperatures and RF power levels seems necessary to accurately model RF properties of HTS films at high powers. However, the development of such a model would require a better understanding of nonlinearities in HTS materials.

In reference to the investigation of NdBCO and YBCO materials, measured temperature characteristics of surface resistance versus temperature for the YBCO buffered NdBCO films under test exhibited lower dependence as commercially available YBCO films. Observed smaller nonlinear effects in NdBCO resonators could give them an advantage over YBCO resonators for applications in microwave filters for mobile communication technologies. However, the rigorous control of the deposition process and appropriate template for NdBCO composition growth are fundamental requirements for high quality materials. The conducted investigation of the materials deposited in the same laboratory using the same co-evaporation technique also adds valuable input to the limited body of knowledge in this area.

As far as a wider application of the improved NdBCO superconducting compound is concerned, its better high power handling capability makes it attractive

for applications in advanced and complex radar systems, deep-space detection, satellite technology, emerging high-performance computing including advanced cryogenic quantum memory technologies, and next generation communication systems. With the electromagnetic spectrum getting more crowded due to increasing user numbers and expanding data services, the all-HTS integrated front-end receivers based on the improved NdBCO superconductors could also become a viable solution to the existing technology.